

Leander D. Eiring and Ulrik K. M. Lullau

Solar-Powered Cold Storage and Microgrid Integration for Sustainable Agriculture in Northern Ghana

Trondheim, 12 2024



NTNU – Trondheim
Norwegian University of
Science and Technology

PROJECT WORK

For

Students Ulrik Lullau and Leander Eiring

Autumn 2024

Solar-Powered Cold Storage and Microgrid Integration for Sustainable Agriculture in Northern Ghana
Soldrevet Kjølelager med Integrert Microgrid for Bærekraftig Landbruk i Nord-Ghana

Background and objective

This master thesis focuses on the initial design of a solar-powered cold storage facility to support sustainable agricultural practices at the TRAX Youth Empowerment Centre in Northern Ghana. The project addresses the critical need for efficient food storage to reduce post-harvest losses in a region challenged by extreme poverty, unemployment, and climate-related issues. The thesis covers the initial design and dimensioning of the solar powered cold storage facility with microgrid support. Through this work, the thesis aims to contribute to food security, sustainable development, and community empowerment in Northern Ghana.

The following tasks are to be considered:

1. Literature review on cold storage solutions in developing countries.
2. Make a simulation model of the total system.
3. Initial design of the full-scale cold storage in Northern Ghana.
4. Make a detailed specification of all the components for the system
5. Propose further work in a master thesis

The project work comprises of 15 + 30 ECTS credits (project and master's thesis).

The work shall be edited as a scientific report, including a table of contents, a summary in Norwegian, conclusion, an index of literature etc. When writing the report, the candidate must emphasise a clearly arranged and well-written text. To facilitate the reading of the report, it is important that references for corresponding text, tables and figures are clearly stated both places.

By the evaluation of the work the following will be greatly emphasised: The results should be thoroughly treated, presented in clearly arranged tables and/or graphics and discussed in detail.

The candidate is responsible for keeping contact with the subject teacher and teaching supervisors.

Risk assessment of the candidate's work shall be carried out according to the department's procedures. The risk assessment must be documented and included as part of the final report. Events related to the candidate's work adversely affecting the health, safety or security, must be documented and included as part of the final report. If the documentation on risk assessment represents a large number of pages, the full version is to be submitted electronically to the supervisor and an excerpt is included in the report.

According to the "Supplementary rules to the study regulations for the technology study/master's engineering program at NTNU", the submitted master's thesis with attachments can be freely used by NTNU for teaching and research purposes. For use in addition to this, such as publication and other financial utilization, a special agreement must be written between NTNU and the candidate.

Submission deadline: December 17th 2024 at 14:00 o'clock

- Work to be done in lab (Thermal engineering lab)
 Field work (Bongo District, Northern Ghana)

Department for Energy and Process Engineering



Trygve M. Eikevik, Prof.
Supervisor

Co-Supervisor(s): Engineers Without Borders.

Abstract

This project thesis is a part of a Master with Meaning (MwM) written in a collaboration between Norwegian University of Science and Technology (NTNU) and Engineers Without Borders (EWB) during the fall of 2024. This project is developed to support the operations of the TRAX Ghana farm by developing an initial design of a Solar-Powered Cold Storage (SPCS) facility for the farm to improve sustainability and address post-harvest losses. Addressing food insecurity and post-harvest losses is critical in regions such as northern Ghana, where agricultural productivity is constrained by a lack of reliable storage infrastructure. SPCS systems have emerged as a sustainable and eco-friendly solution to preserve perishable food, mitigate waste, and improve economic opportunities for small-scale farmers.

Cold storage facilities are crucial for increasing the shelf life of perishable goods such as vegetables and fruits. Rapid cooling shortly after harvest plays an important role in maintaining the quality of vegetables and fruits. Air cooling is a widely used method that utilizes cooling supplied by a refrigeration system to circulate cold air, quickly eliminating field heat from harvested crops. This method is both energy-efficient and cost-effective, making it ideal for rural settings. An initial design of the cold storage facility and the corresponding refrigeration system is presented. This design is in accordance with the specifications provided by TRAX Ghana. Furthermore, the refrigeration system uses relevant theory to create a simulation built on a literature-based estimate of the required refrigeration capacity. The highest refrigeration load in the system is estimated to be 0.96 kW, based on the highest refrigeration load. This load falls on a harvesting day of lettuce day in April, cooling 40 kg from 29.9°C to 1°C. This results in a 300 W compressor using Propane (R290) as the primary refrigerant. An indirect system is the proposed solution, which is ideal for cold storage facilities that require rooms with different temperatures. It features a secondary loop with a mixture of 18.8 % sodium chloride and water as a secondary refrigerant, which circulates between the evaporator and the storage area. This design reduces the required primary refrigerant, mitigates risks associated with refrigerant

leaks, and promotes environmental sustainability.

Given the limited access to reliable grid electricity in areas like northern Ghana, solar Photovoltaic (PV) systems combined with Battery Energy Storage Systems (BESS) are essential to supply sustainable power. Solar energy is abundant in this region, with average irradiance levels of $5\text{-}6 \text{ kWh/m}^2$ per day (Asumadu Sarkodie & Owusu, 2016). However, challenges such as dust accumulation on PV panels and high ambient temperatures can reduce system efficiency. Regular maintenance, optimized panel tilt angles, and cooling technologies are essential to maximize energy output. Battery systems further ensure continuous operation, especially during cloudy periods or at night, which addresses the variability of solar energy.

The solution presented is an integration of a decentralized Direct Current (DC) microgrid and a cooling system that suits such a remote context. By combining the advantages of an intuitive and numerical approach, adjustments were made to size a PV system of 2.83 kWp and 936 Ah in battery capacity, to balance the reliability of this critical load and cost. The suggested battery capacity offers an adequate autonomy of 4 days without excess cost or complexity. These modifications ensure that the initial design is reliable and efficient, enabling it to fully meet energy demand while minimizing excess energy. This integrated approach establishes the basis for future design.

The success of this project could hopefully serve as a model for strengthening sustainable agriculture and renewable energy solutions in similar African contexts.

Sammendrag

Denne prosjektoppgaven er en del av en Master med Mening (MmM) skrevet i samarbeid med NTNU og Ingeniører Uten Grenser (IUG) høsten 2024.

Gjennom et designutkast til et solcelledrevet kjølelager, er målet å lage en fremtidig løsning som kan bistå TRAX Ghana i driften av drivhus. Løsningen skal kunne hjelpe TRAX med å sikre bærekraftig drift ved å redusere tap etter høsting. Å sikre matsikkerhet og redusere tap etter høsting kan være viktige tiltak i regioner som nord-Ghana, hvor landbruk er begrenset av upålidelig strømtilgang og mangel på oppbevaringsmuligheter. Solcelledrevet kjølelagre har vist seg å være en bærekraftig og miljøvennlig løsning for å redusere matavfall og forbedre den økonomiske situasjonen for lokale bønder.

Kjølelagere er avgjørende for å forlenge den tradisjonelt korte holdbarheten til matvarer som frukt og grønnsaker. Derfor spiller rask nedkjøling kort tid etter innhøsting en viktig rolle i å opprettholde kvaliteten. Luftkjøling er en ofte benyttet metode, som utnytter kulde levert av et kjølesystem for å sirkulere kald luft, som raskt fjerner varmen fra innhøstede avlinger. Denne metoden er både energi- og kostnadseffektiv, noe som gjør den ideell for avsidesliggende områder. Et designutkast av kjølelageret og det tilhørende kjølesystemet presenteres i denne oppgaven. Designet er utarbeidet med bakgrunn i spesifikasjoner gitt av TRAX Ghana. Videre benyttes relevant teori om kjølesystemer for å lage en simulering basert på beregninger av nødvendig kjølekapasitet. Av de relevante grønnsakene trenger salat mest energi for å kjøles ned, det medfører at det største nedkjølingsbehovet er basert på en høstedag av salat i april måned, da omgivelsestemperaturene også er høyest. Denne maksimale nedkjølingskapasiteten er estimert til å være 0.96 kW , der 40 kg salat kjøles fra 29.9°C til 1°C . Dette fører til et nødvendig kompressorarbeid på 300 W , hvor R290 brukes som det primære kuldemediumet. Det foreslalte systemet er et indirekte system, ideelt for et kjølelager med flere rom ved forskjellige temperaturer. Det inkluderer en sekundærkrets med et sekundært kuldemedium, som er en blanding av 18,8% natriumklorid og vann, som sirkulerer mellom fordamperen og kjølerommet. Dette designet reduserer mengden av det primære kuldemediumet, minimerer risikoen tilknyttet

lekkasjer og fremmer bærekraft.

I områder som i nord-Ghana, med begrenset tilgang til et pålitelig strømnett, er solcelleanlegg integrert med batterilagring en avgjørende løsning for bærekraftig drift av et kjølelager. Solenergi er rikelig tilgjengelig i disse breddegradene, med en gjennomsnittlig solinnstråling på 5-6 kWh/m^2 per dag (Asumadu Sarkodie & Owusu, 2016). Utfordringer som store mengder støv på solcellepaneler og høye temperaturer kan imidlertid redusere systemets effektivitet. Regelmessig vedlikehold og optimalisering av panelvinkler og kjøleløsninger er nødvendig for å maksimere energiutbyttet. Batterisystemer sikrer ytterligere kontinuerlig drift, spesielt i overskyet vær eller om natten.

Løsningen som er presentert, er en integrasjon av et desentralisert DC-mikrogrid og et kjølesystem som passer en slik avsidesliggende kontekst. Ved å kombinere fordelene med intuitive og numeriske metoder, ble justeringer gjort for å dimensjonere et solcelle-system på 2.83 kWp (Kilowatt peak) og 936 Ah (Ampere-timer) i batterikapasitet for å sikre forsyningssikkerhet til en så viktig last. Den foreslalte batterikapasiteten gir tilstrekkelig autonomi uten å føre til overflødige kostnader eller økt kompleksitet. Disse endringene gjør at designet er både pålitelig, slik at det dekker energibehovet fullt ut. Denne tilnærmingen danner grunnlag for fremtidige design.

Med et suksessfullt design, kan prosjektet forhåpentligvis fungere som en modell for å styrke bærekraftig jordbruk og fornybare energiløsninger i lignende afrikanske sammenhenger.

Preface

This project thesis marks the beginning of the conclusion of our MSc at NTNU in Energy and Environmental Engineering.

We express our gratitude to our partners for their support during this period. Special acknowledgments are given to our supervisor, Trygve Eikevik of the Department of Energy and Process Engineering at NTNU, and our project leader from EWB, Elise Skattum, for their guidance and encouragement throughout the research. We also appreciate the contributions of Mr. Vincent Subbey, director of TRAX Ghana, and our EWB mentors: Torstein Riise and Annika Schartmüller from Multiconsult AS. We are deeply grateful for their advice, insight, and contributions.

Our deep gratitude goes to EWB and NTNU for facilitating our thesis.

Trondheim, May 28, 2025.

Leander D. Eiring

Ulrik K. M. Lullau

Contents

Abstract	iii
Sammendrag	v
Preface	vii
Table of Contents	viii
List of Figures	xii
List of Tables	xiv
Nomenclature	xv
Abbreviations	xix
1 Introduction	1
1.1 Background	1
1.1.1 Engineers Without Borders (EWB)	2
1.2 Motivation	2
1.3 Scope	3
2 Literature review	5
2.1 Normal distribution of harvest	5
2.2 Post-harvest losses in Sub-Saharan Africa	6
2.2.1 The cold chain	6
2.3 Refrigerants	8
2.4 Simulation and modeling tools	9
2.4.1 CoolProp	9
2.4.2 Distributed Energy Systems (Distributed Energy Systems (DES)) .	10
2.5 PV systems in remote areas	11
2.5.1 Solar irradiance	12
2.5.2 Wind speed	13
2.5.3 Ambient temperature	13

2.5.4	Geographical characteristics	14
2.6	Barriers: Solar-Powered Cold Storage	14
3	Theoretical background	16
3.1	Ghana	16
3.1.1	Energy access	16
3.1.2	Climate	17
3.2	Storage of vegetables	17
3.3	Relevant refrigerants	19
3.4	Refrigeration systems	21
3.4.1	Secondary loop refrigerants	23
3.4.2	Bypass valve	24
3.5	Structural cold storage design	25
3.6	Solar energy	28
3.6.1	Solar geometry and angles	29
3.7	Distributed Energy Systems (DES)	30
3.7.1	PV technology	30
3.7.2	PV components	34
3.7.3	Microgrid	35
3.7.4	Microgrid components	36
4	Presentation of the property	38
4.1	TRAX Ghana	38
4.1.1	Climatic conditions and solar potential	39
4.1.2	Energy usage	41
4.1.3	Agriculture on site	42
5	Methods	44
5.1	Data collection	44
5.2	Refrigeration system	45
5.3	Refrigeration loads	48
5.3.1	Crop properties	48
5.3.2	Transmission load	51
5.3.3	Product load	52
5.3.4	Infiltration load	53
5.3.5	Internal load	54
5.3.6	Total load	54
5.3.7	Compressor work	54
5.4	Load profile	55
5.5	Microgrid design	56

5.5.1	Design approach: intuitive and numerical	56
5.5.2	DC Microgrid configuration	57
5.5.3	Component sizing	57
5.5.4	Component selection	58
5.5.5	Parameters	58
5.5.6	Batteries	59
5.5.7	PV modules	60
5.6	PVsyst	61
5.6.1	Meteorological data	62
5.6.2	Inputs and interface	62
5.6.3	System simulation	63
5.6.4	Losses	63
5.6.5	Tilt angle and orientation	64
5.6.6	3D Model	65
6	Results and analysis	66
6.1	Cold storage design	66
6.2	Cold storage simulation and calculation results	68
6.2.1	Refrigeration load calculations	68
6.2.2	Compressor work	75
6.3	Refrigeration system simulation	75
6.3.1	Pump work	77
6.4	Load profile	78
6.5	Microgrid design	80
6.5.1	Component selection	81
6.5.2	Battery design	83
6.5.3	PV system design	84
6.6	PVsyst simulation	85
6.6.1	System overview	85
6.6.2	Energy production and demand	86
6.6.3	Battery performance	88
6.6.4	System efficiency and losses	88
6.7	Comparison of design approaches	89
7	Discussion	92
7.1	Plausibility	92
7.2	Climate and weather considerations	92
7.3	Cold storage	93
7.4	Refrigeration loads	93
7.5	Refrigeration system	95

7.6	Simulation vs. Calculation	95
7.6.1	Pump Work	97
7.6.2	Defrosting the Evaporator	97
7.7	Uncertainty in microgrid design	97
7.7.1	Load profiles	97
7.7.2	System design considerations	98
7.7.3	Additional losses	98
7.7.4	PVsyst	99
7.8	Future work	100
8	Conclusions	102
References		104
Appendix:	A1
A	Appendix A: Github repository	A1
B	Appendix B: Code script	B1
C	Appendix C: Data sheet	C1
C.1	PV Module Datasheet	C2
C.2	PV Module Datasheet	C3
C.3	Battery Datasheet	C4
C.4	Battery Datasheet	C5
C.5	Charge Controller Datasheet	C6
C.6	Charge Controller Datasheet	C7

List of Figures

3.1.1 Map of Ghana.	16
3.3.1 Refrigerating effect comparison between Isobutane (R600a), R290, R134a (Tetrafluoroethane) and R152a (Difluoroethane) from -30 °C to 10 °C.	20
3.4.1 Direct refrigeration system.	22
3.4.2 Indirect refrigeration system with one secondary refrigerant circuit.	22
3.5.1 Conventional wall design.	25
3.5.2 Conventional ceiling design with insulation on the inside of the structural support.	25
3.5.3 Conventional floor design.	26
3.5.4 Apparent thermal conductivity versus density for some common insulation materials.	27
3.5.5 Temperature profile through a typical wall.	28
3.6.1 Figure of solar geometry and Earth angles.	30
3.7.1 Figure of a basic PV cell.	31
3.7.2 Illustration of the temperature influence on the I/V curve for a PV module of 565 W. Extracted from PVsyst.	32
3.7.3 Illustration of the difference in irradiation and its influence on the I/V curve for a PV module of 565 W. STC is 25°C. The plot is extracted from PVsyst.	33
3.7.4 Figure of a PV system configuration with belonging components.	35
4.1.1 The Upper East Region of Ghana.	38
4.1.2 Screenshot from Google Maps. TRAX Ghana from above.	39
4.1.3 Mean monthly climate for TRAX Ghana.	40
4.1.4 Average peak sun hours between the two seasons for Bolgatanga, Ghana.	40
4.1.5 A simple system topology for the off-grid system	41
4.1.6 Average sunshine hours between the two seasons for Bolgatanga, Ghana.	42
5.0.1 Flowchart for the SPCS design.	44
5.2.1 Refrigeration system and corresponding Log (P-H) diagram for the cold storage.	46
5.6.1 Flowchart of the methodology in PVsyst.	62
5.6.2 Figure of the plane optimization tool in PVsyst.	64

5.6.3 Figure of the near shading construction tool in PVsyst.	65
6.1.1 2D and 3D illustrations of the cold storage.	67
6.2.1 Average transmission load for January and April in kW.	72
6.2.2 Average transmission load for the entire year.	72
6.2.3 Maximum total daily load [kW] for the relevant crops.	75
6.4.1 Daily Seasonal Load Profile of the Cold Storage Facility	78
6.4.2 Daily Load Profile of the Cold Storage Facility	79
6.4.3 Daily Load Profile of the Cold Storage Facility	80
6.5.1 A simple system topology for the off-grid system after design	80
6.5.2 Figure of the optimal tilt angle in PVsyst.	83
6.6.1 3D scene of the cold storage facility with 3 modules on 2 strings . Trees are just for aesthetics.	85
6.6.2 Data quality check for Meteonorm inputs in PVsyst.	86
6.6.3 Normalized production and loss factors from the PVsyst simulations.	87
6.6.4 Loss diagram from PVsyst simulations	89

List of Tables

2.2.1 Comparison of bulk cooling methods (Lange et al., 2016)	8
2.4.1 Comparison of software relevant for the modeling of the off-grid PV system (de Souza Silva et al., 2020)	11
3.2.1 Ideal storage temperature, vegetable sensitivity and production of ethylene, and optimal relative humidity inn the storage (American society of heating, 2010)	19
3.4.1 Concentration by volume of different single-phase aqueous solutions at var- ious freezing temperatures.	24
4.1.1 Weather characteristics by season.	39
5.3.1 Vegetable content.	48
5.3.2 Thermal Property Models for Food Components and Water ($-40 \leq t \leq$ $150^{\circ}C$).	49
5.3.3 Classification of Vegetables by Geometric Shape	50
5.3.4 Surface types and their characteristics.	52
5.5.1 Comparison of Available Components	58
5.6.1 Summary of the input data required by PVsyst.	63
5.6.2 Summary of the main simulation results in PVsyst.	63
5.6.3 Summary of default loss parameters from PVsyst (“PVsyst PVsyst 8”, n.d.).	64
6.1.1 Different scenarios for storage of crops.	67
6.2.1 Thermal conductivity, density, and specific heat for the relevant crops. . . .	68
6.2.2 Thickness of the different crops.	69
6.2.3 Time needed for each crop in minutes	69
6.2.4 Room measurements for east/west, south, and north facing walls. . . .	70
6.2.5 Hourly average temperature and transmission load data for April	71
6.2.6 Total heat removal and daily harvest product load required to cool vegeta- bles to the target temperature.	73
6.2.7 Values used in the infiltration load calculation	73
6.2.8 Maximum total daily load [kW] for the relevant crops.	74
6.3.1 Enthalpy and Pressure at Different Stages	76

6.3.2 Coefficient of performance (COP) and compressor work from CoolProp and Excel for lettuce cooling throughout a day in April.	77
6.4.1 Power consumption of various appliances	78
6.5.1 Electrical Parameters at Nominal Operating Cell Temperature (NOCT) for JAM72S30-565.	82
6.5.2 Electrical Parameters at for BYD LVS 8.0 kWh.	82
6.5.3 Summary of the specifications of the Charge Controller	83
6.5.4 Summary of the battery bank configuration	84
6.5.5 Summary of the PV system design	84
6.6.1 Summary of the geographical coordinates.	86
6.6.2 Summary of PVsyst simulation results	86
6.6.3 Monthly energy distribution from PVsyst simulation	87
6.7.1 Comparison of design parameters between intuitive and PVsyst approaches	89
6.7.2 Summary of final optimized design	91
7.6.1 Comparison of estimated compressor work from both Excel and Coolprop.	96

Nomenclature

$(^{\circ}C)$	Degree Celsius	
α	Solar elevation angle	[$^{\circ}$]
α	Thermal diffusivity	[$\frac{m^2}{s}$]
δ	Solar Declination Angle	[$^{\circ}$]
δ	Thickness	[m]
\dot{Q}	Heat flow rate	[W]
γ_s	Azimuth angle	[$^{\circ}$]
ϕ	Latitude angle	
ρ	Density	[$\frac{kg}{m^3}$]
θ	Cooling time	
θ_d	Chosen time interval	[h]
θ_p	Opening-closing time of the door	[s]
θ_z	Solar zenith angle	[$^{\circ}$]
	Overall heat transfer coefficient	[$\frac{W}{m^2 \cdot K}$]
Υ	Specific volume	[$\frac{m^3}{kg}$]
Bi	Biot number	

Cos	Cosine	
Cp	Specific heat capacity	$[\frac{kJ}{kg \cdot K}]$
D_f	Doorway flow factor	
D_t	Doorway open-time factor	
E	Effectiveness of doorway protection	$[m]$
f	Slope of temperature history curve	
F_m	Density factor	
g	Gravitational acceleration	$[9.81 \frac{m}{s^2}]$
h	Enthalpy	$[\frac{kJ}{kg}]$
h	Heat transfer coefficient	$[\frac{W}{m^2 \cdot K}]$
j	Intercept of temperature history curve	
J_0	Bessel function	
J_1	Bessel function	
k	Thermal conductivity	$[\frac{W}{m \cdot K}]$
L	Length from thermal center to surface	
q	Sensible and latent refrigeration load	$[kW]$
q_{evap}	Specific heat absorbed in the evaporator	$[\frac{kJ}{kg}]$
Sin	Sine	
T_i	Initial temperature of the produce	$[^\circ C]$
T_m	Temperature of the cooling medium	$[^\circ C]$
T_w	Wanted temperature for the produce	$[^\circ C]$
Y	Fractional unaccomplished temperature difference	

\dot{m} Mass flow rate [$\frac{kg}{s}$]

η Efficiency

P Pressure [bar]

Abbreviations

List of all abbreviations in alphabetic order:

AC Alternating Current	31
AHRI Air Conditioning, Heating, and Refrigeration Institute	19
BESS Battery Energy Storage Systems	iv
CFCs Chlorofluorocarbons	9
COP Coefficient of performance	xv
DC Direct Current	iv
DES Distributed Energy Systems	viii
DERs Distributed Energy Resources	35
DIN German Institute of Standardization	19
DHI Diffuse Horizontal Irradiation	29
DNI Direct Normal Irradiation	29

DoD Depth of Discharge	36
EWB Engineers Without Borders	iii
GEBA Global Energy Balance Archive Data	44
GHI Global Horizontal Irradiation	29
GWP Global warming potential	20
HCFCs Hydrochlorofluorocarbons	9
HFC-134a 1,1,1,2-Tetrafluoroethane	9
HFCs Hydrofluorocarbon	9
HOMER Hybrid Optimization Model for Electric Renewables	10
IUG Ingeniører Uten Grenser	v
LCOE Levelized Cost of Electricity	36
MmM Master med Mening	v
MPPT Maximum Power Point Tracking	34
MwM Master with Meaning	iii
NOCT Nominal Operating Cell Temperature	xv

NTNU Norwegian University of Science and Technology	iii
ODP Ozone depletion potential	9
PPM Parts per million	21
PPE Personal protective equipment	20
PV Photovoltaic	iv
R22 Chlorodifluoromethane	20
R134a 1,1,1,2-Tetrafluoroethane	21
R152a 1,1-Difluoroethane	21
R290 Propane	iii
R600a Isobutane	xii
R717 Ammonia	9
R744 Carbon dioxide	9
SDGs Sustainable Development Goals	3
SoC State of Charge	36
SoW State of Wear	88

SPCS Solar-Powered Cold Storage	iii
SPCSTs Solar-Powered Cold Storage Technologies	14
SPECSS Solar-Powered Evaporative Cooling Storage System	15
SSA Sub-Saharan Africa	6
YEC Youth Empowerment Center	2
WMO World Meteorological Organization	44

Chapter 1

Introduction

1.1 Background

World hunger and food loss

The World Health Organization states that in 2023, 1 in 11 people worldwide and 1 in 5 people in Africa faced hunger (W. H. Organization, 2024). The report warns that the world will not achieve the goal of zero hunger by 2030 if current trends continue, estimating about 582 million chronically undernourished people by 2030. This goes hand in hand with a growing global population, leading to a higher demand for food, creating significant challenges to ensure food security (Broom, 2020). One of the contributors to this problem is the substantial post-harvest loss of perishable foods (Aemu, 2023). 30 percent of the food produced globally is lost after harvest, often due to inadequate storage facilities and infrastructure (Amjad et al., 2023). In addition, traditional storage methods such as cold rooms and refrigerators are both energy-intensive and costly to operate, particularly in rural and isolated areas (Energypedia, n.d., Coalition, 2020). SPCS systems with BESS have recently become a promising alternative to these conventional methods (Hannes & Brits, 2020). These systems can help tackle food preservation and storage issues, especially in remote or off-grid locations, where they operate using renewable solar energy (Amjad et al., 2023).

Electricity access

In Africa, approximately 53% of the population lacks access to electricity (IEA, n.d.). The increase in renewable energy technologies presents an opportunity to address this problem while reducing the effects of poverty, unreliable electricity supply, and climate change. Africa is home to 40% of the total energy potential in the world (Abdelrazik et al., 2022). However, the widespread adoption of solar projects faces significant barriers,

such as financial constraints and logistical challenges (Ibegbulam et al., 2023).

TRAX Ghana

In the Bongo district of northern Ghana, communities face extreme poverty, high unemployment, and food insecurity, worsened by a dry climate and cultural practices such as early marriage and teenage pregnancies. TRAX Ghana, a non-profit organization, addresses these challenges through initiative solutions aimed at improving food security, education, and gender equality. Key projects include a greenhouse for vegetable production, a goat farm, and the establishment of the Youth Empowerment Center (YEC), which provides vocational and agricultural training to empower youth, particularly girls.

Despite these efforts, the lack of adequate storage facilities limits the full utilization of agricultural potential, resulting in significant food waste and financial loss. Addressing this gap through a sustainable solar-powered cold storage facility would align with the vision of TRAX Ghana for eco-friendly solutions that improve food preservation and economic opportunities in the region.

1.1.1 Engineers Without Borders (EWB)

EWB Norway was founded on 7 February 2011 and is a nonprofit organization dedicated to exploring engineering and technological solutions for projects in developing nations. Through partnerships with other aid organizations, EWB provides technical expertise to address local challenges. Their operations are guided by their vision: Technology and engineering competence for a sustainable and equitable world. EWB addresses specific challenges and offers custom-made solutions for each project. These solutions are managed by the local community and improves lives around the world.

Master with Meaning (MwM)

Master with Meaning is a program that gives master's-level students the opportunity to use their theoretical and practical expertise to contribute to positive development in low-and middle-income countries. As a Master with Meaning student, with the support of an EWB mentor, you get the opportunity to work on concrete issues in vulnerable and important areas globally.

1.2 Motivation

This master's thesis is motivated by a passion to contribute to sustainable development in one of the most vulnerable regions in Ghana. This area faces the challenges of extreme poverty, food insecurity, and a harsh climate compounded by cultural practices. TRAX

Program Support Ghana (TRAX Ghana) is a charitable organization dedicated to collaborating with rural communities in northern Ghana. Founded in 1989, the organization has worked with these communities for more than 26 years, driven by the philosophy of a demand-oriented social approach. In 2016, TRAX Program Support Norway (TRAX Norway) was formed and registered as a charitable organization in Norway with the purpose of conducting fundraising initiatives to help TRAX Ghana's efforts. Currently, TRAX Ghana is focusing on six project areas that they believe can help reduce poverty and increase food security in northern Ghana:

- Sustainable agriculture
- Youth and education
- Gender equality
- Environmental sustainability
- Alternative livelihoods
- Community capacity building

This project is designed to support the mission of TRAX Ghana by combining these focus areas, particularly improving agricultural sustainability and youth empowerment.

In addition, this project aligns with the Sustainable Development Goals (SDGs), specifically targeting several key areas. It focuses on Goal 1: No Poverty, Goal 2: Zero Hunger, Goal 8: Decent Work and Economic Growth, Goal 12: Responsible Consumption and Production, and Goal 13: Climate Action. By addressing these goals, the project aims to contribute to global progress and sustainability.

In particular, SDGs 12.3 states: "By 2030, reduce global food waste per capita at the retail and consumer levels and reduce food losses along production and supply chains, including post-harvest losses" (United Nations, n.d.). The success of this project could hopefully serve as a model for strengthening sustainable agriculture and renewable energy solutions in similar African contexts. It aligns with the visions of TRAX Ghana and supports the mission of EWB Norway, to develop technology for a sustainable and fair world.

1.3 Scope

The scope of this project work is to support the mission of TRAX Ghana by developing an initial design of a SPCS facility. The cold storage facility will be designed to operate entirely on natural refrigerants and solar energy, focusing on energy efficiency, sustainability, and reliability to meet the long-term needs of the farm.

The project begins with a detailed analysis of the required refrigeration capacity for the cold storage facility. Based on this, the optimal size of the solar PV system, including

battery storage for consistent power supply during the night and cloudy periods, will be determined. The integration of microgrid technology ensures sustainability and adaptability to the rural, off-grid environment of northern Ghana.

This initiative seeks to improve food security and create sustainable employment opportunities, especially for young women with limited educational and economic prospects due to early marriage and teenage pregnancy. By addressing post-harvest losses, the project will propose a reliable and eco-friendly storage solution.

Chapter 2

Literature review

Reducing post-harvest losses is a significant challenge in the agriculture sector, particularly in regions with limited access to reliable storage facilities. In developing countries, this problem is further worsened by the lack of infrastructure and energy resources, leading to substantial food waste and economic losses for farmers. SPCS systems present a promising solution to this problem by helping to preserve the quality and extend the shelf-life of perishable crops.

This section will explore patterns and gaps in existing literature on SPCS systems in similar contexts, focusing on their potential applications, benefits, and challenges in addressing post-harvest losses. In addition, barriers in employing these kinds of technologies will be examined.

2.1 Normal distribution of harvest

Since the 1970s, the question of whether crop yields are normally or non-normally distributed has been raised (Ramirez, 2001). Although the general idea was that the crop yield is not normally distributed, Hennessy (2009) argues that the validity of all previous findings could be questioned due to statistical testing problems and model specifications. Furthermore, Ramirez (2001) concludes that in the case of corn and soybean yields, the yields are skewed left, thus validating the non-normality of these crop yields. However, Just and Weninger (1999) points out that soil and climate variations cause the results to vary, causing disagreement around the topic. With this being said, Just and Weninger (1999) states that most academic papers on the subject lean towards a negative skewness for crop yields.

2.2 Post-harvest losses in Sub-Saharan Africa

In Sub-Saharan Africa (SSA) in 2011, approximately 8 % of all initial food production was lost or wasted during the post-harvest phase due to poor storage conditions, and approximately 50% of all initial production was lost or wasted (Bernstad et al. (2016), F. a. A. Organization (2011)). This goes hand in hand with the number of undernourished people, which increased from 172 to 264 million between 2010 and 2020 (agricultural organization, 2021). There are measures in SSA to combat food loss (Chege & Carson, 2017), but there is still substantial work to be done to decrease undernourishment in SSA (Makule & Dimoso, 2022). One way to combat the loss of initial food production is by implementing a functioning cold chain (Makule & Dimoso, 2022).

2.2.1 The cold chain

The objective of a cold chain is to preserve temperature-sensitive products, such as vegetables, from production to consumption in low-temperature environments (Bamakan & Manshadi, 2021). To be defined as a cold chain, a process must consist of one or more of the following phases: pre-cooling, bulk storage, distribution, retail cooling, and household refrigeration (Makule & Dimoso, 2022). However, typical for small-scale farmers in rural SSA is the lack of capital to implement a cold chain (Utz, 2011). The cold chain offers environmental protection through waste reduction that provides an efficient use of natural resources, accelerates economic growth, and increases income, which would greatly benefit small-scale farmers (Lange et al., 2016, Utz, 2011).

The paper by Makule and Dimoso, 2022 provides five general recommendations for strengthening the cold chain and cold storage for fresh fruits and vegetables:

- Improving cold chain management with good infrastructure throughout, including a stable source of energy that can come from an off-grid renewable energy source.
- Sufficient training of the cold chain staff to efficiently operate and maintain the cold storage and cold chain. This includes training small-scale farmers in their respective fields.
- Grading of fruit and vegetables to avoid unnecessary energy loss from cooling spoiled products. In cases of mold, rot, or other forms of spoilage that can spread, it is especially important to remove these.
- Fragmentation of the cold chain due to a large number of stakeholders and intermediaries should be avoided. That means reducing the number of people involved in the cold chain to improve efficiency and viability.
- Respecting the cold storage capacity and leaving enough space between storage crates is essential for proper circulation and efficient cooling of the products.

2.2.1.1 Precooling

To prolong and maintain the quality of food, it is necessary to cool the goods as quickly as possible, making pre-cooling shortly after harvest essential (Brosnan, 2001). For example, after harvesting vegetables and fruits, they continue to respire and transpire (Baldwin, 2003). However, the rate of respiration decreases along with temperatures above the freezing point, indicating the importance of a rapid temperature decrease (Singh & Meher, 2014). Furthermore, when they are still attached to the mother plant, the losses are replaced by water, energy, and minerals, but after harvest, these losses are not replaced, causing deterioration (Kader, 1980). There are several ways to pre-cool newly harvested crops, and the optimal solution depends on the nature of the product, the packaging requirements, and the flow of the product (Brosnan, 2001). Some crops, such as strawberries and broccoli, thrive at temperatures near the freezing point, while others are damaged by it (Edeogu et al., 1997). Some of the most common precooling techniques include air cooling, contact or package icing, hydrocooling, and vacuum cooling (Brosnan, 2001).

Air cooling is an established method that produces cold air from refrigeration equipment to remove heat from the product (of Agriculture, 1961). There are different varieties of air cooling, such as forced ventilation through circulation, i.e. a fan, which is cost-effective and requires simple equipment (Xiang & Zhang, 2023). However, there are some concerns about the potential extension of the cold chain, as this solution is variable and does not always handle large quantities of produce well (Fordham & Biggs, 2008). Another form of air cooling is differential pressure precooling, creating a pressure difference inside and outside the boxes (Yuan et al., 2020). Although this form of air cooling is energy-efficient, it requires complex equipment and therefore the cost is high (Xiang & Zhang, 2023).

Before modern advances in the field of pre-cooling, **ice cooling** was popular (Baladhiya & Doshi, 2016). One of the benefits of this precooling method is that ice not only removes heat instantly when applied but also continues to do so through absorption while melting (Brosnan, 2001). Ice cooling also helps prevent drying of the product, but can cause problems when the ice melts as it could create a warm, wet surface easily susceptible to the formation of diseases and soft rot (Thompson, 1998, Alegbeleye et al., 2022).

Hydrocooling first emerged in 1923, making it an established and popular pre-cooling method (F. Faubion & A. Kader, 1997). The concept of hydrocooling refers to immersion, flooding, or spraying of the product with cold water (Subedi et al., 2022). Brosnan, 2001 states that the products should tolerate surface wetness and not deteriorate, like leafy produce tends to do with exposure to excessive moisture.

Xiang and Zhang, 2023 states that **vacuum precooling** is a rapid form of precooling and consists of four parts: control system, drainage system, vacuum system, and refrigeration system. Furthermore, the paper talks about the basic principle of this method, which is to reduce the pressure within cold storage to vaporize water vapor and absorb environmental heat. This process, combined with the cooling power delivered to the vacuum chamber by the refrigeration system through a refrigerant, will absorb the water vapor (Xiang & Zhang, 2023). However, the product must be able to facilitate diffusion through a porous structure, such as lettuce (Zheng & Sun, 2004). In 1948, the first commercial vacuum cooling facility was built to reduce the field heat of lettuce (McDonald & Sun, 2000). Since then, vacuum cooling has been applied to other food industries, such as bakeries and fisheries (Sun & Wang, 2001).

2.2.1.2 Bulk storage

Bulk storage refers to the process in the cold chain after the initial precooling, where larger quantities of the product are stored under low-temperature conditions (Makule & Dimoso, 2022). Common methods for bulk storage systems are evaporative cooling systems, sorption systems and vapor compression systems, and the choice of the correct system will depend on factors such as temperature and relative humidity (Lange et al., 2016). Table 2.2.1 illustrates a brief comparison of the three methods.

Table 2.2.1: Comparison of bulk cooling methods (Lange et al., 2016).

Methods	Common systems (Design)	Temperature provided	Refrigerant
Evaporative coolers	Zero-Energy Cooling Chamber	$\geq 15^{\circ}\text{C}$	Water
	USDA-Portacooler		Not specified
	Charcoal cooler		Not specified
Sorption coolers	Cooler (Solar adsorption cooling) Solar Polar (Adsorption cooling)	4 °C to 8 °C Not specified	Distilled water Ammonia-water
Vapor compression coolers	Cold Storage Chamber Chest-type cooler Walk-in cold room	-10 °C to 10 °C 2 to 12 °C (refrigerator) or -20 to -10 °C (freezer) 2 °C and above	Not specified Halogenated (R134a) Natural refrigerant

2.3 Refrigerants

In the last 100 years, refrigeration has become one of the most important achievements along with space travel, computers, and the Internet (Constable & Sommerville, 2003). In 2020, around 20% of the total worldwide energy consumption came from air conditioning and refrigeration (McLinden & Huber, 2020). Refrigerants are an essential part

of refrigeration systems and are used in heat transfer from heat sinks or sources, often undergoing a phase change (Vuppaldadiyam et al., 2022). In 1930, natural refrigerants that had been used since the 1800s were replaced by synthetic refrigerants, mainly Chlorofluorocarbons (CFCs), due to their performance, safety, and durability (Abas et al., 2015). After a while, synthetic refrigerants were recognized as a cause of stratospheric ozone depletion (Stephen A. et al., 2018), which led to them being ruled out at the Montreal convention in 1987 (Abas et al., 2015). However, it should be noted that these refrigerants do not pollute if they are enclosed in secure refrigeration cycles, but leakage, poor maintenance, and unsafe disposal lead to the leakage of harmful environmental gases into the atmosphere (Maina & Huan, 2015).

In reality, it took time to implement the prohibition of synthetic refrigerants, and it was not before the Kyoto Protocol in 1997 that developed countries ruled out CFCs (Mahmood et al., 2020). The third generation of refrigerants was then introduced mainly consisting of Hydrochlorofluorocarbons (HCFCs) which reduced the damage done to stratospheric ozone (Vuppaldadiyam et al., 2022). Then came Hydrofluorocarbon (HFCs), which are replacing HCFCs (Mahmood et al., 2020). However, 1,1,1,2-Tetrafluoroethane (HFC-134a), a common variation of HFCs, has a zero Ozone depletion potential (ODP), but is a potential greenhouse gas (Sicard & Baker, 2020). This has led to a global focus on natural refrigerants such as Carbon dioxide (R744), R290, Ammonia (R717), R600a, and other less risky synthetic refrigerants (Dilshad et al., 2019).

2.4 Simulation and modeling tools

Precise modeling and simulation are essential for the development of microgrid technologies and refrigeration systems. This is especially crucial in contexts with significant uncertainty and stochastic behavior. This section covers tools used to model and design both off-grid energy systems and refrigeration systems, ensuring optimal performance and reliability.

2.4.1 CoolProp

This section is based on the theory of the paper by Bell et al., 2014, which evaluates the database of thermophysical properties *CoolProp*, unless otherwise stated. When designing and simulating refrigeration systems, numerous thermodynamic states and properties must be found. There are a number of thermophysical property libraries that exist, such as *REFPROP*, which is the most widely used. However, the only open-source and reliable library is *CoolProp*, which enables engineers and researchers worldwide to gain easy access to high-accuracy properties. In *CoolProp*, the implementation of thermodynamic properties is based on Helmholtz energy-explicit equations of state, further described in

Bell et al., 2014. One limitation of *CoolProp* is the poor handling of fluid mixtures.

2.4.2 Distributed Energy Systems (DES)

Designing and optimizing DES requires specialized software to ensure that energy demand is met under varying environmental and operational conditions. With diverse conditions and multiple factors to analyze, Jakica, 2018 identified and compared more than 200 solar design tools to characterize the abilities and limitations of PV performance modeling in general. Among numerous PV system modeling software tools, some of the most popular and established include Hybrid Optimization Model for Electric Renewables (HOMER), PV*SOL, and PVsyst (Freeman et al., 2014). The choice of software depends entirely on the user's specific needs. For example, HOMER is notable for its strong engineering aspect, while PV*SOL offers robust features for shading analysis and detailed loss calculations, and PVsyst provides comprehensive simulations of off-grid PV energy systems (Dirlik et al., 2024). Therefore, the focus of this study is on HOMER, PVSYST, and PV*SOL due to their global recognition and simulation performance accuracy.

PVsyst is a European-based PV energy system simulator developed by the University of Geneva for the European Energy Center and is widely used in academia. It receives meteorological data from Meteonorm and NASA-SSE, while also allowing the use of external databases (“PVsyst | PVsyst 8”, n.d.). It supports modeling with or without grid connection and includes advanced shading and 3D modeling capabilities (Lalwani et al., 2010).

PV*SOL, developed by Valentin Software, is designed to plan, design, and simulate PV systems from a few modules to solar parks (Dirlik et al., 2024). It sources meteorological data from Meteonorm and the German Meteorological Service, providing analyses for both electric vehicle integrations and grid-connected or off-grid systems, and specializes in shading, 3D modeling, and visual design Valentin Software, 2020.

HOMER, developed by the National Renewable Energy Laboratory (NREL), receives meteorological data from NASA-SSE (Dirlik et al., 2024). Although it lacks 3D modeling capabilities, it can perform calculations with or without grid connections and analyze various hybrid renewable energy systems Lambert et al., 2005.

Multiple studies, such as de Souza Silva et al., 2020 and Freeman et al., 2014, have been conducted to validate and compare the precision of these tools for freestanding PV solutions. These studies indicate that the tools achieve results close to real generation and annual errors within $\pm 8\%$ compared to quality-controlled measured performance data (Freeman et al., 2014). The studies also noticed optimism regarding HOMER, conservatism regarding PV*SOL and closer to the real values with PVsys.

In Table 2.4.1, you can observe a comparison between the possibilities and resources of each software relevant for the modeling of the off-grid PV system. This comparison is performed by de Souza Silva et al., 2020.

Table 2.4.1: Comparison of software relevant for the modeling of the off-grid PV system (de Souza Silva et al., 2020).

Object	Description	HOMER	PV*SOL	PVSYST
System Simulations	Stand-alone (Off-grid)	✓	✓	✓
	Grid-Tie PV systems (On-grid)	✓	✓	✓
	Pump systems		✓	✓
	Hybrid systems PV and Battery	✓	✓	
	Others Hybrid systems	✓		
	PV System for Electric Vehicles		✓	
Site Parameters	Analysis of the terrain data			
	Weather database	✓	✓	✓
	Temperature Settings of the Site	✓	✓	✓
Building Physics	Building 3D modeling		✓	✓
	Image capturing/Geo maps		✓	
	Import maps image		✓	✓
	Shading analysis		✓	✓
Building Energy Performance	Monthly	✓	✓	✓
	Hourly	✓	✓	✓
Mounting Forms System	Ground	✓	✓	✓
	Roof	✓	✓	✓
	Roof integrated	✓	✓	✓
	Facade integrated			✓
	Solar Tracker	✓	✓	✓
Financial	Payback prediction	✓	✓	✓
	Direct Finance	✓	✓	✓
	Loan/Lease/Mortgage	✓	✓	✓
Emissions avoided	CO ₂	✓	✓	✓

2.5 PV systems in remote areas

One of the key barriers to the application of PV systems in remote areas is the local climate and geographical conditions (Amoah, 2022). In northern Ghana, these factors determine the amount of solar radiation, the temperature, humidity, the efficiency of energy conversion, and the overall reliability of the system. Understanding these impacts is crucial for optimizing the design and deployment of PV systems in this region. Several case studies highlight the impact of local climate and geographic conditions on PV performance in similar contexts. Studies in Nigeria, Burkina Faso, and Mali, countries that share similar climatic conditions with northern Ghana, demonstrated that seasonal variations in wind, humidity, and dust accumulation significantly affect PV efficiency (Bello et al.,

2022, Diarra and Akuffo, 2002).

2.5.1 Solar irradiance

Solar irradiance is the primary factor that affects the performance of PVs. Northern Ghana benefits from high solar irradiance levels, receiving an average solar radiation of about 5-6 kWh/m^2 per day (Asumadu Sarkodie & Owusu, 2016). However, seasonal variations in atmospheric conditions, such as the Harmattan winds, can affect solar irradiance. For example, a study of eight different cities in Ghana shows a trend in the decrease in solar irradiance between April and September, highlighting the need for storage solutions to fully harness and utilize these solar resources for all seasons (Asumadu Sarkodie & Owusu, 2016).

Harmattan, a dry and dusty monsoon wind, which usually occurs between November and March, can cause dust accumulation on PV modules (Bello et al., 2022). This can reduce the amount of solar energy absorbed. A study in Walewale, northern Ghana, investigated the effect of settling harmattan dust on PV modules. They recorded an efficiency reduction of up to 5-6%, depending on the tilt angle (Owusu - Brown, 2016). Similar effects of dust accumulation on PV energy have also been found in other parts of the world; for example, a reduction of 32% was found in Saudi Arabia (Mani & Pillai, 2010).

The literature consistently shows that regular maintenance, including cleaning schedules and optimization strategies such as tilt angle adjustments, is crucial for maintaining PV system efficiency, especially in dusty environments. Studies in Senegal, Mali, and Nigeria emphasize the importance of these measures in minimizing efficiency losses due to soiling. Without regular intervention, significant efficiency losses can occur, as evidenced by the reductions in efficiency 18% and 78% in PV modules reported in Senegal (Ndiaye et al., 2013). Furthermore, research conducted in Mali suggests that regular cleaning can recover up to 7% of the daily capacity, strengthening the effectiveness of scheduled maintenance (Younis & Onsa, 2022). Anti-soiling coatings and advanced cleaning systems offer additional benefits in sustaining performance, given the ineffectiveness of natural cleaning methods during dry seasons, as pointed out in the Nigerian study (Chanchangi et al., 2020).

In particular, most studies on dust-related effects have been conducted in regions such as Africa and the Middle East, where seasonal dust storms and/or generally low rainfall levels dominate. These findings confirm that dust accumulation reduces PV performance; however, studies limited to specific seasons, such as the 5-month study in Kathmandu, do not capture the full seasonal cycle (Paudyal & Shakya, 2016). This highlights the need for comprehensive research throughout the year to better understand the impact of dust

on PV performance across all seasons.

2.5.2 Wind speed

Wind speed in northern Ghana can have both a negative and a beneficial effect on PV systems Chanchangi et al., 2020. Both Said et al., 2018 and Goossens and Van Kerschaever, 1999 state that dust accumulation increases with an increase in wind speed, supporting the recommendation of regular cleaning of the PV module to avoid performance degradation. However, moderate wind speeds can help cool PV modules, improving their efficiency by reducing operating temperatures. The cooling effect is more pronounced when the front surface of the PV module faces the windward side (Mehdi et al., 2023). However, in northern Ghana, this scenario is unlikely during the Harmattan season, as the trade winds come from the north (Bello et al., 2022). However, high wind speeds, especially during the Harmattan season, can pose structural risks and require robust mounting solutions (Owusu - Brown, 2016).

2.5.3 Ambient temperature

Ambient temperature is another critical factor in the efficiency of the PV system. Northern Ghana experiences high temperatures, often exceeding 35°C during the dry season (Fage & Maier, 2024). For every 1°C increase in module temperature, the PV efficiency drops by approximately 0.5% due to increased resistance and reduced voltage output (Kumari et al., 2023). Studies suggest that cooling methods such as air and water-based systems reduce PV temperatures, which combined with the selection of PV technologies with better temperature coefficients can significantly increase overall output (Harmailil et al., 2024). Some proposed methods for hot climates include passive methods, such as phase change materials and active systems that have been shown to extend the life and efficiency of the PV module by stabilizing temperature fluctuations (Ahmed et al., 2024). Although cooling methods have been shown to help reduce the effect of temperature on PV efficiency, the costs associated with the implementation of technologies make the economic argument unfeasible (Amoah, n.d.).

In addition to temperature, the single rainy season in the region, from May to September, introduces benefits and challenges. Although rain can help naturally clean PV modules by washing away accumulated dust, exposure to moisture can increase the risk of corrosion and require additional waterproofing measures. A case study in Kathmandu stated that relative humidity, while generally less impactful on PV efficiency than other factors, contributes to the adhesion of dust over time, especially during dry conditions when airborne particles settle on the surface of the modules (Paudyal & Shakya, 2016). In a study conducted in Doha, a correlation was observed between relative humidity and a

decrease in PV power output in different PV technologies (Touati et al., 2013). Higher humidity levels introduce a variety of water vapor particles into the atmosphere, which interact with incoming solar radiation, leading to reduced levels of irradiance, especially for tropical countries such as Malaysia (Mekhilef et al., 2012). This emphasizes the impact of humidity when designing PV systems prone to high atmospheric moisture during, for example, rainy seasons.

2.5.4 Geographical characteristics

Geographical characteristics also play a role. The latitude of northern Ghana provides a favorable solar angle, although seasonally adjusting tilt angles can maximize year-round energy capture. A study from China on seasonal tilt optimization in similar latitudes found that seasonal adjustments can increase PV energy by up to 15% compared to fixed tilt installations (Liu et al., 2022). In addition, the relatively flat terrain of the region reduces shading and improves module exposure. A study conducted in Ethiopia also showed that a seasonal optimal tilt angle could increase efficiency by maximizing exposure to sunlight rather than a fixed (annual) optimal tilt angle, especially in regions with defined dry and wet seasons (Ashetehe et al., 2022).

Studies from Kenya and Uganda highlight that equatorial regions benefit from higher and more consistent irradiance than areas further north or south, which makes them ideal for PV deployment but requires careful planning for tilt adjustments to capture peak sunlight (Eddie Sembatya et al., 2022). Ghana's closeness to the equator results in relatively stable solar irradiance throughout the year, with minimal seasonal variation in daylight hours.

2.6 Barriers: Solar-Powered Cold Storage

When it comes to the implementation of Solar-Powered Cold Storage Technologies (SPCSTs) in rural areas, there are several obstacles. In Tanzania, for example, the adoption of these technologies is limited due to factors such as limited awareness, high investment costs, low pay capacity among farmers, and consumer preference for non-refrigerated foods (Rutta, 2022). Similarly, on Mangur Island, the lack of access to electricity has led to the use of SPCS systems as a solution to help fishermen preserve fish catches. The high initial investment in the solar PV system is a significant barrier, despite the potential of the system to pay back in about 6 years and 4 months (Wantira et al., 2023). In northeast Nigeria, a study highlights challenges such as high importation costs for solar modules and components, along with bottlenecks at border crossings. Furthermore, it underscores the current lack of understanding in this field (Hiroyuki et al., 2021).

The literature suggests several solutions to overcome barriers to cold storage technologies.

Rutta, 2022 highlights several options to address these issues. The enforcement of policies that attract investment and improve affordability through flexible payment options is essential. Furthermore, this study also focuses on addressing sociocultural barriers that originate from strong cultural preferences along with increasing public awareness of the environmental and financial benefits. This is also highlighted in (Yadav et al., 2020), where increasing awareness and knowledge of products in communities can be successful in promoting the acceptance of PV technology in the rural market.

Research shows that SPCSTs in horticulture markets increased sales and revenues, reducing food loss and extending product shelf life (Hiroyuki et al., 2021). A study in rural Nigeria found that a Solar-Powered Evaporative Cooling Storage System (SPECSS) significantly extended the shelf life of fruits and vegetables compared to traditional storage (Olosunde et al., 2016). These findings indicate that technological innovation is key to overcoming the challenges in the adoption of SPCSTs.

PV systems operate automatically, starting and stopping without human involvement. However, regular maintenance is essential. The literature highlights the need for scheduled cleaning, diagnostics, and repairs that require qualified technicians. As noted in Chaurey and Kandpal, 2010 and Diarra and Akuffo, 2002, rural areas often lack the technical expertise and infrastructure needed for the maintenance and repair of PV systems, and training local operators or establishing maintenance programs is critical, but can be challenging due to cost constraints and the lack of qualified personnel.

Chapter 3

Theoretical background

This and the next chapter provide the theoretical foundation for the project work, including a detailed review of the literature on the key concepts and technologies relevant to the project. By combining insights from various fields, this chapter aims to establish a solid theoretical basis for the initial design of the SPCS facility.

3.1 Ghana



Figure 3.1.1: Map of Ghana.

Source: (“Ghana”, 2024)

3.1.1 Energy access

Since the 1990s, Ghana has made significant steps in expanding energy access in recent decades. In 2018, the electrification rate was approximately 84% (“Africa Energy Out-

look 2019”, 2019), and efforts are underway to achieve universal access. This progress is largely due to the implementation of the National Electrification Scheme (NES), along with initiatives such as mini-grids and decentralized energy systems to address the needs of off-grid communities (“National Electrification Scheme”, n.d.). Despite this progress, challenges remain, including ensuring a reliable energy supply and reducing dependence on fossil fuels, which still dominate the energy mix (Kipkoech et al., 2024).

Ghana has significant renewable energy resources, such as hydropower, solar, wind, and bioenergy (Takase et al., 2022). These resources play an important role in transitioning to low-carbon development and are backed by policies that encourage renewable energy investments. However, several obstacles have hindered the expansion of the sustainable energy sector, including limited technological expertise, inadequate experience in the development of sustainable energy, as well as sociocultural and human barriers (Kipkoech et al., 2024).

3.1.2 Climate

Ghana is classified into five distinct agroecological zones, each defined by unique climates, vegetation, and agricultural capacities. The climate is primarily tropical, characterized by two main seasons: a dry season and a rainy season. Located in the northernmost agroecological zone, the Upper East region is within the Sudan Savannah zone. This region receives an average annual rainfall ranging from 750 to 1050 mm during May through October, followed by an extended dry period that extends from November to April (Antwi-Agyei et al., 2021). These areas experience a hotter and drier climate compared to the South. The southern part of the country experiences a double-peaked rainfall season, with a major rain season between April and July and a minor rain season between September and November (The World Bank Group, n.d.). Harmattan winds during the dry season can bring cooler mornings, but also lead to dusty conditions, potentially affecting agricultural activities and solar energy production due to reduced sunlight irradiance (Owusu - Brown, 2016).

3.2 Storage of vegetables

After harvest, the quality of the vegetables can only be preserved. Therefore, the temperature and humidity at which they are stored must be correctly specified, as vegetables are easily perishable (Iderawumi, 2021).

For the greenhouse at the farm, the **relevant vegetables** are:

- Tomatoes
- Bell pepper

- Hot pepper
- Lettuce
- Cabbage
- Cucumber

Storage temperature:

One of the most important factors that influence vegetable quality is the storage temperature, where the decay speed increases 2 to 3 times per 10 °C (Iderawumi, 2021). The ideal storage temperature will vary depending on the vegetable, but common for all at the TRAX farm is that they do not freeze well. When cucumbers are stored below 7°C, they develop pitting, water-soaked spots and begin to decay. Peppers stored below 7°C start to rot, while mature green tomatoes begin to decay and soften (Iderawumi, 2021). For lettuce and cabbage, they can be stored at temperatures as low as 1 degree. However, when frozen, they undergo irreversible damage that causes them to appear watery and yellow or dark brown (Liu et al. (2024), R. Wang et al. (2019)). The optimal storage temperature for all relevant vegetables is listed in table 3.2.1.

Relative humidity:

Furthermore, the relative humidity in a storage unit greatly influences the quality of vegetables. Relative humidity is the relationship between the amount of water vapor in the air and how much water vapor air can actually hold at that temperature, given in percentage (“Relative humidity”, n.d.). If the relative humidity is lower than the water activity on the surface of the vegetable, it will lose moisture, reducing the quality and total mass, resulting in a lower price on the market. However, if the relative humidity is equal or higher than the water content, the vegetable will decrease the rate of deterioration (Tapia-Hernandez & Katouzian, 2017).

The optimal relative humidity in storage for the different vegetables is listed in Table 3.2.1. To keep the relative humidity of the cold storage high, the temperature difference between a heat exchanger / evaporator and the cold storage should not exceed 5°C (FrigoSys, n.d.). To achieve this, the surface area of the evaporator/heat exchanger should be quite large, as this allows more efficient heat transfer (Apollo.learn, n.d.).

Mold and fungal growth:

Dagnas and Membre (2013) discuss the effect of water activity and temperature on mold and fungal growth, as well as methods to address this problem. The book states that due to the high water activity, there is a risk of growth if the vegetables are contaminated. Temperature is also a determining factor in mold and fungal growth, as some grow at temperatures as low as 0°C. Methods for preventing mold and fungal growth are discussed

in the book. One of the main methods is proper packaging, as most types of mold require oxygen to grow. Other ways to tackle this issue are to use preservatives such as benzoic acid, lactic acid bacteria, which has an inhibitory effect on mold, and by using heat treatment.

Ethylene production and sensitivity:

Some crops release a gas called ethylene, which causes certain vegetables to ripen faster (for Community Health, n.d.). This must be taken into account when storing multiple vegetables together, as this could severely decrease the quality of ethylene-sensitive vegetables. Wageningen (n.d.) discuss some ways to solve this problem:

- Store them separately.
- Cooling the crops, as a lower temperature can reduce ethylene production and sensitivity.
- Reduce oxygen and increase carbon dioxide levels, as this contributes to lower ethylene production and sensitivity.
- Ethylene removers or converters, also called scrubbers, can remove ethylene from the air.

Table 3.2.1 summarizes the optimal storage conditions for the relevant vegetables presented in 3.2. This will be a major factor when designing the cold storage facility.

Crop	Storage temperature [°C]	Ethylene production	Ethylene sensitivity	Relative humidity [%]
Tomatoes	13	High	Low	85 to 95
Bell peppers	10	Low	Low	85 to 95
Hot peppers	10	Low	Moderate	85 to 95
Lettuce	1	Very Low	High	95 to 98
Cabbage	1	Low	High	95 to 98
Cucumber	10	Low	High	85 to 95

Table 3.2.1: Ideal storage temperature, vegetable sensitivity and production of ethylene, and optimal relative humidity inn the storage (American society of heating, 2010)

3.3 Relevant refrigerants

A report from the Environmental Protection Agency, Gloel (2022), discusses the availability of natural refrigerants in Ghana. They state that R290, R600a, and R717 are available according to the recommended standards of the Air Conditioning, Heating, and Refrigeration Institute (AHRI) and the German Institute of Standardization (DIN).

R290:

R290 has zero ODP, as well as a very low Global warming potential (GWP) of 20, and in comparison Chlorodifluoromethane (R22), a variation of a HCFC refrigerant, has a GWP of 1700 as discussed by Choudhari and Sapali (2018). Furthermore, the paper talks about the beneficial thermodynamic properties of R290, the low cost, and its compatibility with most materials in a refrigeration system. The only downside presented is the high flammability, which has caused R290 to be neglected as a refrigerant due to safety concerns. However, storing R290 cylinders in a well ventilated, secure area free from sparks, in conjunction with the use of a leak detection system and a fire suppression system, substantially minimizes the risk of injury (“Safety Data Sheet R290”, 2021). Furthermore, R290 is not harmful to vegetables, but high concentrations of R290 could decrease the amount of oxygen in the air, causing symptoms of suffocation (“Hazardous Substance Fact Sheet”, 2015). Therefore, Personal protective equipment (PPE) should be worn when servicing or handling R290.

R600a:

R600a was compared with R290 and some harmful refrigerants in a study by Soni et al. (2023). They showed that similar to R290, it has zero ODP and a very low GWP of 4, making it a great environmental substitution for harmful refrigerants. The study also compared the refrigerating effect for a temperature range of -30°C to 10°C as shown in Figure 3.3.1.

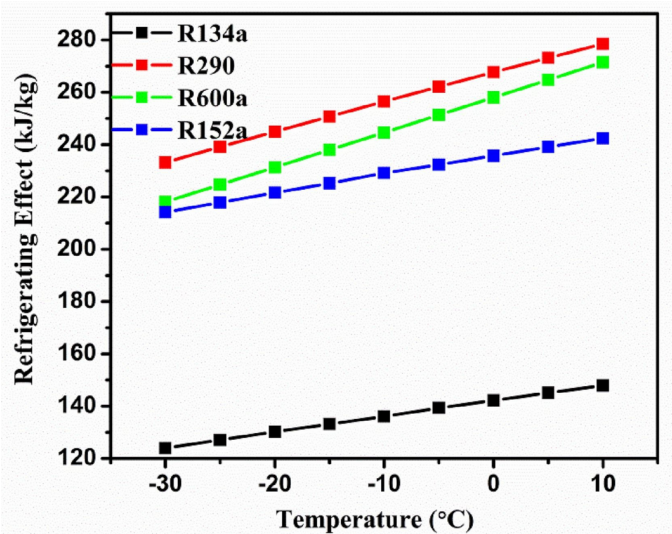


Figure 3.3.1: Refrigerating effect comparison between R600a, R290, R134a (Tetrafluoroethane) and R152a (Difluoroethane) from -30 °C to 10 °C.

Source: (Soni et al., 2023).

In the figure, it can be observed that the natural refrigerants R600a and R290 have a

higher refrigerating effect than 1,1-Difluoroethane (R152a) and 1,1,1,2-Tetrafluoroethane (R134a), which are common refrigerants in developing countries, according to the study. Furthermore, similarly to R290, R600a is highly flammable, which means that the same safety precautions are necessary (Danfoss, 2000). In addition, R600a should not be in contact with the eyes, skin, or be inhaled or digested, as it can cause acute or delayed injury (A-GAS, 2018), making PPE necessary.

R717:

Unless otherwise stated, this section will be based on the theory from the book (Pearson, 2008). R290 is a well-known and widely used refrigerant for industrial refrigeration systems, including food processing and cold storage. One of the reasons for the established use of R717 is its excellent thermodynamic properties, leading to a generally higher COP than other refrigerants. Furthermore, R717 have no effect on ODP or GWP. However, copper cannot be used with R717, one of the main components of heat exchangers, as it can form a brittle copper-ammonia complex (Meier, n.d.). Aluminum is used as a substitute in R717 heat exchangers, which achieves a similar heat transfer performance. Another characteristic of R717 is its strong and pungent smell, which can be traced at a concentration of 5 Parts per million (PPM). When handling R717, it is important to be aware of the consequences of higher concentrations. From concentrations of 150 to 200 PPM, the eyes become irritated, but without long-term damage. At 1000 PPM, one can no longer breathe, and at 1500 PPM or more, the retinas are destroyed or severely damaged. At 5000 PPM, all life is destroyed in 30 minutes. Therefore, PPE should be used and the room should be left immediately if the ammonia smell is strong.

3.4 Refrigeration systems

This section is based on the books Melinder (2015), American society of heating (2010), and Pearson (2008) unless otherwise noted. Most refrigeration systems are divided into **direct** and **indirect** systems.

Direct refrigeration system:

The direct system uses the refrigerant to directly transport heat from the refrigeration room to the heat discharge space. Figure 3.4.1 illustrates the direct system.

The standard direct refrigeration system consists of an evaporator, a compressor, a condenser, and an expansion valve. The evaporator vaporizes the incoming refrigerant fluid when it absorbs heat. A compressor pumps the vapor produced in the evaporator and compresses the refrigerant to a higher pressure and temperature. The gas will then flow through the condenser, where it rejects heat to a coolant, like air. After the condenser,

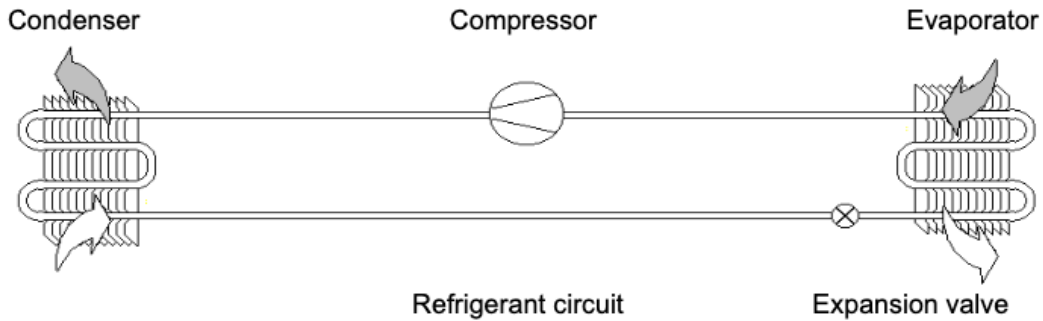


Figure 3.4.1: Direct refrigeration system.

Source: (Melinder, 2015).

the condensed refrigerant passes through an expansion valve, further reducing its pressure and temperature. The liquid is then returned to the evaporator again.

Indirect refrigeration system:

Indirect systems, on the other hand, are divided into two circuits. The primary refrigerant circuit is often a traditional direct expansion loop with one or two circuits with a secondary refrigerant.

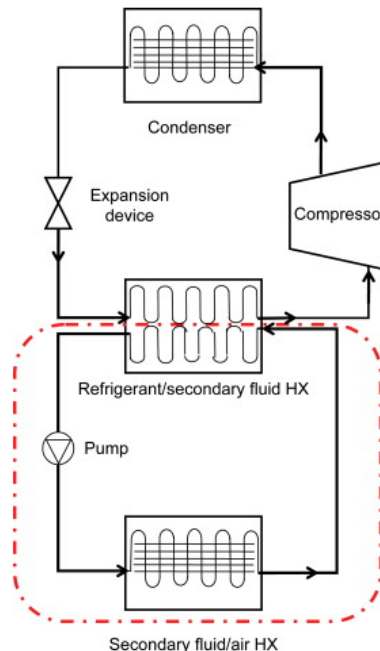


Figure 3.4.2: Indirect refrigeration system with one secondary refrigerant circuit.

Source: (K. Wang et al., 2010).

Figure 3.4.2 illustrates a version of an indirect system. The main refrigeration loop consists of a compressor, an evaporator or heat exchanger, an expansion valve, and a condenser. In the primary loop, the condenser releases heat to the environment. The fluid pump in

the secondary refrigeration loop circulates the secondary refrigerant through the cooling unit, transferring heat from the refrigeration room to the circuit, before passing through the evaporator, releasing heat to the primary circuit. Indirect systems are used in air conditioning, heat pumps, commercial or supermarket refrigeration, ice rinks, and dairy. Indirect systems have often been used for applications where there are multiple places to be cooled, especially if they have different requirements for temperature and humidity.

Although the basic principles are similar for direct and indirect systems, the indirect system has some additional components. The pump in the secondary refrigerant system is a central part of the circuit. As indirect systems become more common, circulation pumps are being increasingly used in refrigeration. They must be properly dimensioned with respect to the density and viscosity of the refrigerant, to avoid unnecessary energy consumption. To dimension the circulation pumps, one must first calculate the flow and pressure drop in the system. The pump will also vary depending on the secondary refrigerant chosen, due to the thermodynamic properties of the fluid. In addition, the indirect system has a heat exchanger or an evaporator located inside the desired refrigeration space.

Furthermore, there are several advantages of an indirect system instead of a direct system. The first benefit is that the primary refrigeration circuit can be built more compactly and installed in a secondary room. The primary refrigerant charge will also be lower, as the refrigerant pipe network is only required in the machine room. The maintenance of the system can also happen mostly inside the machine room, resulting in less traffic in and out of the refrigerated space. However, a disadvantage of the indirect refrigeration system is the increased energy demand due to the lower evaporation temperature of the refrigeration system and the addition of a fluid pump. This can be minimized if the secondary refrigerant is an evaporating and condensing fluid (Haukås, 2016).

3.4.1 Secondary loop refrigerants

This subsection will be based on information from K. Wang et al. (2010), unless otherwise stated. Secondary refrigerants can be divided into two groups; the single phase fluids and the two phase fluids.

Single-phase fluids:

Single-phase fluids are often variations of an antifreeze fluid, such as water solutions of ethylene or propylene glycol, or sodium chloride commonly known as table salt, which have been used as secondary fluids for a long time. When considering single-phase fluids, the freezing point is the most important factor. Typically, the freezing point of these fluids is set to be 5 to 10°C below the operating temperature of the system. The thermophysical

properties of some single-phase fluids are listed in Table 3.4.1, showing the concentration by volume and freezing temperature.

Freezing temperature	-15°C (5°F)	-30°C (-22°F)	-40°C (-40°F)
Aqueous solution	Concentration by volume (vol.%)		
Ethylene glycol/water	30.5	45.4	52.8
Propylene glycol/water	33.0	48.0	54.0
Ethyl alcohol/water	24.5	40.9	53.1
Methyl alcohol/water	20.0	33.6	41.0
Glycerol/water	39.5	56.0	63.0
Sodium chloride/water	18.8	-	-

Table 3.4.1: Concentration by volume of different single-phase aqueous solutions at various freezing temperatures.

Source: (K. Wang et al., 2010).

Two-phase fluids take advantage of latent heat released or absorbed during phase change. The two-phase fluids are often ice slurry or R744. The ice slurry consists of ice particles and an aqueous solution. The ice slurry can be transported best if the ice particles are small and have a cooling capacity of four to six times higher than normal chilling water.

However, R744 have gain more traction as a secondary refrigerant recently, due to its benefits as a two-phase fluid. Advantages of using R744 is smaller pipe size, lower pumping power, low cost, beneficial heat transfer properties, and good compatibility with materials. However, the availability of components and the relatively low critical temperature are disadvantages.

3.4.2 Bypass valve

This section is based on information from the book Zijdemans (2014), unless otherwise stated. If the secondary loop circulates an aqueous fluid, a bypass valve can be used to regulate flow through a thermal actuator, thus controlling the temperature of the evaporator / heat exchanger (Qviller, n.d.). The bypass valve has three streams connected, and there can be two types of bypass valve, a mixing valve and a distribution valve. The mixing valve has two inlet streams and the purpose is to mix the streams of different temperatures to achieve the desired output temperature. The distribution valve, on the other hand, receives one stream, which is distributed to the other two streams, depending on the desired outlet flow or temperature. For example, if a refrigerated room has reached the desired temperature, the distribution valve can bypass the heat exchanger / evaporator. If the temperature in the refrigerated room is above the freezing point, the distribution valve can also be a method of defrosting the evaporator. When the distri-

bution valve bypasses the evaporator, the temperature inside the refrigerated room rises, thus defrosting the evaporator.

3.5 Structural cold storage design

This section is based on information from the books by Granyd et al. (1999) and American society of heating (2010), unless otherwise stated. Correctly designing a cold storage is crucial to prevent unnecessarily large transmission loads and problems with water vapor diffusion. Figure 3.5.1, Figure 3.5.2 and Figure 3.5.3 shows a conventional wall, ceiling, and floor design, respectively.

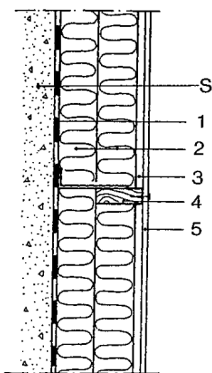


Figure 3.5.1: Conventional wall design.

Source: Granyd et al., 1999

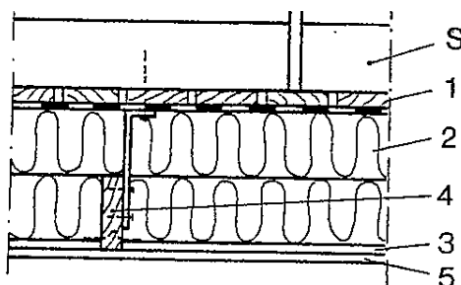


Figure 3.5.2: Conventional ceiling design with insulation on the inside of the structural support.

Source: Granyd et al., 1999

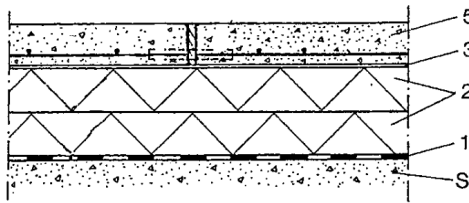


Figure 3.5.3: Conventional floor design.

Source: Granyd et al., 1999

For all three figures, the symbols are equal and listed below.

- S. Structural support (e.g., brick, wood, or concrete).
- 1. Water vapor diffusion barrier (especially important for cold storage).
- 2. Insulation.
- 3. Air ventilation (or channels for the floor).
- 4. Insulation anchoring.
- 5. Inside cover (e.g. plastic or metal sheet, concrete for floor).

Insulation:

Insulation as a thermal barrier in a cold storage is crucial for any room with a temperature different from the outside to avoid unwanted temperature increase or decrease. This will apply to walls, the roof, and the floor. Insulation is designed to prevent heat transfer through both convection and radiation. To prevent heat transfer through convection, it is often designed to hold a gas, such as air or a gas with lower thermal conductivity, stagnant. The insulation material is usually cellular, foam, or fibrous. If the chosen material is fibrous, it does not contain the necessary structural strength and must be attached to the wall, as shown in Figure 3.5.2 and Figure 3.5.1. The thermal conductivity of insulation must be low in order to prevent high heat transfer, and some common insulating materials are presented in Figure 3.5.4, where polyurethane and polystyrene have the lowest thermal conductivity in the density range between 0 and $96 \frac{kg}{m^3}$.

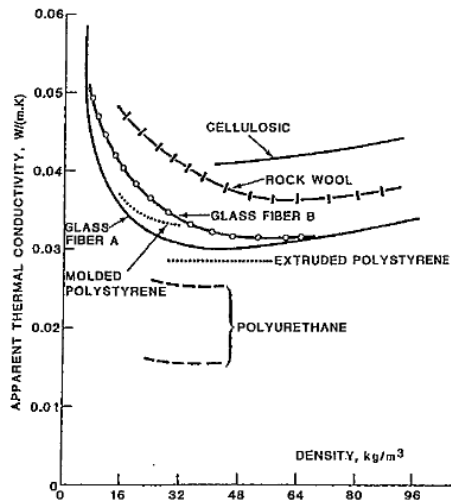


Figure 3.5.4: Apparent thermal conductivity versus density for some common insulation materials.

Source: (Granyd et al., 1999)

Vapor barrier:

Through a wall, there will be a mass transfer of water vapor through diffusion. Therefore, a vapor barrier is needed to prevent condensation in the insulating material, as this increases the thermal conductivity and can result in mold growth (Unal, 2019). To avoid condensation, the vapor barrier should be placed on the warm side of the wall. For cold storage, this means between the outer wall and the insulation. Condensation will occur if the partial pressure of water vapor in the wall at any point exceeds the saturation pressure. Figure 3.5.5 shows a temperature profile, a water vapor pressure profile, and a saturation profile (dotted line) through a typical wall. There is a slight temperature drop through the outer layer and a large linear temperature drop through the insulation. In addition, there will be no condensation in this particular example as the partial pressure of water vapor is lower than the saturated pressure throughout the entire wall.

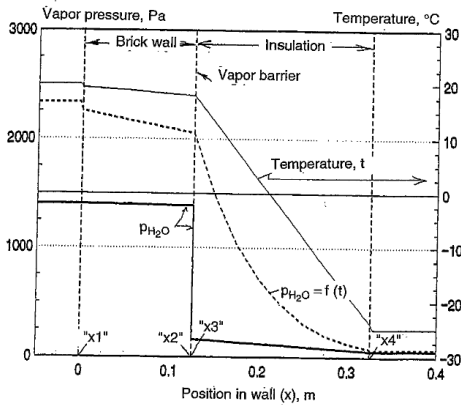


Figure 3.5.5: Temperature profile through a typical wall.

Source: (Granyd et al., 1999)

Air and vapor leakage at junctions:

When building a cold storage, Air and vapor leakage at junctions can be an issue. The structural elements can contract when the temperature is lowered, causing the wall to be pulled from the roof. Therefore, there must be a proper vapor/air seal. For this, an air/vapor flashing sheet, which is a transition from the vapor barriers on the ceiling, floor, and walls. The flashing sheet must be air and vapor-tight, flexible, and durable and should be designed to:

- Withstand movements in the building due to temperature changes.
- Have minimal penetration that might cause leaks.
- Have a proper lapping between the vapor barriers in the ceiling, floor, and walls.

Additional considerations for cold storage design should also take into account electrical wiring and cold storage doors. Electrical wiring should penetrate the refrigeration room in as few places as possible to ensure that the integrity of the vapor barrier is kept intact. The cold storage doors should be strong but light enough for quick and easy opening/closing.

3.6 Solar energy

Solar energy is a significant renewable energy source and is considered radiant light and heat from the Sun. Yearly, the Earth intercepts solar energy more than 10,000 times the global energy consumption (Nations, n.d.). Available worldwide, solar energy is expected to significantly contribute to future energy mixes. The highest solar potential areas lie around the equator, particularly in Africa, Australia, South America, South Europe, and Asia (Gürel et al., 2023). The solar energy received per square meter ranges from 700 to more than 2200 kWh annually, decreasing with distance from the equator (Hofstad,

2024). Technologies such as PV cells, which effectively convert sunlight into electricity, have reduced costs by more than 90% in the last ten years and could contribute to 27% of the global energy supply by 2050 (Ritchie (2024), Hofstad (2024)).

The power output of solar PV systems is significantly influenced by solar irradiance, which refers to the solar power received per unit of area and is measured in watts per square meter (W/m^2) (Ben, n.d.). For PV systems, the primary measure of irradiance is the Global Horizontal Irradiation (GHI), which is the total solar radiation received on a horizontal surface. It includes both direct sunlight (Direct Normal Irradiation (DNI)) and diffuse sunlight (Diffuse Horizontal Irradiation (DHI)) scattered by the atmosphere. The amount of solar radiation that a specific location receives depends on several factors, including geographical location, time of day, season, elevation of the land, and local weather conditions. Because the Earth's surface is curved, sunlight reaches it at various angles throughout the day and year, creating fluctuations in energy levels. In this context, the concept of *peak sun hour* becomes crucial, serving as an effective measure of solar irradiance. It represents an hour when the intensity of sunlight averages 1,000 watts per square meter (Castañer et al., 2012).

3.6.1 Solar geometry and angles

The potential for solar energy is influenced by the position of the sun relative to Earth, which is determined by various Earth angles that affect the intensity and duration of sunlight (Martinez-Gracia et al., 2019). Understanding these angles is essential for optimizing solar systems.

An important angle, *solar declination angle* (δ), is between the sunbeams and the equatorial plane, varying annually due to Earth's axial tilt of 23.5° . This causes seasonal changes in day length and sunlight intensity, peaking at solstices. The *solar elevation angle* (α), observable in Figure 3.6.1 as the distance between the horizon and the position of the Sun, peaking at solar noon and affecting the intensity of sunlight. The *solar zenith angle* (θ_z) is the angle between the sunbeams and a line perpendicular to the surface, visible in Figure 3.6.1. A zenith angle near zero indicates direct sunlight, optimal for solar energy.

The *hour angle* (H) measures the time from solar noon, useful for tracking sunlight throughout the day, with the rotation of the Earth at 15° per hour equal to 360° in 24 hours (Rajput, 2017). The *azimuth angle* (γ_s), seen in Figure 3.6.1 as the horizontal angle of the sun rays relative to the horizon. This indicates the direction in which the sunlight is coming. In the northern hemisphere, an orientation towards the equator will result in an azimuth of 0° , while in the southern hemisphere, 0° indicates north and 180° indicates south. The *latitude angle* (ϕ) shows the impact of latitude on the variation of sunlight and the optimal tilting of the module, especially at higher latitudes (Skouri et al., 2016).

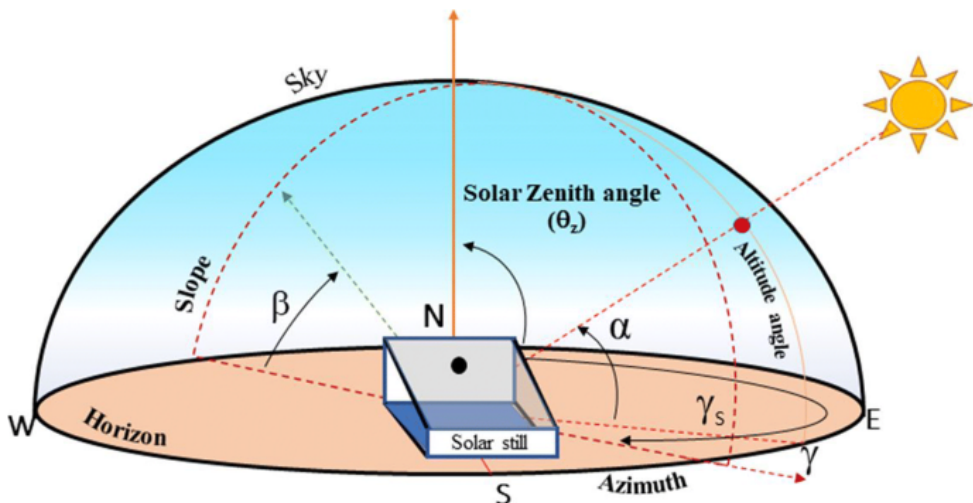


Figure 3.6.1: Figure of solar geometry and Earth angles.

Source: Arunkumar et al., 2021

3.7 Distributed Energy Systems (DES)

Distributed Energy Systems (DES) refer to energy solutions that involve decentralizing and distributing energy generation. These systems are often associated with microgrids and utilize various renewable energy sources, such as solar modules, wind turbines, and small-scale hydroelectric plants, to produce energy closer to the point of consumption (Mavromatidis et al., 2018). This approach improves energy security, reduces transmission losses, and supports sustainable development.

3.7.1 PV technology

3.7.1.1 PV cell:

PV systems generate electricity by directly converting solar radiation into electrical energy through a process called the PV effect (Onar & Khaligh, 2015). In this process, the electrons in the atoms of a PV cell become energized when they absorb energy from sunlight. Once the electrons gain enough energy, they move away from their normal positions in the semiconductor material, generating an electric current.

The semiconductor material in a PV cell comprises two layers: a negatively charged n-type layer and a positively charged p-type layer. When these layers come into contact, an electric field forms because n-type silicon contains excess electrons, whereas p-type silicon contains excess holes. This electric field causes the energized electrons to move toward the negative surface of the cell, creating a current flow (Appleyard, 2006). At the same time, the holes move toward the positive surface, waiting for the returning electrons. This PV process can be visualized in Figure 3.7.1.

The current output from a solar PV cell is given as DC. Everyday appliances often use Alternating Current (AC), therefore, a power electronic device (inverter) is required to convert direct current to alternating current to make energy usable (Berwal et al., 2017).

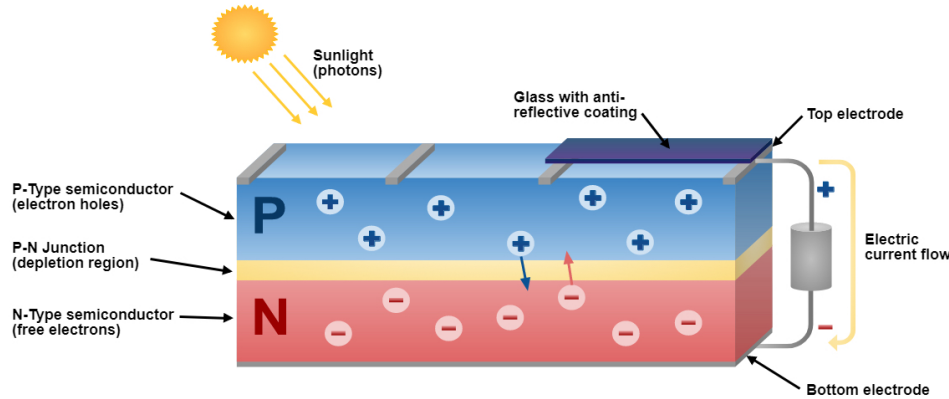


Figure 3.7.1: Figure of a basic PV cell.

Source: “How a PV Module Works”, n.d.

3.7.1.2 PV Module

A PV module consists of multiple PV cells, typically up to 72 in a string (Franklin, 2018). When multiple PV modules are connected, they form a PV array that makes up the structure of a PV system. The performance of a PV system can be customized by configuring the PV modules in series or parallel connections. The series connection increases the voltage, and the modules connected in parallel increase the current output (Onar & Khaligh, 2015), which can be designed to meet specific needs. PV modules are normally mounted on an inclined structure to receive the maximum annual insolation, keeping the inclination at the location’s latitude (Kalogirou, 2014, p. 481-540).

3.7.1.3 Shading

Shadows on PV modules can significantly reduce their effectiveness by reducing the amount of sunlight reaching solar cells. In a series connected cell, if some become shaded, the maximum allowable current decreases, resulting in a reduction in total power output (Abdelaziz et al., 2022). Furthermore, shaded cells can heat up excessively, causing a hotspot effect that might lead to permanent damage to the PV module. To minimize these efficiency losses, bypass diodes are frequently employed in PV modules. These diodes are installed parallel to the solar cell strings and provide a path for the current to bypass any shaded or malfunctioning cells, reducing the effects of shadowing on the total power output of the PV system (Abdelaziz et al., 2022).

3.7.1.4 Temperature

Temperature also plays a crucial role in the efficiency of PV modules. Typically, as the temperature of solar modules increases, its efficiency decreases. This is due to the increase in the energy band gap of the semiconductor material with increasing temperature (Dubey et al., 2013). As a result, the voltage output of the solar cells decreases and the short-circuit current increases, leading to lower power generation. This can be observed in Figure 3.7.2, where the voltage drops as the temperature increases. Manufacturers often provide a temperature coefficient, which indicates the percentage decrease in efficiency per °Celsius increase in the module temperature.

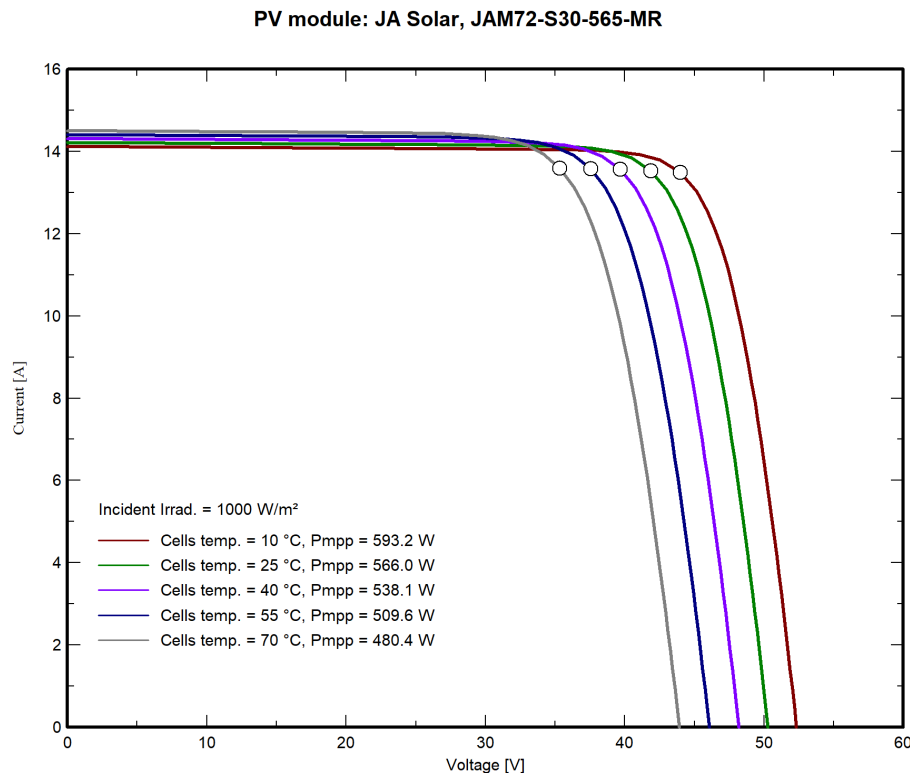


Figure 3.7.2: Illustration of the temperature influence on the I/V curve for a PV module of 565 W. Extracted from PVsyst.

Source: “PVsyst | PVsyst 8”, n.d.

3.7.1.5 Soiling

Soiling losses can lead to a reduction in energy output up to 6% for most locations due to accumulation of dirt, dust, and other particles on the surface of solar modules (Kimber et al., 2006). These particles block sunlight from reaching the PV cells, thus reducing efficiency and energy production. The extent of soiling erosion can vary significantly depending on geographic location, weather conditions, and the frequency of rain, which can naturally clean modules (Adekanbi et al., 2024).

3.7.1.6 Optimal plane tilt and orientation

Optimizing solar radiation exposure is essential to maximize energy generation. The effect of different levels of irradiation can be observed in Figure 3.7.2, where a higher irradiation results in a higher power output. In optimizing solar radiation, tilt and azimuth angles are critical factors (Kalogirou, 2014). The tilt angle is the angle between the PV module and the horizontal plane, while azimuth, as mentioned, refers to the module's orientation in the east-west direction. In the northern hemisphere, a south-facing tilt aligns better with the Sun's path, maximizing solar energy capture compared to a horizontal surface. In contrast, in the southern hemisphere, north-facing tilts capture more solar energy (Ben, n.d.). In further sections of this thesis, the location of the site in the northern hemisphere will be considered.

Latitude plays a significant role in determining the optimal tilt angle. Near the equator, a lower tilt angle is generally optimal, although a tilt less than 10° is not recommended due to reduced natural cleaning from rain and wind, which can lead to increased soiling losses (Ben, n.d.). In addition, if the modules are installed closer to the ground or roof, the airflow behind them is reduced. Increasing the spacing between modules in series and strings can result in a decrease in the heat loss from the modules.

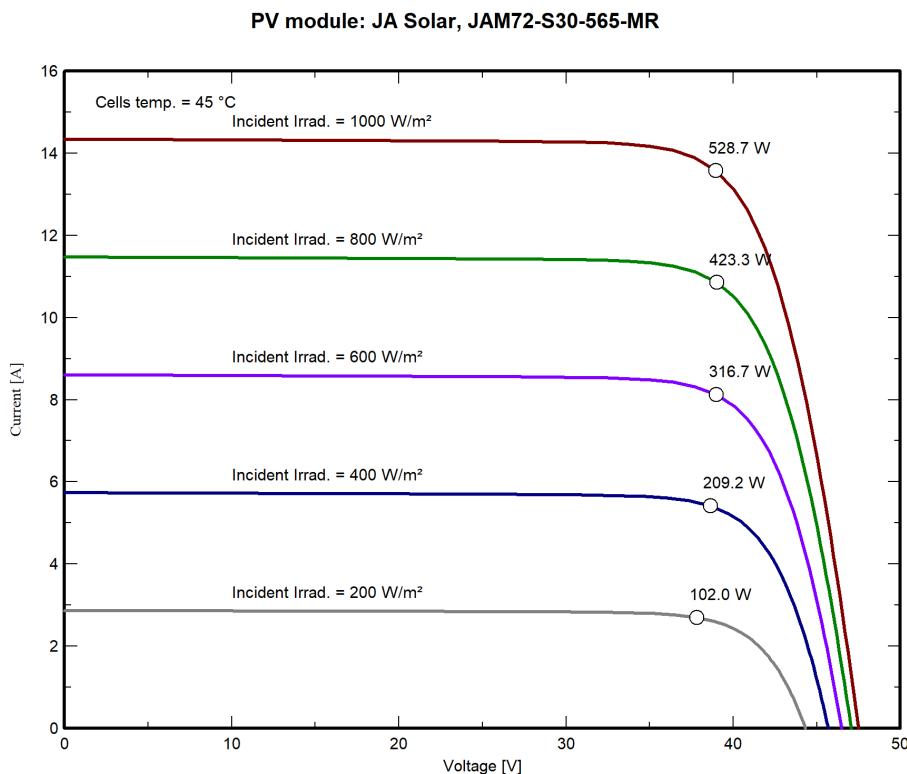


Figure 3.7.3: Illustration of the difference in irradiation and its influence on the I/V curve for a PV module of 565 W. STC is 25°C. The plot is extracted from PVsyst.

Source: “PVsyst | PVsyst 8”, n.d.

3.7.2 PV components

Inverter

As described, an inverter converts DC electricity from sources such as batteries to AC electricity. The converted AC electricity can be designed to deliver any required voltage and can power AC equipment. In a PV system context, a solar inverter, also known as a PV inverter, is a crucial component. It converts the variable DC output of the solar module into a utility frequency alternating current that a local electrical network outside the grid can use (Akorede, 2022).

Solar inverters often have specialized features for use with PV arrays, one of the most important being the Maximum Power Point Tracking (MPPT). MPPT is a technique that solar inverters use to extract the maximum possible power from a PV array. This technique is based on the complex relationship between solar irradiation, temperature, and resistance, resulting in a non-linear output efficiency represented by the current-voltage curve (I-V curve) (Eltawil & Zhao, 2013). The MPPT system works by continuously monitoring the output of solar cells and adjusting the resistance to maximize power generation. In essence, MPPT determines the optimal current that the inverter should draw from the PV array to achieve the highest possible power, since power is the product of voltage and current.

Controller

The charge controller is a device connected between the PV array and the battery that regulates the flow of electricity from the PV array to the battery. It works by ensuring that the maximum output of solar arrays is used to charge batteries without causing overcharging or damage (Qazi, 2017). When the controller detects that the battery is fully charged, it reduces or stops the flow of electricity from the PV array. This process helps maintain efficiency and prolong the lifespan of the equipment.

Battery

Batteries store the electricity produced by the PV system. The energy storage capacity of a battery is measured in watt-hours, which is calculated by multiplying the amp-hour rating by the voltage (Rajput, 2017). As the battery offers the opportunity to store energy, it allows the solar energy system to be used even when the sun is not shining. This is crucial to achieve energy independence and reliability in solar power systems.

Working of the system

To sum up the workings of the components, also visualized in Figure 3.7.4, it all starts with the PV array's output being sent to the charge controller, which then regulates the flow

of electricity from the PV array to the battery. The controller ensures that the battery remains fully charged without overcharging. The battery output is then connected to the input of the inverter, which converts DC electricity into AC electricity and then supplies it to the connected load.

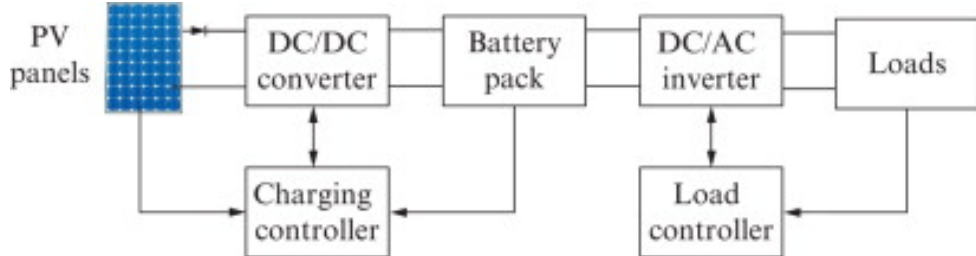


Figure 3.7.4: Figure of a PV system configuration with belonging components.

Source: Onar and Khaligh, 2015.

Losses

Due to the workings of the system, various types of losses can affect efficiency (“PVsyst | PVsyst 8”, n.d.) . Cable losses occur as a result of resistance in electrical cables, leading to energy dissipation as heat. Losses in components, such as in inverters and controllers, are unavoidable as the energy is converted from DC to AC. Degradation is another factor that affects system performance over time. Jordan and Kurtz (2013) suggests an average annual degradation rate of 0.5% for PV modules, affecting their long-term efficiency.

3.7.3 Microgrid

A microgrid is a modern energy infrastructure commonly used in DES that integrates and coordinates various loads and Distributed Energy Resources (DERs) (Shuai et al., 2016). These systems can function either interconnected with the main utility grid or autonomously in island mode. Today, microgrids are characterized by decentralized power generation and improved local adaptability (Suwi & Justo, 2024). Typically, they employ various renewable energy technologies such as PV panels, wind turbines, and small-scale hydropower plants. These decentralized arrangements improve grid efficiency and are beneficial in meeting local electricity demand.

Microgrids play an especially critical role in less developed regions, where they provide increased energy security and reliability in areas with limited or no access to centralized grids. Their applications range from serving isolated communities, individual buildings, and manufacturing centers, to supporting local power networks. Depending on specific needs, microgrids can operate using AC and DC power configurations and may operate as single-phase or three-phase systems (Ustun et al., 2011).

3.7.4 Microgrid components

Microgrids differ from traditional centralized grids primarily due to their distributed infrastructure and integration of renewable energy resources. In the following subsections, the key components and technical aspects of microgrids are presented.

Battery:

Energy storage systems, primarily batteries, are crucial in stabilizing the power supply by storing excess energy for later use. The performance of batteries in a microgrid is often defined by the following terms:

- **State of Charge (SoC):** The current charge level of the battery as a percentage of its total capacity (Spiers, 2012)
- **Depth of Discharge (DoD):** The percentage of the battery's total capacity that has been used. A higher DoD means more capacity has been discharged (Spiers, 2012)
- **Cycle life:** The number of charge and discharge cycles a battery can undergo before its available capacity is reduced to approximately 80% of its original capacity (Spiers, 2012). The type of battery technology influences the cycle life (Wenzl, 2009). As the battery degrades over time, also with age (due to corrosion), the capacity also reduces.
- **Days of Autonomy:** Days of Autonomy represent the number of days a battery bank can supply power to an average electrical load without requiring recharge, until it is fully depleted (Louie, 2018b, p.401).
- **Lead-acid and Lithium-ion batteries:** Two most common battery technologies used in microgrids. Lead-acid batteries are cost-effective but have a shorter cycle life, while lithium-ion batteries offer higher efficiency, longer life, and lower maintenance, but at a higher initial cost (Makola et al., 2023). Ayeng'o et al. (2018) found from comparing both storage systems for off-grid applications that lithium-ion batteries have a lower Levelized Cost of Electricity (LCOE) mainly due to both the longer life of lithium-ion batteries and the reduced price as a result of increased global production. In addition, the energy storage efficiency is higher, leading to higher charge and discharge rates.

Converters:

Converters play an essential role in adapting different voltage levels within the microgrid. A DC/DC converter is used to increase or decrease the DC voltage to meet the needs of the system (Louie, 2018b). For PV systems, MPPT converters are generally considered

the best. They optimize the power output from the PV array by continually adjusting the DC/DC converter to operate at the maximum power point. According to Baharudin et al. (2017), the DC-DC buck converter is more appropriate for PV arrays arranged in series, while the DC-DC boost converter is effective for PV arrays connected in parallel. The DC-DC buck-boost converter has proved the most efficient means of generating the maximum output power of PV power regardless of the conditions.

Inverters:

As presented in subsection 3.7.2, inverters are essential for the effective incorporation of renewable energy into microgrids. In off-grid PV systems, micro inverters are commonly favored because they improve the performance of individual solar modules (“Pros & Cons Inverteres”, n.d.). This feature is especially useful when modules are subjected to shading or facing different directions, as it allows each module to function independently (Famoso et al., 2015). String inverters, on the other hand, are employed in systems with multiple strings per inverter and several modules in each string, resulting in high voltage. Central inverters are typically found in larger systems with higher power demands and operate similarly to string inverters. As for solar inverters, their expected lifespan is between 10 and 15 years.

Controllers:

The controller of a microgrid is the brain of the system, ensuring proper coordination of all components, managing load distribution, energy storage and generation, and optimizing power flow based on real-time conditions (Louie, 2018b).

AC and DC Microgrids:

Microgrids can be configured to operate on AC or DC, or even as hybrid systems that combine both.

- **AC Microgrids:** These are more common due to the dominance of AC in traditional grids and most appliances. However, AC systems involve higher losses in conversion and transmission (Justo et al., 2013).
- **DC Microgrids:** DC microgrids are gaining attention due to the direct output of renewable energy sources such as solar PV and battery systems, which naturally produce DC power. With only DC loads, the need for conversion equipment is removed, making them more efficient in some applications (Justo et al., 2013).
- **Hybrid Microgrids:** Hybrid systems combine AC and DC distribution, providing greater flexibility and efficiency, especially in systems that rely heavily on renewable energy (Mishra & Viral, 2022)

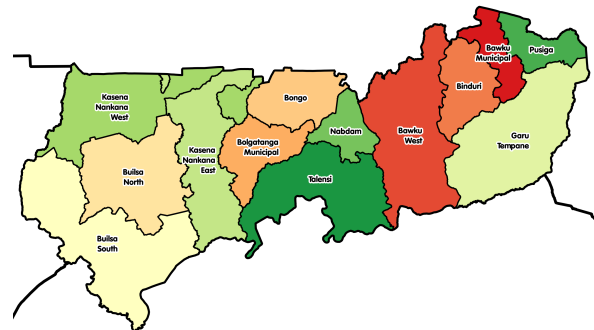
Chapter 4

Presentation of the property

4.1 TRAX Ghana



(a) Map of Ghana with the Upper East Region highlighted.



(b) Map of the districts of the Upper East Region.

Figure 4.1.1: The Upper East Region of Ghana.

Source: “Upper East Region”, 2024

TRAX Ghana is located near Bolgatanga, Bongo District, in northern Ghana. The property is located at an elevation of approximately 200 meters above sea level; the geographical coordinates of the site are 10.85 °N latitude and -0.73 °W longitude (“PVsyst | PVsyst 8”, n.d.).

The TRAX facility consists of three primary buildings (visualized in Figure 4.1.2) that

support its operational and community-focused activities. These include a farm building, library, IT center, and greenhouse, which make up the facilities for educational and agricultural activities.



Figure 4.1.2: Screenshot from Google Maps. TRAX Ghana from above.

Source: “Google Maps”, n.d.

4.1.1 Climatic conditions and solar potential

Table 4.1.1: Weather characteristics by season.

Source:“intro - Meteonorm (de)”, n.d., Ampadu et al., 2020

Season	Avg. temperature (°C)	Avg. rainfall (mm)	Avg. sun hrs (h)	Peak sun hrs (h)
Rainy	28.64	150.01	6.67	5.78
Dry	29.12	11.12	8.49	5.95

The region experiences two main seasons:

- **Rainy season** (May to October): Characterized by lower temperatures and frequent rainfall, which affects agricultural cycles and slightly reduces solar radiation.
- **Dry season** (November to April): Characterized by higher temperatures and sunny conditions, offering optimal conditions for solar energy generation.

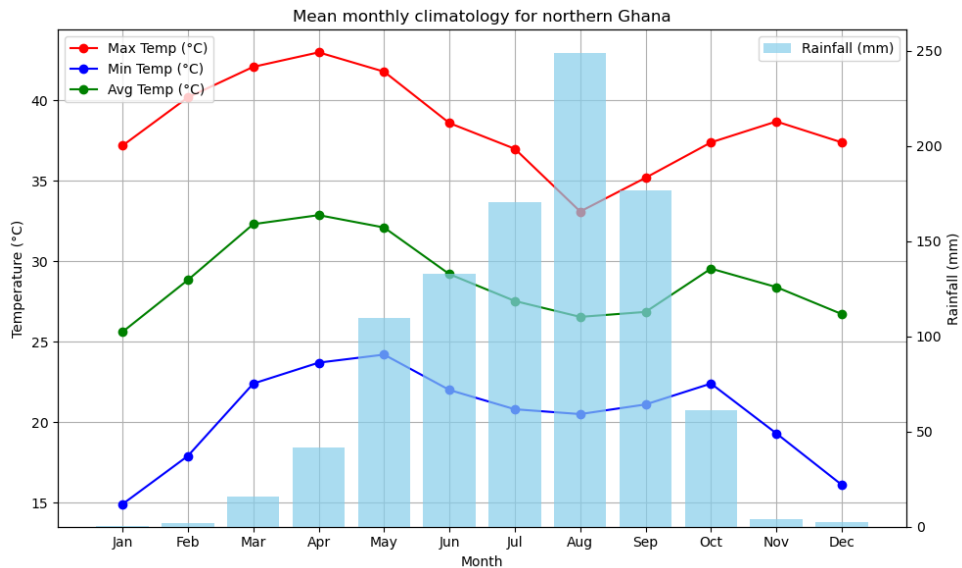


Figure 4.1.3: Mean monthly climate for TRAX Ghana.

Sources: (“intro - Meteonorm (de)”, n.d., Ampadu et al., 2020).

As visualized in Figure 4.1.3, the site experiences an annual temperature fluctuation between 15 °C and 43 °C. Solar irradiance (GHI) varies significantly, with the lowest monthly GHI recorded in the rainy season and peaks during the dry season, supporting the use of PV systems throughout the year. This is visualized in Figure 4.1.4 as the peak sun hours, indicating periods when the intensity of the sunlight averages 1000 W/m^2 . The months during the dry season are colored yellow, while the months during the rainy season are colored blue.

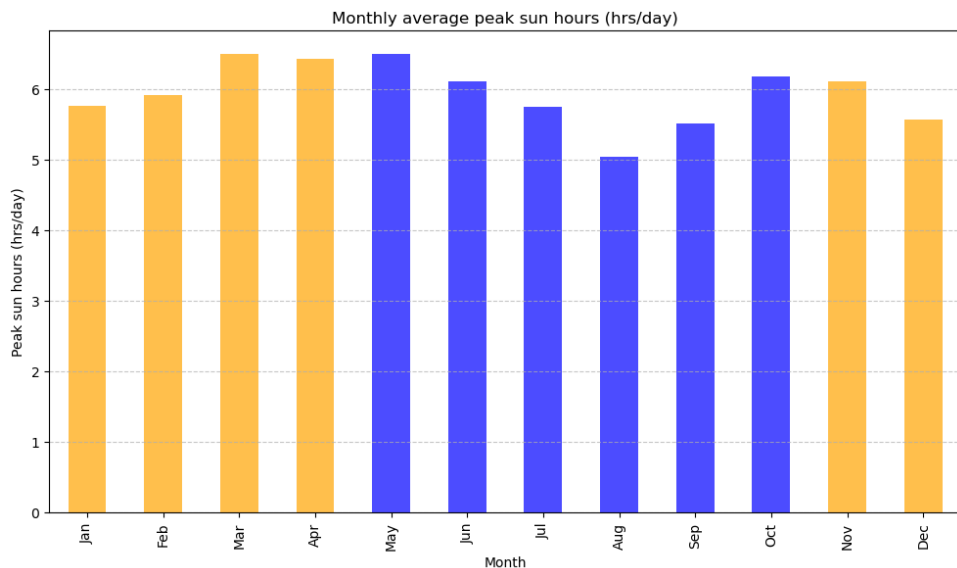


Figure 4.1.4: Average peak sun hours between the two seasons for Bolgatanga, Ghana.

4.1.2 Energy usage

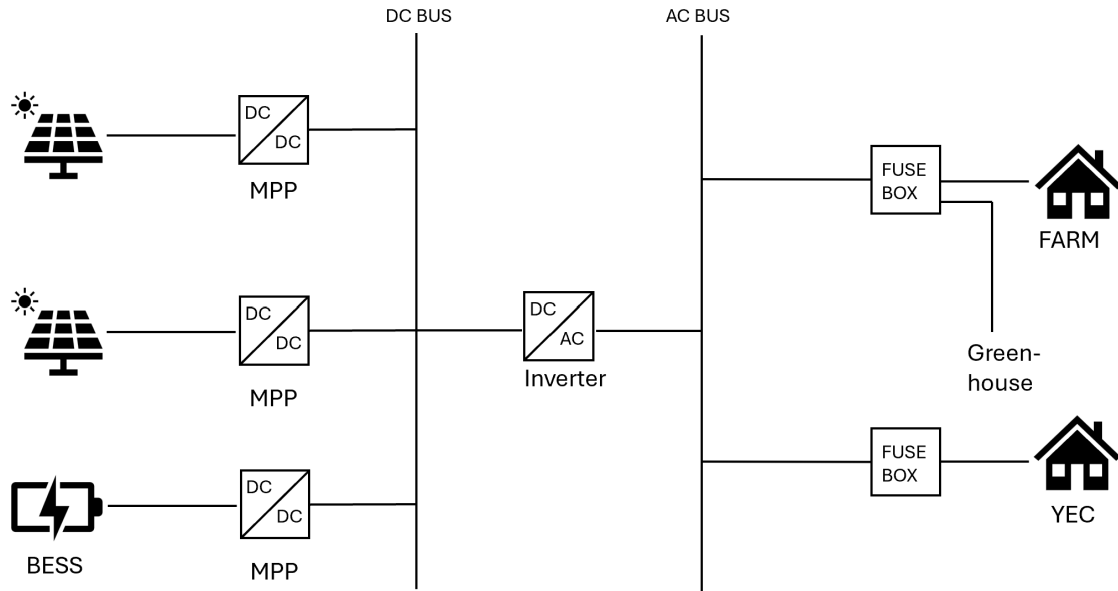


Figure 4.1.5: A simple system topology for the off-grid system

Source: All icons are either made by student or taken from Microsoft PowerPoint's icon library.

System Topology

A simple topology is visualized in Figure 4.1.5, where the PV system that supplies the farm consists of 30 PV modules, each with a nominal capacity of 285 Wp, arranged in four strings (“Installasjon av solcelleanlegg”, n.d.). This results in a solar array output of approximately 4.1 kWp and an output voltage of approximately 70V. Two strings are connected to one charge controller each, which regulates the voltage and current to the batteries and inverter. The inverter is powered by solar modules or the battery bank, depending on the availability of sunlight.

The battery bank comprises 8 batteries, each 100Ah/12V, connected in series and parallel to achieve a 48V output with a total capacity of 9.6 kWh. The system’s inverter, with a capacity of 10 kVA, converts the 48V DC to 230V AC. Currently, the available capacity of the PV system is approximately 2.9 kW after accounting for the existing load of the farm, including the main house lighting (50 W), ventilation (100 W) and the water pump (1000 W). This leaves sufficient capacity to meet the energy demands of the planned greenhouse facilities. Further adjustments are required for power connections for the installation of additional greenhouses, including a new circuit in the container fuse box.

In December 2024, a newly established system upgrade was established for the YEC with remote monitoring, 12 new PV modules of 565 Wp and eight 5.0 kWh lithium-ion

batteries. This results in a solar array output of 6.78 kWp and 40 kWh of battery storage capacity.

4.1.3 Agriculture on site

Energy demand in the region is strongly influenced by the agricultural calendar, with higher usage during harvest seasons, particularly in the late rainy season, when crop cooling and storage requirements are peak. During this time, the area receives an average of 8–10 hours of sunlight a day, as shown in Figure 4.1.6, reducing the dependence on external energy sources.

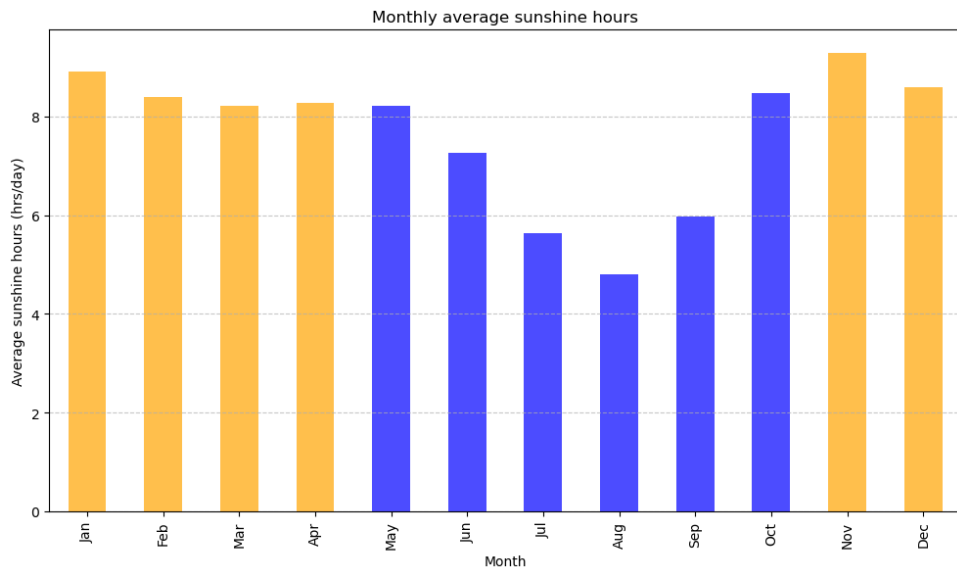


Figure 4.1.6: Average sunshine hours between the two seasons for Bolgatanga, Ghana.

Harvest seasons and crop yield

The harvest season in the Bongo district spans from June to October and December to May, occurring twice a year, with a three-month interval between each cycle. During these periods, production peaks and cooling needs are at their highest. The current setup on the farm includes one greenhouse that produces around 516 kg of bell peppers per cycle. There are plans to expand to four greenhouses, increasing total production to 2064 kg. This will support continuous production throughout the year and increase income for TRAX Ghana. Choosing which vegetables to grow for each cycle will be based on research of the current market.

Having several greenhouses that grow different crops would make the farm versatile on the market, allowing it to adapt to market fluctuations. Possible vegetables that can be grown on the farm are bell peppers, cucumbers, lettuce, tomatoes, hot peppers, and cabbage. In addition, harvesting occurs weekly to maintain freshness during the harvesting season. A cold storage facility would be used to manage peak periods when market prices are lower.

This will be during the abundance season that lasts from June to October. Although market competition intensifies during the rainy season, it decreases in the dry season, as open field farming becomes more challenging. This in turn leads to increased market demand and prices, making it profitable to sell stored produce at this time.

The average weight of the crops harvested during a 12-week three-month cycle for one greenhouse is $\frac{516kg}{12} = 21.5kg$ for the two combined daily harvests. However, since there is no conclusive research on the normal distribution of harvesting cycles, it is assumed that the maximum harvest during a day is a total of $40kg$, which also takes into account some possible overlap between greenhouse production cycles. Future calculations are based on the assumption that there will be an expansion to four greenhouses.

Chapter 5

Methods

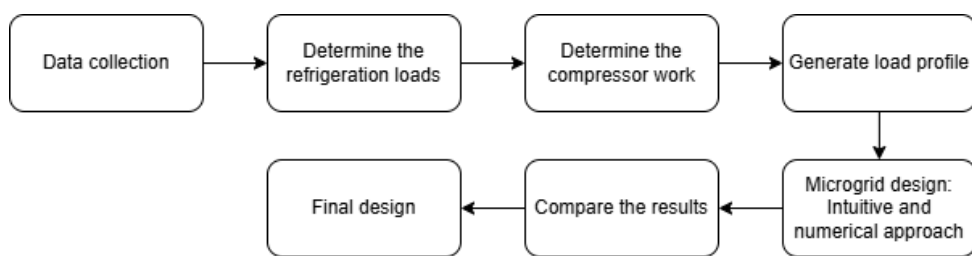


Figure 5.0.1: Flowchart for the SPCS design.

5.1 Data collection

Accurate and comprehensive data collection was essential for this project to maintain the reliability of the findings and to effectively customize the solutions to the needs of TRAX Ghana. The key data sources for this study include interviews with stakeholders and internal reports from a previous project, supplemented by external datasets.

Meteonorm

Meteonorm, a well-established software for meteorological data, was used to collect weather parameters on an average basis from 1991 to 2010. The data collected included solar radiation, temperature, and other environmental conditions. Meteonorm provides exclusive access to the Global Energy Balance Archive Data (GEBA). GEBA data are sourced from national weather services and meet the quality standards of the World Meteorological Organization (WMO) (“intro - Meteonorm (de)”, n.d.). The data serve as the basis for assessing temperature variations and the potential for energy generation. To precisely simulate PV installations or manage battery systems, reliable time series of solar irradiance are crucial. In addition, the data were used to calculate the needed refrigeration capacity of the system, which means how much heat the system needs to remove to

maintain the desired temperature.

Interviews and internal reports

Interviews were conducted with key contributors at the center, including farm managers and local workers. These interviews were aimed at understanding the operational challenges, the energy requirements, and the contextual differences. The insights from these discussions were the main contributors to system design and integration strategies, ensuring that all practical needs and constraints were met.

Internal reports, including historical energy usage logs, system performance assessments, and previous studies, were reviewed to establish baseline conditions and identify gaps in the existing system. This combination of primary and secondary data sources ensured a solid understanding of the project environment, which is important to make informed decisions.

5.2 Refrigeration system

Figure 5.2.1 illustrates the initially designed refrigeration system alongside the corresponding logarithmic pressure-enthalpy (P-H) diagram. This configuration represents an indirect system comprising two circuits, each circulating different refrigerants. The primary circuit operates as a conventional single-stage vapor compression cycle, which incorporates a compressor, a condenser, an expansion valve, and an evaporator. The energy in the primary system is supplied by the compressor. The transfer of heat occurs from a low-temperature region (evaporator) to a high-temperature region (condenser) through phase transitions of the refrigerant. In the secondary circuit, the system includes a fluid pump, two bypass valves, and two heat exchangers. The fluid pump circulates the secondary refrigerant throughout the system. Bypass valves, equipped with thermal actuators, manage fluid flow based on temperatures in refrigerated rooms. This is done by bypassing the heat exchangers once the refrigeration rooms achieve their desired temperatures. The two bypass valves vary the cooling requirements, with the first valve regulating Room 1 and the second valve regulating Room 2.

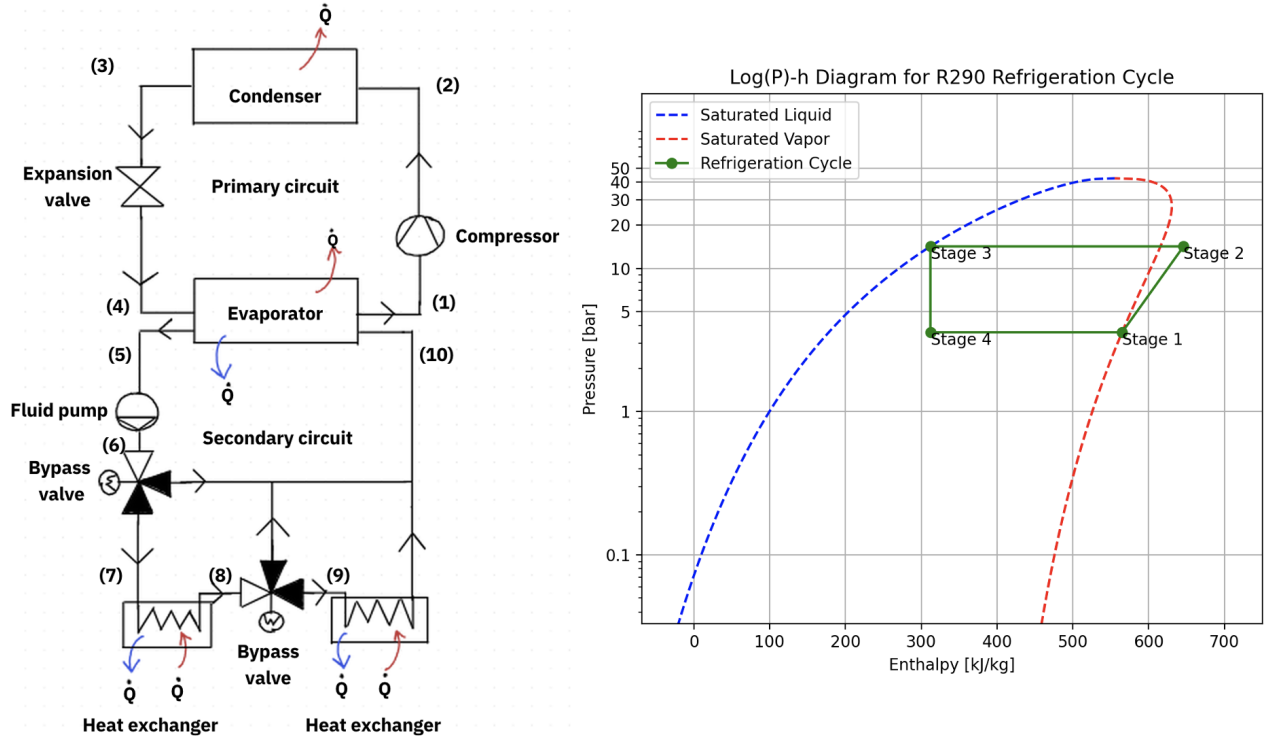


Figure 5.2.1: Refrigeration system and corresponding Log (P-H) diagram for the cold storage.

Using thermodynamic principles, the state points of the fluid throughout the cycle can be identified if there are some initial inputs. These are mainly the isentropic efficiency, refrigerant type, ambient temperature, and desired temperature of the cold reservoir. **Stage 1** is the outlet of the evaporator and the inlet of the compressor, which will be at the saturated vapor line with the same pressure as in the evaporator. From this, pressure, enthalpy, and entropy can be found. **Stage 2** is the outlet of the compressor and the inlet of the condenser. Here, the compressor has compressed the saturated vapor to a superheated vapor. Assuming isentropic compression and knowing the temperature in the outlet of the condenser, the pressure in the condenser is found and the specific compressor work can be calculated through Equation 5.1:

$$w_{comp} = h_2 - h_1 [\text{kJ/kg}] \quad (5.1)$$

h_2 is the real enthalpy and is found using Equation 5.2:

$$h_2 = h_1 + \frac{h_{2s} - h_1}{\eta_{is}} [\text{kJ/kg}] \quad (5.2)$$

Stage 3 is the condenser outlet and is at the saturated liquid line. Pressure and enthalpy can be found using this relation. **Stage 4** is the outlet of the expansion valve and the

inlet of the evaporator, which will be a two-phase fluid. The enthalpy in Stage 4 is equal to Stage 3.

Furthermore, the specific heat absorbed in the evaporator can be expressed as Equation 5.3:

$$q_{evap} = h_1 - h_4 [kJ/kg] \quad (5.3)$$

The mass flow of the refrigerant can be determined through Equation 5.4, when the total amount of heat that needs to be removed from the system, \dot{Q}_{tot} , is known:

$$\dot{m} = \frac{\dot{Q}_{tot}}{q_{evap}} [kg/s] \quad (5.4)$$

From this, the compressor work can be calculated with Equation 5.5:

$$\dot{W}_{comp} = \dot{m} * w_{comp} [W] \quad (5.5)$$

The COP of the system is the degree of compressor performance and is defined as the amount of heat supplied or removed from the system, compared to the input from work. A higher COP relates to higher efficiency, lower energy consumption, and lower operating cost (Donev, 2024). Equation 5.6 shows the COP:

$$COP = \frac{q_{evap}}{w_{comp}} \quad (5.6)$$

The determination of the necessary work for the fluid pump within the secondary circuit is made by applying Equation 5.7:

$$W_{pump} = \dot{m} \cdot v \cdot \Delta P [kW] \quad (5.7)$$

Where v is the specific volume, ΔP is the pressure drop over the heat exchangers, and the mass flow rate \dot{m} of the secondary refrigerant is found from Equation 5.8:

$$\dot{m} = \frac{\dot{Q}_{tot}}{C_p \cdot \Delta T} [\frac{kg}{s}] \quad (5.8)$$

Here, \dot{Q}_{tot} is the total refrigeration load, the specific heat capacity, C_p , is for the secondary refrigerant, and ΔT is the temperature difference in the secondary circuit.

5.3 Refrigeration loads

This section of the chapter outlines the considerations for calculating cold storage loads, primarily based on the reference book (American society of heating, 2010), unless mentioned otherwise. In these estimations, there are two main loads and two minor loads. The main loads are the transmission load and the product load from cooling of the vegetables. The two minor loads are the infiltration load and the heat gain from people inside the building. All of these must be calculated to estimate the size of the compressor, and create a functioning load profile for the energy system.

5.3.1 Crop properties

Upon storage, the harvested vegetables are at the same temperature as the outside environment. Therefore, they need to cool down to preserve quality. To calculate the heat that must be removed, one must establish the different properties of the vegetables.

Content of crops

Common for most food is that they consist of water, protein, fat, carbohydrates, fiber, and ash. The amount of each component will vary for different foods, thus affecting their thermal properties. Table 5.3.1 shows the composition of the relevant vegetables.

Crop	Moisture content [%]	Protein [%]	Fat [%]	Carbohydrates [%]	Fiber [%]	Ash [%]
Tomatoes	93.76	0.85	0.33	4.64	1.1	0.42
Bell peppers	92.00	1.00	0.30	6.00	2.1	0.87
Hot peppers	88.00	1.87	0.44	8.81	1.5	0.87
Lettuce	95.89	1.00	0.19	2.09	1.4	0.48
Cabbage	92.15	1.44	0.27	5.43	2.3	0.071
Cucumber	96.01	0.69	0.13	2.76	0.8	0.41

Table 5.3.1: Vegetable content.

Source: American society of heating, 2010.

Thermal properties

To perform calculations on the refrigeration of food items, the thermophysical properties are crucial to know, as they determine the internal heat and mass transfer. Table 5.3.2 shows the thermal property models for k , C_p and ρ that depend on both the crop components and the temperature.

Thermal Property	Food Composition	Thermal Property Model
Thermal conductivity [$\frac{W}{m \cdot K}$]	Water	$k_w = 5.7109 \times 10^{-1} + 1.7625 \times 10^{-3}t - 6.7036 \times 10^{-6}t^2$
	Protein	$k = 1.7881 \times 10^{-1} + 1.1958 \times 10^{-3}t - 2.7178 \times 10^{-6}t^2$
	Fat	$k = 1.8071 \times 10^{-1} - 2.7604 \times 10^{-4}t - 1.7749 \times 10^{-7}t^2$
	Carbohydrate	$k = 2.0141 \times 10^{-1} + 1.3874 \times 10^{-3}t - 3.3312 \times 10^{-6}t^2$
	Fiber	$k = 1.8331 \times 10^{-1} + 1.2497 \times 10^{-3}t - 3.1683 \times 10^{-6}t^2$
	Ash	$k = 3.2962 \times 10^{-1} + 1.4011 \times 10^{-3}t - 2.0969 \times 10^{-6}t^2$
Density [$\frac{kg}{m^3}$]	Water	$\rho_w = 9.9718 \times 10^2 + 3.1439 \times 10^{-3}t - 3.7574 \times 10^{-2}t^2$
	Protein	$\rho = 1.3299 \times 10^3 - 5.1840 \times 10^{-1}t$
	Fat	$\rho = 9.2559 \times 10^2 - 4.1757 \times 10^{-1}t$
	Carbohydrate	$\rho = 1.5991 \times 10^3 - 3.1046 \times 10^{-1}t$
	Fiber	$\rho = 1.3115 \times 10^3 - 3.6589 \times 10^{-1}t$
	Ash	$\rho = 2.4238 \times 10^3 - 2.8063 \times 10^{-1}t$
Specific heat [$\frac{kJ}{kg \cdot K}$]	Water (0 to 150°C)	$c_w = 4.1289 - 9.0864 \times 10^{-5}t + 5.4731 \times 10^{-6}t^2$
	Protein	$c_p = 2.0082 + 1.2089 \times 10^{-3}t - 1.3129 \times 10^{-6}t^2$
	Fat	$c_p = 1.9842 + 1.4733 \times 10^{-3}t - 4.8008 \times 10^{-6}t^2$
	Carbohydrate	$c_p = 1.5488 + 1.9625 \times 10^{-3}t - 5.3999 \times 10^{-6}t^2$
	Fiber	$c_p = 1.8459 + 1.8306 \times 10^{-3}t - 4.6509 \times 10^{-6}t^2$
	Ash	$c_p = 1.0926 + 1.8896 \times 10^{-3}t - 3.6817 \times 10^{-6}t^2$

Table 5.3.2: Thermal Property Models for Food Components and Water ($-40 \leq t \leq 150^\circ C$).

Source: American society of heating, 2010.

Cooling time of the produce The cooling time of the produce varies depending on the shape, thermal diffusivity, geometry, thickness, Biot number, and initial and desired temperature. Common for the geometries to the relevant vegetables, namely spheres, slabs, and cylinders, are the formulas for the Biot number, thermal diffusivity, and cooling time.

The Biot number provides information on whether or not food is more controlled by internal or external heat transfer, and can be found using formula 5.9.

$$Bi = \frac{h \cdot L}{k} \quad (5.9)$$

The thermal diffusivity, α , is presented in Equation 5.10.

5.10:

$$\alpha = \frac{k}{Cp \cdot \rho} \left[\frac{m^2}{s} \right] \quad (5.10)$$

The cooling time, given in hours, is found by applying Equation 5.11:

5.11:

$$\theta = \frac{-f}{2.303} \ln\left(\frac{Y}{j}\right) \quad (5.11)$$

where Y is a dimensionless temperature relationship between the initial, wanted and cooling medium temperature, and is given in formula 5.12:

$$Y = \frac{T_w - T_m}{T_i - T_m} \quad (5.12)$$

In Equation 5.12, the subscripts w, i, and m stand for the initial desired, and the cooling medium, respectively, with respect to the temperature.

The slope and intercept of the temperature history curve, f and j , vary depending on the geometry, the characteristic dimension described as the length from the thermal center to the surface and the thermal diffusivity. The equations assume a uniform initial temperature of the vegetables, a constant temperature of the surrounding medium, convective heat transfer at the surface, and constant thermophysical properties throughout the calculations.

Vegetables are classified primarily into three shapes: sphere, cylinder, and slab. However, bell pepper is an exception; it is treated as a slab but uses the area of a sphere. This is illustrated in Table 5.3.3

Table 5.3.3: Classification of Vegetables by Geometric Shape

Geometric Shape	Vegetables
Sphere	Tomatoes, Cabbage, Lettuce
Cylinder	Hot Peppers, Cucumber
Slab	Bell Peppers

Spheres

For the spheres, if $0.1 < Bi < 100$, f and j can be found by Equations 5.13 and 5.14, respectively:

$$f = \frac{L^2 \cdot \ln(Bi)}{\alpha \cdot 3Bi} \quad (5.13)$$

$$j = \frac{2 \cdot (\sin(w) - w \cdot \cos(w))}{w - \sin(w) \cdot \cos(w)} \quad (5.14)$$

L is the radius of the vegetable, and w is presented in Equation 5.15:

$$w = 1.57 + 0.64 \cdot \ln(Bi) + 0.047 \cdot \ln(Bi)^2 - 0.035 \cdot \ln(Bi)^3 - 0.0049 \cdot \ln(Bi)^4 + 0.0015 \cdot \ln(Bi)^5 \quad (5.15)$$

Cylinders

Similarly to the sphere, if the Biot number of cylinders is $0.1 < Bi < 100$, f and j are expressed as 5.16 and 5.17, respectively:

$$f = \frac{L^2 \cdot \ln(10)}{\alpha \cdot w^2} \quad (5.16)$$

$$j = \frac{2 \cdot J_1(v)}{v \cdot [J_0^2(v) - J_1^2(v)]} \quad (5.17)$$

where J_0 and J_1 are Bessel functions, commonly described as solutions to the Bessel differential equation (Weisstein, n.d.), L is the half thickness and v is found in Equation 5.18:

$$v = 1.26 + 0.49 \cdot \ln(Bi) + 0.025 \cdot \ln(Bi)^2 - 0.027 \cdot \ln(Bi)^3 - 0.0029 \cdot \ln(Bi)^4 + 0.0011 \cdot \ln(Bi)^5 \quad (5.18)$$

Slabs

Slabs as well are calculated similarly to the other geometries, and f and j are expressed in Equations 5.19 and 5.20 when $0.1 < Bi < 100$:

$$f = \frac{L^2 \cdot \ln(10)}{\alpha \cdot u^2} \quad (5.19)$$

$$j = \frac{2 \cdot \sin(u)}{u + \sin(u) \cdot \cos(u)} \quad (5.20)$$

Here, L is the half thickness and u can be found using equation 5.21:

$$u = 0.86 + 0.31 \cdot \ln(Bi) + 0.0079 \cdot \ln(Bi)^2 - 0.0162 \cdot \ln(Bi)^3 - 0.0011 \cdot \ln(Bi)^4 + 0.0006 \cdot \ln(Bi)^5 \quad (5.21)$$

Identifying the time it takes for each vegetable to reach the desired internal temperature equal to the storage temperature is necessary to calculate the product load in Equation 5.26.

5.3.2 Transmission load

The transmission load is defined as the sensible heat gain through the surfaces of a building, such as the walls, floor, windows, and ceiling. It can be calculated through Equation 5.22:

$$\dot{Q}_{trans} = U \cdot A \cdot \Delta T \quad (5.22)$$

In this context, ΔT represents the difference between the ambient temperature, which

fluctuates with seasons and time of day, and the internal storage temperature. The overall heat transfer coefficient U is described in Equation 5.23:

$$U = \frac{1}{\frac{1}{h_i} + \frac{\delta}{k} + \frac{1}{h_o}} \quad (5.23)$$

where h_i and h_o are the convective heat transfer of the inside and outside surfaces.

Generally, a value of 1.6 is given for h_i for a cold storage with still air. If the wind speed reaches 25 km/s , h_o could increase to 6. However, if the walls have a thick insulation with low thermal conductivity, h_i and h_o can be neglected in the calculations. This leaves Equation 5.24 for the overall heat transfer coefficient:

$$U = \frac{1}{\frac{\delta}{k}} \quad (5.24)$$

Furthermore, since the cold storage is located in Ghana, the sunlight that shines on the outer surfaces will increase the temperature. This means for the duration of daily sunlight, $\Delta T = T_{amb} + T_{sun} - T_i$, where the subscripts amb, sun, and i are the ambient temperature outside, the temperature increase due to sunlight and the temperature inside the storage, respectively. Table 5.3.4 shows the temperature increase due to sunlight.

Table 5.3.4: Surface types and their characteristics.

Source: American society of heating, 2010

Surface Type	Examples	East/West Wall [K]	South Wall [K]	Flat Roof [K]
Dark-colored surfaces	Slate, tar roofing, black paint	5	3	11
Medium-colored surfaces	Unpainted wood, brick, red tile, dark cement, red/gray/green paint	4	3	9
Light-colored surfaces	White stone, light-colored cement, white paint	3	2	5

Furthermore, the area A in the equation 5.22 is calculated for each wall, the roof, and the floor. Therefore, the total transmission load will be the sum of every section with its respective area, the overall heat transfer coefficient, and the temperature difference.

5.3.3 Product load

The product load refers to the heat required to cool the product to its storage temperature and the heat it generates. Equation 5.25 shows the heat that needs to be removed to bring it to storage temperature:

$$Q_{prod} = m \cdot Cp \cdot \Delta T \quad (5.25)$$

Since there are six different vegetables grown throughout the year, the load of the product will vary depending on the crops grown. Since equation 5.25 is given in kJ without regard to the cooling time, equation 5.26 will be used to calculate the product load in kW :

$$\dot{Q}_{prod} = \frac{m \cdot Cp \cdot \Delta T}{3600 \cdot t} \quad (5.26)$$

where t is the time given in hours. This will be the only product load considered, as the heat emitted from the product is minor compared to that of the heat removed from the product.

5.3.4 Infiltration load

Infiltration load occurs due to the heat gain from infiltration air when the door is open. This is a result of density differences inside and outside the room, where the cold air inside the storage is flowing out at ground level, while the warm air is flowing in above. Furthermore, the heat gain from the door is described in Equation 5.27:

$$\dot{Q}_t = q \cdot D_t \cdot D_f \cdot (1 - E) \quad (5.27)$$

where, \dot{Q}_t is the average heat gain over a defined time period in kW . The doorway protective device's effectiveness, denoted as E , varies between 0.95 and 0, where 0 indicates no protection. For fully established flow, the sensible and latent refrigeration load q is given by formula 5.28:

$$q = 0.221 \cdot A \cdot (h_i - h_r) \cdot \rho_r \cdot \left(1 - \frac{\rho_i}{\rho_r^{0.5}}\right) \cdot (g \cdot H)^{0.5} \cdot F_m \quad (5.28)$$

where A equals the area of the door, h_i and h_r are the enthalpies of the infiltration air and the air inside the cold storage. ρ_i and ρ_r are the densities of the infiltration air and the air inside the cold storage. H is the height of the door and F_m is the density factor given in Equation 5.29:

$$F_m = \left[\frac{2}{1 + (\frac{\rho_r}{\rho_i})^{\frac{1}{3}}} \right]^{1.5} \quad (5.29)$$

From 5.28, the doorway flow factor D_f is 0.8 for storage areas where the temperature difference between the inside and outside is greater than 16 K. The open time factor of the doorway D_t is given by Equation 5.30:

$$D_t = \frac{P\theta_p + 60\theta_o}{3600\theta_d} \quad (5.30)$$

with P being the number of doorway passages, θ_p the opening-closing time of the door in seconds. θ_o is the time the door is open, in minutes, and θ_d is a chosen time interval in

hours. For high-speed doors, 5 to 10 seconds are used, while for pull-cord-operated doors, 15 to 25 seconds is standard.

5.3.5 Internal load

The internal load of a cold storage is the sum of the heat from electrical equipment such as fans, lights, and trucks, the processing equipment, the people who occupy the room, and the heat from the defrosting of the evaporator. Although the heat emitted from people depend on factors such as clothing type, ambient temperature, a person's size, and type of work, the heat load can be estimated using Equation 5.31:

$$\dot{Q}_p = 272 - 6 \cdot T \quad (5.31)$$

where T is the temperature in the storage room.

5.3.6 Total load

The total load will be the sum of all the loads stated above plus a correction factor of 10% to account for unexpected additional increases in the total load. Equation 5.32 gives the heat that needs to be removed from the system:

$$\dot{Q}_{\text{tot}} = (\dot{Q}_{\text{trans}} + \dot{Q}_{\text{prod}} + \dot{Q}_t + \dot{Q}_p) \cdot (1.1) \quad (5.32)$$

The subscripts trans, prod, t and p are transmission load, product load, infiltration load, and internal load, respectively.

5.3.7 Compressor work

To make an initial estimate of the compressor work required to facilitate the calculated refrigeration load, the COP must be estimated. Equation 5.33 shows the COP for a Carnot refrigeration cycle with cycle efficiency η (campus, 2022):

$$COP_R = \eta \cdot \frac{T_L}{T_H - T_L} \quad (5.33)$$

where T_L and T_H are the temperatures inside the cold storage and the ambient temperature. From the estimated COP and the calculated \dot{Q}_{tot} , the initial estimate of the compressor work can be found in Equation 5.34:

$$\dot{W}_{\text{comp}} = \frac{\dot{Q}_{\text{tot}}}{COP} \quad (5.34)$$

5.4 Load profile

For microgrids, accurate load modeling is important, particularly since some data depend on interviews and limited harvest data. The creation of the load profile for the cold storage facility involves a systematic approach that incorporates deterministic and stochastic factors to represent the demand for power over time. The facility is designed to operate four greenhouses continuously throughout the year, ensuring a steady supply of crops.

A typical day is divided into three primary duty cycles based on the harvesting and storage schedule:

- *Intensive duty* (Morning harvest period): This occurs during peak harvest activity, usually between 7:00 and 9:00 AM when the compressor is operating at maximum capacity to rapidly cool newly harvested produce.
- *Intermediate duty* (Afternoon period): From late morning to mid-afternoon (10:00 AM to 4:00 PM), cooling demand stabilizes, maintaining a steady load. This period accounts for the change in ambient heat while avoiding excessive energy consumption.
- *Low duty* (evening and nighttime periods): During the evening and night (4:00 PM to 6:00 AM), the compressor activity drops significantly. This lower duty cycle is set to maintain the cold storage temperature.

The methodology begins with defining the deterministic components of the load. This includes the baseline power demand from the fans, which operate continuously to maintain the set temperatures. The compressor's power demand is then characterized based on its operational cycle, which varies with external factors such as ambient temperature and crop harvest schedules.

Next, stochastic elements are introduced to capture variability in crop removal for sales. This involves adding a margin that covers random events, such as the timing and quantity of crops taken out of storage.

The load profile and the load duration curve are constructed using a Python script, which can be found in the Appendix section B. A time series is generated for each day, where the fan load serves as a constant baseline, and the compressor load acts as a variable component. This data is arranged in a CSV file, structured with columns representing each month and rows detailing hourly power values. The variable component accounts for daily and seasonal variations, with adjustments for maximum cooling loads during crop loading events. Furthermore, the load profiles were generated by averaging hourly loads to form a 24-hour daily load profile using average monthly data for ambient conditions and incorporating stochastic variations for crop handling.

To create the load duration curve, the hourly load values were sorted in descending order. This allowed for the calculation of key metrics such as total energy consumption, peak load, and utilization time. Total energy is the annual sum of the hourly loads, peak load is the highest observed load, and utilization time is the ratio of total energy to peak load, indicating the number of hours the system operates at peak capacity.

Finally, plots for daily and monthly load profiles and the load duration curve were generated, with peak load and utilization times clearly marked to visualize the system's operational characteristics.

5.5 Microgrid design

The microgrid design methodology for the cold storage facility is structured to ensure simplicity, reliability, and robustness, in accordance with the challenges of a rural location off-grid. The design process incorporates both intuitive and numerical approaches, each with its own variations. It is important to note that the methods discussed in this thesis represent only few of many possible strategies, and there could be several optimal approaches to address this design challenge.

5.5.1 Design approach: intuitive and numerical

The intuitive design approach requires minimal input data and relies on simpler calculations, often based on 'rules of thumb' or formal standards such as IEEE 1526, IEEE 1013, and IEC TS 62257 (Louie, 2018b, p.396). Although this method is straightforward and suitable for initial design stages, it provides limited feedback on how design choices impact overall system performance. Consequently, this approach may lead to designs with insufficient or excessive reliability. To address this limitation, a numerical approach is employed to complement the intuitive method, providing detailed insights that guide and improve design decisions.

The intuitive approach used in this thesis is based on the methodology presented in Louie (2018a), Section 12.7. The initial design of the system will use a DC-coupled configuration with a PV array as the primary energy source, supported by a battery bank to ensure energy availability during low-sunlight periods. By aligning the microgrid with the DC appliances of the cold storage facility and the storage components, the need for DC-AC power conversions is eliminated, improving overall efficiency. An MPPT charge controller is selected to maximize battery lifespan and optimize energy capture.

Numerical approaches, such as those implemented using simulation software's, provide more detailed insight into system performance, including energy balance, losses, and component interactions. These methods enable fine-tuning of design parameters and provide a

comprehensive understanding of system reliability and efficiency under various conditions.

The methodology was validated by comparing the results of the intuitive approach with numerical simulations performed using PVsyst. This ensured that the design met the operational requirements while complying with the constraints of simplicity, cost-effectiveness, and reliability.

5.5.2 DC Microgrid configuration

The system was designed as a DC microgrid to minimize complexity and potential failure points, particularly for the rural off-grid context of TRAX Ghana. The choice of a DC configuration was guided by the following considerations:

- **Component compatibility:** All essential components, such as fans, compressor, and battery, are equipped with DC power capability. This eliminates the need for an inverter, reducing both initial costs and the need for maintenance.
- **Simplicity and maintainability:** In rural off-grid settings, it is a rule of thumb to keep the system as simple as possible to reduce maintenance requirements and minimize the risk of component failure.
- **Energy efficiency:** By operating entirely on DC, the system avoids the inefficiencies introduced by power conversion processes, maximizing the use of solar energy.

This configuration ensures that the system is robust, cost-effective, and suitable for the rural environment while meeting the operational requirements of the cold storage facility.

5.5.3 Component sizing

The energy needs were estimated based on the load profile developed, taking into account both peak and average energy demands. The sizing process included:

- Calculation of the total daily energy requirement, accounting for monthly variations in solar insolation.
- Identification of the month with the lowest solar insolation using *Peak Sun Hours*, as defined in Equation (5.35):

$$\text{Peak Sun Hours} = \frac{\text{Total Solar Energy (Wh/m}^2\text{)}}{\text{Benchmark Irradiance (W/m}^2\text{)}} \quad (5.35)$$

where the benchmark irradiance is 1000 W/m^2 (Castañer et al., 2012).

- Incorporation of a design margin to account for uncertainties, ensuring that the system could handle unexpected conditions, such as extended periods of low solar insolation.

5.5.4 Component selection

PV modules and batteries were selected based on their availability and suitability for local conditions, with a preference for local suppliers to ensure the accessibility and reliability of the components. A comparative analysis of two sets of components available at the site is presented in Table 5.5.1.

Table 5.5.1: Comparison of Available Components

Component	Option 1	Option 2
PV Module	JA Solar JAM72-S30 565 Wp	Victron Solar Panel 330 Wp
Battery	BYD LVS 8.0KWh Lithium (51.2V)	Victron Gel Deep Cycle 12V/220Ah

5.5.5 Parameters

Voltage level

According to Louie (2018a), voltage levels of 12, 24, or 48 V should be chosen to ensure compatibility with most charge controllers and inverters. A general guideline is to use 12 V for systems with a load less than 1 kWh/day, 24 V for loads between 1 and 4 kWh/day, and 48 V for loads exceeding 4 kWh/day. Given the proximity of the BESS to the load, transmission losses are minimal. In addition, a higher voltage enhances efficiency and minimizes the risk of voltage drops over long distances.

Charge controller

The charge controller is a critical component that ensures compatibility between PV modules, batteries, and the overall system. An MPPT charge controller maximizes energy harvesting from the PV array and extends battery lifespan. The selection process prioritized meeting the following criteria, as recommended by Louie (2018a):

- **Voltage:** The maximum voltage of the controller must exceed that of the PV module V_{oc} at the lowest ambient temperatures.
- **Current:** The controller must meet the maximum short-circuit current of the PV module (I_{sc}).
- **Power:** The controller must handle the peak power output of the PV array without overload.
- **Battery safety:** The controller must ensure that charging and discharging currents remain within the BESS's maximum limits.

These criteria ensure that the system operates reliably, even under challenging environmental conditions.

Optimal Orientation

The orientation of the PV array plays a critical role in maximizing the energy yield. In order to optimize the sunlight exposure, the array tilt was designed to correspond to the site's latitude, and the azimuth was adjusted to face the equator. This was recommended after performing a sensitivity analysis using PVsyst. In addition, the tilt angle will reduce dust accumulation and withstand Harmattan winds by increasing airflow around the modules. These considerations are vital to maintain the efficiency of the system and minimize maintenance needs.

5.5.6 Batteries

Battery selection and sizing are based on three key factors: the nominal voltage of the DC bus, the discharge current, and the reliability requirements, as measured by Days of Autonomy. Days of Autonomy indicate how long the system can function without solar power, typically between 2 and 12 days during the rainy season (Louie, 2018b, p. 401). This factor increases costs due to the need for a larger battery-bank capacity.

The daily average load the battery need to cover is calculated in Equation 5.36:

$$C_{battery,avg} = \frac{P_{load,avg}}{V_{battery\ bank}} \quad (5.36)$$

where $C_{battery,avg}$ is the battery capacity and $P_{load,avg}$ is the load average consumption in kWh. Now, taking the reliability into account:

$$C_{battery} = \text{Days of Autonomy} \times C_{battery,avg} \times 1/\text{end-of-life rating} \quad (5.37)$$

where the end-of-life rating is normally stated in the data sheet.

To prolong battery life, DoD, as explained in subsection 3.7.4, must be taken into account. Normally, at least 20% of the battery charge should be kept after discharge to avoid battery degradation (Ameur et al., 2021). That taken into account, the new battery capacity is:

$$C'_{battery} = C_{battery} \times 1/\text{DoD} \quad (5.38)$$

Now, this should be compared to the battery's cycle life, found in the datasheet, to ensure that the chosen DoD is not too low compared to the expected lifetime. A design margin should also be added to account for the potential under-dimensioning of the load and losses in the BESS:

$$C''_{battery} = C'_{battery} \times (1 + \text{design margin}) \quad (5.39)$$

The final step in designing the BESS is to find the number of series and parallel batteries. To find the number of batteries in series, divide the nominal voltage of the battery bank by the nominal voltage of a single battery as specified in the datasheet. The number of parallel strings required to meet the necessary current is found by dividing the calculated battery bank capacity by the nominal capacity of a single battery from the datasheet. This gives the following equations:

$$\text{Number of series} = \frac{V_{\text{battery bank}}}{V_{\text{battery,nom}}} \quad \text{and} \quad \text{Number of strings} = \frac{C''_{\text{battery}}}{C_{\text{battery,nom}}} \quad (5.40)$$

5.5.7 PV modules

The first step in the design of the PV system is to estimate the total potential energy production. For the month with the lowest solar radiation, the potential for energy production in watt-hours could be found by dividing the average aggregated load by the average insolation, and normally the efficiency of the inverter (Louie, 2018a, p. 407):

$$P_{PV} = \frac{\text{Aggregated load}}{\bar{I}} \quad (5.41)$$

where \bar{I} is the average insolation for the month with the lowest insolation.

In the following equations, generation and storage losses are taken into account (Louie, 2018a, p. 408). This could be factors such as aging, cable losses, temperature, module shading, or dust accumulation, which have been proven to pose a problem for the region. Since there is no inverter losses, the corrected potential energy production will be:

$$P'_{PV} = \frac{P_{PV}}{(1 - loss)} \quad \text{and} \quad P''_{PV} = 100 \times \frac{P'_{PV}}{(100 - \alpha_p \times {}^\circ C)} \quad (5.42)$$

where $loss$ is the total loss (between 0 and 100%), α_p is the the temperature coefficient, given in the data sheet, reflecting the power loss per ${}^\circ$ Celsius increase above the design temperature.

Since the system is designed to provide energy to such a critical load, the design has increased reliability. This contributes to additional energy in the scenario of low insolation or discharged batteries during a period. Louie (2018a) recommends margins up to 0.4 for more critical loads. The PV production with the design margin will be:

$$P'''_{PV} = \frac{P''_{PV}}{(1 - \text{design margin})} \quad (5.43)$$

Determining the number of modules required can be found by dividing PV production by

the nominal power of the module, and is rounded up to the nearest whole number:

$$\text{Number of modules} = \frac{P_{PV}'''}{W_{p,module}} \quad (5.44)$$

To minimize wiring complexity and losses, the array was configured with the maximum number of modules per string, constrained by the controller's V_{oc} rating and current limits:

$$\text{Number of strings} = \frac{\text{Controller rating}}{V_{oc}}$$

where V_{oc} is given by Louie (2018b), p. 411:

$$V_{oc}(T_{ambient}) = V_{oc}(T_{design})(1 + \alpha_v \times (T_{ambient} - 25))$$

In addition, the short-circuit current must not exceed the rating of the charge controller. This can be checked by multiplying the short-circuit current from the datasheet by the number of strings. As short-circuit currents increase proportionally with insolation, a margin of 0.25 should be added (Louie, 2018b, p. 411).

5.6 PVsyst

PVsyst was selected for this project as a comparative method to the intuitive approach to optimize the design of energy systems. Known for its industry-standard simulations, PVsyst provides a comprehensive collection of analytical tools for evaluating system performance. These include detailed evaluations of component reliability, energy balance, and system size, producing results that closely mirror real world conditions (“PVsyst | PVsyst 8”, n.d.). The software’s ability to handle complex scenarios and generate practical insights made it particularly well-suited for the requirements of this off-grid cold storage facility.

Figure 5.6.1 outlines the design methodology in PVsyst, including data input, component selection, and evaluation of results. Each step is explained in the following subsections.

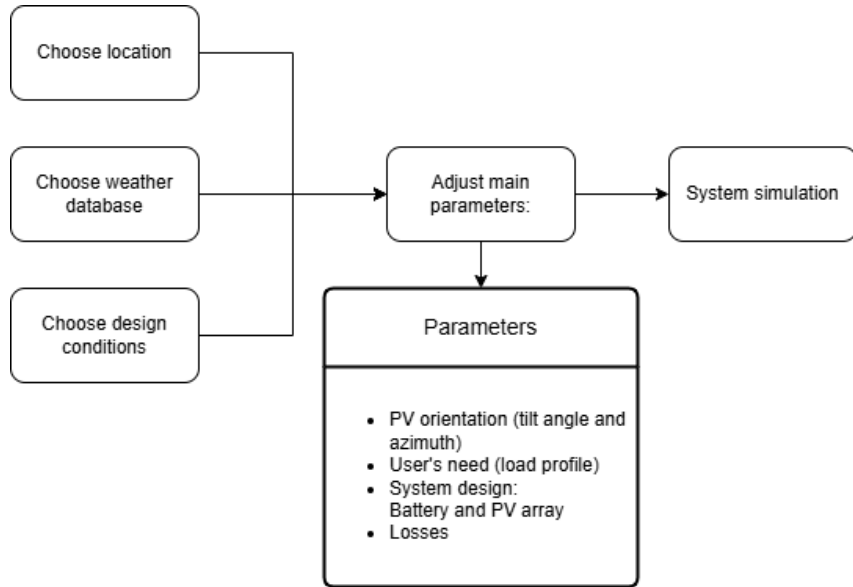


Figure 5.6.1: Flowchart of the methodology in PVsyst.

5.6.1 Meteorological data

Accurate meteorological data are critical for PVsyst simulations, as they directly influence the design and performance predictions. Meteonorm data, already used in other parts of this project, were chosen for consistency. These data were collected for Bolgatanga, the nearest weather station to the cold storage facility. The detailed simulation process was based on the following hourly weather parameters (“PVsyst | PVsyst 8”, n.d.):

- Horizontal Global Irradiance,
- Ambient Temperature,
- Horizontal Diffuse Irradiance (optional, reconstructed using models if unavailable),
- Wind velocity (optional, for module temperature calculations).

These inputs were stored in Meteonorm (*.MET) files and verified for accuracy within PVsyst’s built-in tools. For example, the alignment of solar geometry calculations with time was ensured using the Time Shift parameter, as errors in this alignment could lead to significant inaccuracies in irradiance values.

5.6.2 Inputs and interface

PVsyst requires various input parameters to model standalone systems effectively. These parameters, summarized in Table 5.6.1, include meteorological data, load profiles, and technical specifications for the components of the system. For this project, the load profile was imported as a .CSV file containing hourly data derived from the estimated energy consumption of the cold storage facility. The Python-generated data are detailed in Appendix B.

The choice of components are the same as for the intuitive approach,

Table 5.6.1: Summary of the input data required by PVsyst.

Parameter	Description
Longitude & latitude	Location details for solar and weather data.
Load profile	Hourly energy consumption data.
PV module	Specification of the PV module.
Charge Controller	Specification of controller
Battery	Specification of battery.
Battery voltage	Voltage rating of the battery bank.
Autonomy	Days of Autonomy for the battery pack.
Cost	Component costs.

5.6.3 System simulation

The simulation process in PVsyst was critical to evaluate the system design. Key performance indicators, such as energy demand, excess energy, and losses, were evaluated to validate the system's ability to meet the facility's energy needs. Table 5.6.2 summarizes the available PVsyst results, providing information on system efficiency and highlighting areas for potential optimization.

Table 5.6.2: Summary of the main simulation results in PVsyst.

Parameter
Energy demand [kWh/year]
Useful energy [kWh/year]
Missing energy [kWh/year]
Excess energy [kWh/year]
Array losses

By iterating simulations and adjusting parameters such as array tilt, battery autonomy, and module configuration, the design was refined to achieve a balance between performance, cost, and reliability. This iterative approach underscored the importance of site-specific modeling to ensure the system's robustness.

5.6.4 Losses

The losses within the system were analyzed and optimized using the default PVsyst and user-defined loss parameters. These include thermal losses, module mismatch losses, and

soiling losses, as summarized in Table 5.6.3. Understanding these losses allowed for targeted design improvements, such as optimizing the layout of the array and the tilt angle to reduce shading and thermal inefficiencies.

Table 5.6.3: Summary of default loss parameters from PVsyst (“PVsyst | PVsyst 8”, n.d.).

Parameter	Type	Value	Unit
Constant loss factor (thermal)	Thermal	29	$\text{W}/\text{m}^2\text{K}$
Ohmic loss	Loss fraction at STC	1.5	%
Voltage drop across series diode	Electrical	0.7	V
Module quality	Module mismatch losses	0.5	%
	Module efficiency loss	0.7	%
Soiling loss (annual)	Environmental	3	%

5.6.5 Tilt angle and orientation

PVsyst’s tilt angle optimization tool, illustrated in Figure 5.6.2, enables users to determine the optimal tilt and azimuth angles to maximize the energy yield. The software provides appropriate graphs for the assessment of the transposition factor, where the transposition factor is marked by a violet dot. This tool enables quick evaluation of orientation choice based on site and weather capabilities (“PVsyst | PVsyst 8”, n.d.). The transposition factor will be considered with respect to the annual yield.

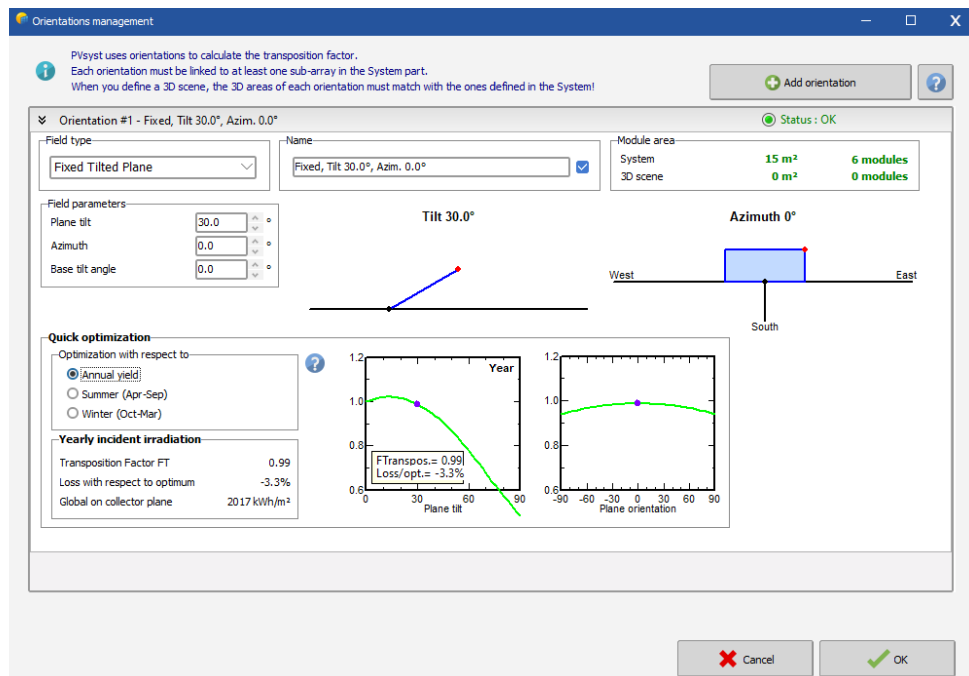


Figure 5.6.2: Figure of the plane optimization tool in PVsyst.

Source: “PVsyst | PVsyst 8”, n.d.

5.6.6 3D Model

The near-shading 3D construction tool in PVsyst, visualized in Figure 5.6.3, is used to create a 3D model of the solar installation site. Using the 3D shading tool, the placement and orientation of the PV modules can be optimized to avoid shading losses. The shading risk is assumed to be zero, as the placement and orientation of the cold storage will be optimized on-site.

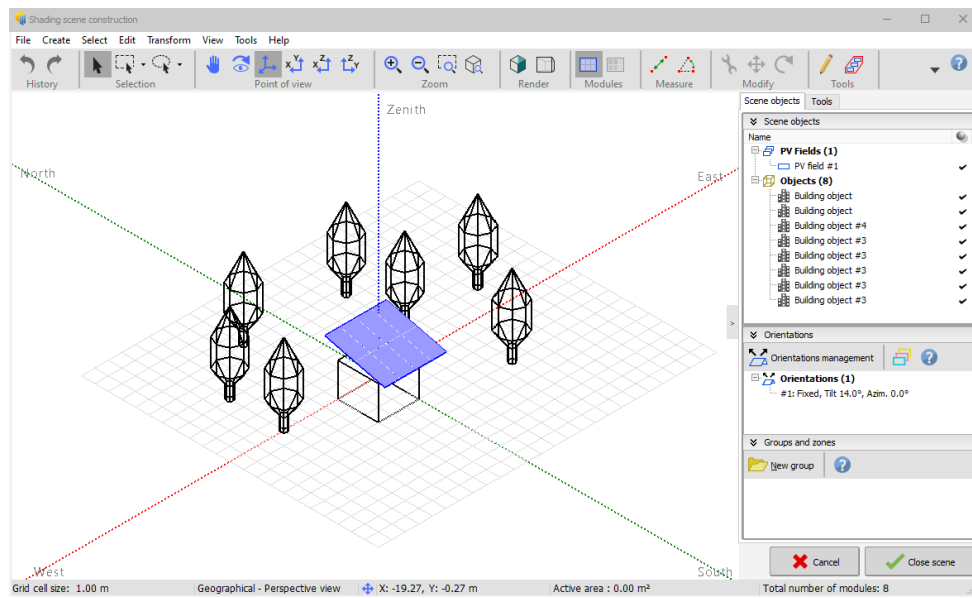


Figure 5.6.3: Figure of the near shading construction tool in PVsyst.

Source: “PVsyst | PVsyst 8”, n.d.

Chapter 6

Results and analysis

6.1 Cold storage design

During initial design discussions with TRAX Ghana about the cold storage unit, they listed some suggestions for the dimensions and the amount of vegetables they should be able to store, as seen in the following list:

- Small: 2m x 2m x 2m ($8m^3$), 600-900 kg.
- Medium: 3m x 3m x 2.5m ($22.5m^3$), 1500-2250 kg.
- Large: 4m x 4m x 4m ($48m^3$), 3000-4500 kg.

The final design chosen is the medium option, where the decision was based on the assumption that the farm expand with three additional greenhouses, producing a total of 2064 kg of vegetables per year. Therefore, even if the entire yearly production is stored, there is no need to expand the cold storage.

The building must be insulated to prevent heat from entering the room. American society of heating (2010) states that for cold storage between -4 and 4 °C, the minimum insulation should be 75 mm thick for a location in the southern United States. For this cold storage, the insulation will be 100 mm thick, to further reduce the transmission load. The insulation chosen is polyurethane with a thermal conductivity of $k = 0.037[\frac{W}{mK}]$ (American society of heating, 2010). To prevent moisture from entering the cold storage, there will be a vapor barrier between the outer wall and the insulation. In the interior of the cold storage, a thin wall will be installed to protect the insulation from external penetration. Furthermore, there will be a simple plastic air curtain outside the entrance of the cold storage to prevent the free flow of air to enter the cold storage when the door is open.

In addition, the cold storage is designed to facilitate optimal storage of the relevant vegetables listed in section 3.2. Table 3.2.1 specifies the storage requirements, and the chosen

solution is to divide the cold storage unit into two rooms with equal relative humidity but different temperature. However, there will be an issue when storing tomatoes, as the optimal storage temperature is 13 °C, and produces high amounts of ethylene. Therefore, it is essential to plan crop production, with possible production scenarios demonstrated in Table 6.1.1:

	Scenario 1		Scenario 2		Scenario 3	
	Room 1	Room 2	Room 1	Room 2	Room 1	Room 2
Vegetables	Lettuce, Cabbage	Bell peppers, Hot peppers, Cucumber	Lettuce, Cabbage	Tomatoes	Bell peppers, Hot peppers, Cucumber	Tomatoes
Temperature [°C]	1	10	1	13	10	13
Relative humidity [%]	90	90	90	90	90	90

Table 6.1.1: Different scenarios for storage of crops.

There are other options than the three scenarios in Table 6.1.1, such as storing tomatoes, hot peppers, and bell peppers together, as they are not ethylene sensitive. However, this means storing tomatoes at 10 °C, which could cause damage due to low temperature, or store bell peppers and hot peppers at 13 °C, which would cause faster deterioration.

In addition, to ensure rapid crop cooling, a small tunnel is included in the design of each of the two rooms. In these tunnels, there will be a heat exchanger and a fan to circulate the cool air. This form of air cooling is forced ventilation through circulation, described in subsubsection 2.2.1.1. The tunnel is designed to fit three plastic storage boxes with dimensions: 53 x 36 x 29 cm, which means that the dimensions of the tunnel design are: 159 x 40 x 33 cm. Figure 6.1.1 and Figure 6.6.1 show the final sketches and simple 3D model of the cold storage, based on the parameters listed above.

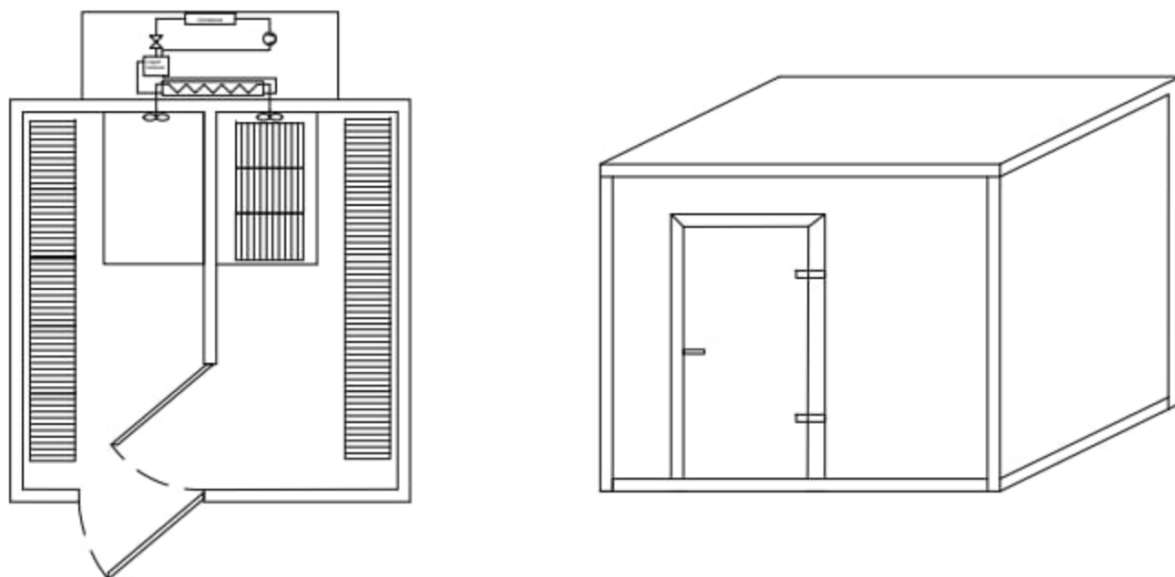


Figure 6.1.1: 2D and 3D illustrations of the cold storage.

6.2 Cold storage simulation and calculation results

6.2.1 Refrigeration load calculations

The refrigeration loads are estimated using a combination of Microsoft Excel and the programming language Python. This means that temperature and time-variable functions will be simulated in Python before being inserted into an Excel sheet to calculate the refrigeration load. For each specific section, this will be specified. Furthermore, ambient temperatures will greatly affect the refrigeration loads. Therefore, the calculations will be based on the highest monthly average temperature, which is in April. Table 6.2.5 shows the hourly temperatures in April, where the yellow markings between 08:00 and 17:00 are the hours with sunlight.

6.2.1.1 Thermal properties

The thermal properties are temperature dependent but do not differ widely in the relevant temperature ranges because there are no phase changes. Therefore, an average value is utilized to model the thermal properties in Python as presented in Table 5.3.2. This means the difference between the ambient temperature outside and the desired temperature inside the storage, divided by two. The ambient temperature will vary depending on the time of day, so the highest temperature is used to find the maximum refrigeration load. As for the constituents of the vegetables, although similar, each composition will vary. The vegetable compositions listed in Table 5.3.1 could have small variations, but are derived from a credible source in American society of heating (2010). The simulation of the thermal property models calculates the total thermal property by summing all constituent properties. Table 6.2.1 shows the results of the simulation for thermal conductivity, density, and specific heat.

Crop	Thermal conductivity [$\frac{W}{m \cdot K}$]	Density [$\frac{kg}{m^3}$]	Specific heat [$\frac{kJ}{kg \cdot K}$]
Tomatoes	0.57	1030	3975
Bell peppers	0.56	1044	3935
Hot peppers	0.55	1063	3832
Lettuce	0.58	1011	4026
Cabbage	0.57	1021	3932
Cucumber	0.58	1019	4030

Table 6.2.1: Thermal conductivity, density, and specific heat for the relevant crops.

6.2.1.2 Cooling time

The cooling time is simulated in Python and uses the thermal conductivity, the specific heat and the density of the vegetables from the simulated thermal property models in Table 6.2.1. The Biot number and the thermal diffusivity given in Equation 5.9 and Equation 5.10 are considered constants and are calculated as part of the cooling function. Furthermore, in equation 5.9, h is the convective heat transfer coefficient that is in contact with the produce. As discussed previously, the cooling will be done mainly inside the cooling tunnels. Therefore, the heat transfer coefficient will be larger here than in the rest of the storage, because a fan is located at the beginning of the tunnel. This value is difficult to find theoretically and therefore a predefined value of $25 \frac{w}{m^2 \cdot K}$ is used.

Furthermore, the thickness of the crops is listed in Table 6.2.2 and are essential for calculating the cooling times.

Crop	Thickness [cm]
Tomatoes	5.6 (Schwartz et al., 2014)
Bell peppers	1 (Decorexpo, 2024)
Hot peppers	0.75 (Starkeayres, 2020)
Lettuce	17 (Sreejariya et al., 2016)
Cabbage	17 (Rana et al., 2019)
Cucumber	4 (Wikipedia, n.d.)

Table 6.2.2: Thickness of the different crops.

As harvesting is predicted to be split into two equal parts during the day, the cooling time will vary as a result of the increasing temperature throughout the day. After internal discussions with TRAX Ghana, harvesting is expected to occur between 07:00 and 08:00. The cooling times for each product at 07:00 and 08:00 with temperatures of 28.4°C and 29.9°C, respectively, are listed in Table 6.2.3:

Crop	Cooling time at 07:00 [minutes]	Cooling time at 08:00 [minutes]
Tomatoes	29	31
Bell peppers	27	29
Hot peppers	12	13
Lettuce	329	335
Cabbage	330	336
Cucumber	46	48

Table 6.2.3: Time needed for each crop in minutes

6.2.1.3 Transmission load

Calculations are performed in an Excel spreadsheet using Equation 5.22. Due to the low thermal conductivity of the insulation, the insulating effect of the outer steel layer, the plastic coating, and the inner wall is neglected due to their high thermal conductivity and small thickness. Furthermore, the cold storage is chosen to be white, which means that the values of the temperature increase from direct sunlight for light-colored surfaces in Table 5.3.4 are used. However, since there will be a solar panel on the roof of the cold storage, the increase in temperature on the roof is negligible. In addition, the surface areas of the different walls are shown in Table 6.2.4. Here, the eastern and western wall is divided between the two rooms, room 1 is facing north, and room 2 is facing south.

	Room 1 (1 °C)	Room 2 (10 °C)	Unit
East/West	3.75	3.75	m^2
South	0	7.5	m^2
North	7.5	0	m^2

Table 6.2.4: Room measurements for east/west, south, and north facing walls.

Furthermore, due to fluctuations in temperature during the day, the calculations are performed hourly and it is assumed that the temperature below the floor is 3°C lower than the ambient temperature. This results in a maximum $\dot{Q}_{trans} = 0.587kW$. Table 6.2.5 illustrates the average transmission load for April.

Time	Temperature [°C]	Transmission load [kW]
01:00	29.8	0.432
02:00	29.0	0.419
03:00	28.6	0.412
04:00	28.2	0.404
05:00	27.9	0.399
06:00	27.8	0.398
07:00	28.4	0.408
08:00	29.9	0.435
09:00	31.6	0.465
10:00	33.5	0.497
11:00	35.2	0.527
12:00	36.7	0.553
13:00	37.8	0.572
14:00	38.4	0.583
15:00	38.7	0.587
16:00	38.3	0.582
17:00	37.4	0.566
18:00	36.2	0.544
19:00	34.9	0.521
20:00	33.9	0.505
21:00	33.0	0.489
22:00	32.1	0.474
23:00	31.2	0.458
00:00	30.3	0.442

Table 6.2.5: Hourly average temperature and transmission load data for April

In addition, the lowest ambient temperature will be in January, resulting in the lowest transmission load. The total average transmission loads for January and April are $Q_{trans} = 8.64\text{kWh}$ and $Q_{trans} = 11.67\text{kWh}$, respectively. These are presented on an average hourly basis in Figure 6.2.1.

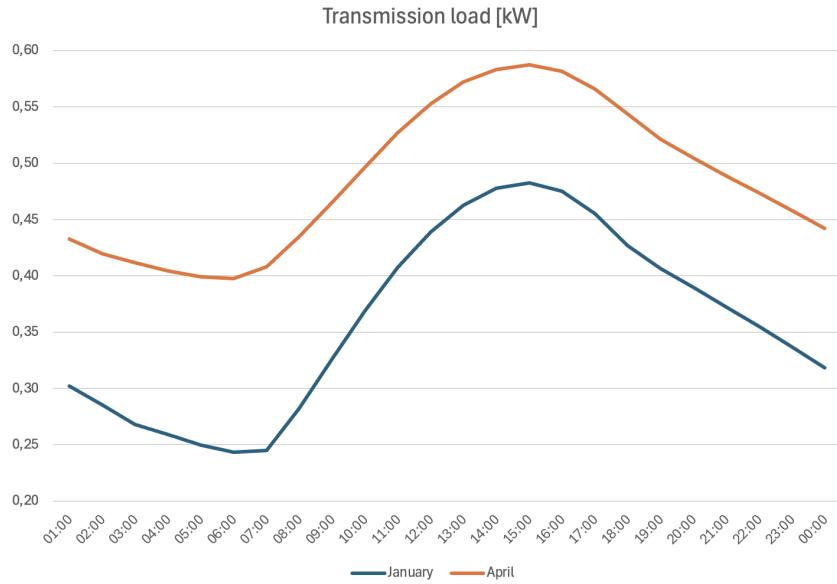


Figure 6.2.1: Average transmission load for January and April in kW.

The average transmission load for the entire year is presented in Figure 6.2.2.

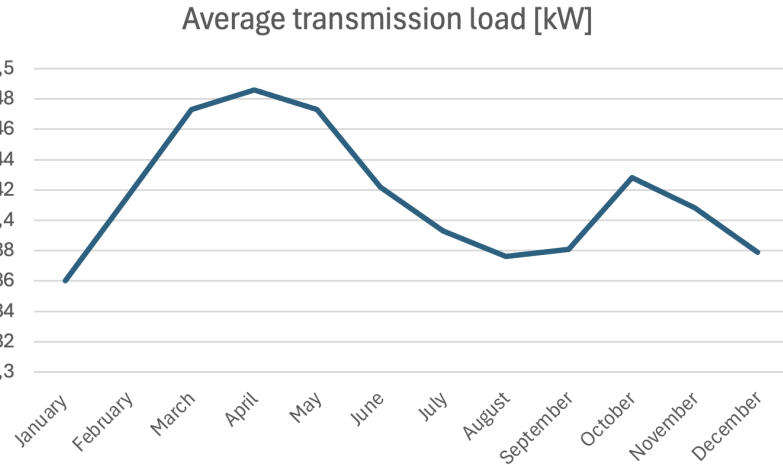


Figure 6.2.2: Average transmission load for the entire year.

6.2.1.4 Product load

The product load calculations are performed in Excel and are based on the thermal properties listed in Table 6.2.1, the cooling time in Table 6.2.3, the temperatures in Table 6.2.5, and the largest predicted mass. To decrease the product load, harvesting will occur twice daily, once at 07:00 and once at 08:00. Harvesting in the morning will also result in the vegetables having a lower temperature when entering the cold storage, further reducing the product load. The maximum harvest during a day is assumed to be a total of 40 kg combined for the two daily harvests, which is estimated to be 20 kg for each. The product load in kW is calculated using Equation 5.26 and remains

constant throughout the cooling time specified in Table 6.2.3. Furthermore, lettuce has the highest total amount of heat that must be removed; $Q_{lettuce} = 1.29 \text{ kWh}$, as it has a high heat capacity and the lowest optimal storage temperature. However, due to the predicted cooling time, cucumber has the highest product load of $\dot{Q}_{cucumber} = 0.45 \text{ kW}$. The compressor is sized to manage the cooling load of lettuce at $\dot{Q}_{lettuce} = 0.23 \text{ kW}$, which can increase the cooling duration of tomatoes, bell peppers, hot peppers and cucumbers due to its lower peak capacity. The heat that must be removed for each product is listed in Table 6.2.6.

Crop	Heat removed [kJ]	Heat removed [kWh]	Product load per daily harvest [kW]
Tomatoes	2688	0.75	0.37
Bell peppers	3140	0.87	0.44
Hot peppers	3049	0.85	0.43
Lettuce	4655	1.29	0.12
Cabbage	4545	1.26	0.11
Cucumber	3208	0.89	0.45

Table 6.2.6: Total heat removal and daily harvest product load required to cool vegetables to the target temperature.

6.2.1.5 Infiltration load

The calculations are based on some assumptions made during internal discussions with TRAX Ghana about the number of times they enter the room in a day. All harvesting should be done within two hours in the morning, resulting in a specified time interval. As each crate would be able to contain about 20 kg of produce, the door will be opened four times a day. However, in reality, the door will open more due to unforeseen events. Therefore, as an overestimate of the maximum open times, the number 16 is used, which also accounts for the door being opened to remove crops. Furthermore, the area of the door is 2 m^2 and the enthalpies and densities for air inside and outside the cold storage are found in the book Moran et al. (2014). Since the type of door could vary depending on the availability in the area, the estimated time used in the calculations is 20 seconds per opening/closing. This equals a total of 321 seconds spent open per day. The doorway protection chosen is air curtains, which have a protection value of 0 to 0.7. The value chosen for this cold storage is 0.6. This leads to $\dot{Q}_t = 32 \text{ W}$ as the infiltration load. These assumed parameters are listed in 6.2.7:

P	$\theta_p[\text{s}]$	$\theta_o[\text{min}]$	$\theta_d[\text{h}]$	D_f	E_f
2	321	5.35	2	0.8	0.6

Table 6.2.7: Values used in the infiltration load calculation

6.2.1.6 Internal load

The internal load of this cold storage is calculated in the Excel spreadsheet as $\dot{Q}_p = 266W$. This is the heat gain of the people who occupy the room. Furthermore, the heat gained from the fan will be neglected, as this amounts to an insignificant heat gain due to the predicated small power consumption. The potential additional heat from defrosting the evaporator will also be neglected. As it is uncertain how long and how many times people will occupy the room, the internal load is assumed constant throughout the two hours of harvest, to ensure an over- rather than an underestimation.

6.2.1.7 Total load

As described earlier, the maximum refrigeration load will fall on a harvesting day in April, as this is the warmest month. Therefore, the total refrigeration capacity will be dimensioned according to this. The total maximum load will fall between 08:00 and 09:00 and is calculated as $\dot{Q}_{tot} = 0.43 + 0.23 + 0.3 = 0.96[kW]$. Table 6.2.8 and Figure 6.2.3 illustrate the maximum daily total load for each of the vegetables.

Time	Temperature [°C]	Total load [kW]					
		Lettuce	Tomatoes	Bell peppers	Hot peppers	Cabbage	Cucumber
01:00	29.8	0.43	0.43	0.43	0.43	0.43	0.43
02:00	29	0.42	0.42	0.42	0.42	0.42	0.42
03:00	28.6	0.41	0.42	0.41	0.41	0.41	0.41
04:00	28.2	0.40	0.40	0.40	0.41	0.40	0.40
05:00	27.9	0.82	1.05	1.11	1.10	0.82	1.12
06:00	27.8	0.43	0.46	0.46	0.46	0.43	0.47
07:00	28.4	0.96	1.09	0.96	0.99	0.96	1.06
08:00	29.9	0.75	0.55	0.53	0.53	0.75	0.53
09:00	31.6	0.72	0.57	0.57	0.57	0.72	0.58
10:00	33.5	0.68	0.55	0.55	0.54	0.68	0.58
11:00	35.2	0.62	0.58	0.58	0.58	0.62	0.58
12:00	36.7	0.59	0.59	0.59	0.59	0.59	0.59
13:00	37.8	0.54	0.53	0.54	0.54	0.54	0.54
14:00	38.4	0.50	0.51	0.50	0.50	0.50	0.51
15:00	38.7	0.47	0.47	0.47	0.47	0.47	0.47
16:00	38.3	0.44	0.44	0.44	0.44	0.44	0.44
17:00	37.4	0.57	0.57	0.57	0.57	0.57	0.57
18:00	36.2	0.54	0.54	0.54	0.54	0.54	0.54
19:00	34.9	0.52	0.52	0.52	0.52	0.52	0.52
20:00	33.9	0.50	0.50	0.50	0.50	0.50	0.50
21:00	33	0.49	0.49	0.49	0.49	0.49	0.49
22:00	32.1	0.47	0.47	0.47	0.47	0.47	0.47
24:00	31.2	0.46	0.46	0.46	0.46	0.46	0.46
00:00	30.3	0.44	0.44	0.44	0.44	0.44	0.44

Table 6.2.8: Maximum total daily load [kW] for the relevant crops.

The total maximum load takes into account the predicted cooling time for each of the crops, resulting in a larger peak load for tomatoes, bell peppers, hot peppers, and cucumbers at 07:00 and 08:00.

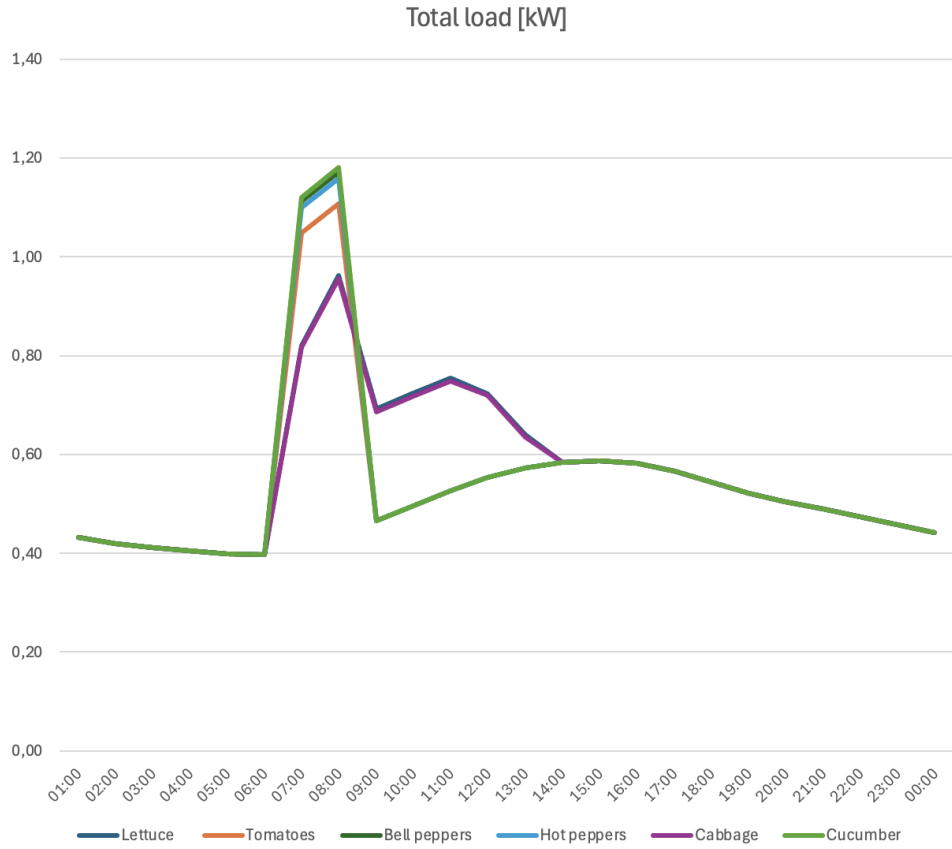


Figure 6.2.3: Maximum total daily load [kW] for the relevant crops.

6.2.2 Compressor work

The compressor load was initially estimated in Excel using the COP from Equation 5.33. The temperature T_L was set to 1°C , and T_H was adjusted according to the hourly average temperature in April. A cycle efficiency $\eta = 0.4$ was assumed. Based on this setup, Equation 5.34 was used to determine the compressor work. Table 6.3.2 outlines the predicted COP and the equivalent compressor work required for cooling lettuce, with an extra 1.1 factor for safety, as advised by American society of heating (2010).

6.3 Refrigeration system simulation

Although direct systems remain the common choice for refrigeration, an indirect system was selected for this cold storage facility. There are two primary reasons for this. The first is due to the different temperatures in the two cold rooms. Having a separate heat exchanger in each of the two rooms facilitates easier temperature regulation. As men-

tioned previously, the indirect system performed better when multiple heat exchangers were involved. The second reason is the flammable nature of the selected refrigerant, R290. From section 3.3, it was stated that the natural and environmentally sustainable refrigerants R717, R290, and R600a are available in Ghana. Following internal discussions at NTNU and consultations with people at the farm, refrigerant R290 was chosen. The primary refrigeration cycle circulating R290 is enclosed in a container equipped with fire safety mechanisms to enhance protection against leaks and potential ignition.

The chosen secondary refrigerant is a water and sodium chloride mixture, which is considered the least harmful single-phase option for humans. Circulating within cold storage, this refrigerant benefits from its non-flammable properties. This mixture will contain 18.8% sodium chloride to avoid freezing, with a freezing point of -15°C. The mixture will operate solely in a single phase, necessitating the use of countercurrent air heat exchangers instead of evaporators. These heat exchangers will have a relatively large surface area and operate at a maximum temperature difference of 5°C with the cold storage, in order to maintain high relative humidity inside the rooms.

Stage:	Enthalpy [kJ/kg]	Pressure [bar]
1	565	3.57
2	649	15
3	319	15
4	319	3.57

Table 6.3.1: Enthalpy and Pressure at Different Stages

The simulated stages of the primary refrigeration cycle is presented in Table 6.3.1. For the highest refrigeration load of $\dot{Q} = 0.96 \text{ kW}$, using Equation 5.5, the simulated compressor work is $\dot{W}_{comp} = 0.278 \text{ kW}$. Similarly to subsection 6.2.2, a factor of 1.1 is added as a margin for the compressor work. Additionally, the mass flow rate needed to handle the refrigeration load is estimated to be $\dot{m} = 0.0035 \text{ kg/s}$ from Equation 5.4. Both compressor work and COP for a lettuce harvesting day in April are listed in Table 6.3.2.

Time	Coolprop		Excel	
	COP	\dot{W}_{comp} [kW]	COP	\dot{W}_{comp} [kW]
01:00	3.80	0.124	3.68	0.129
02:00	3.90	0.119	3.77	0.122
03:00	3.95	0.114	3.83	0.118
04:00	3.99	0.110	3.89	0.114
05:00	3.97	0.109	3.93	0.112
06:00	3.97	0.109	3.94	0.111
07:00	3.97	0.227	3.86	0.234
08:00	3.79	0.278	3.66	0.289
09:00	3.60	0.211	3.46	0.220
10:00	3.41	0.232	3.28	0.243
11:00	3.25	0.254	3.11	0.267
12:00	3.11	0.255	2.99	0.266
13:00	3.02	0.233	2.90	0.242
14:00	2.97	0.215	2.85	0.225
15:00	2.94	0.221	2.86	0.228
16:00	2.98	0.214	2.86	0.224
17:00	3.05	0.205	2.89	0.212
18:00	3.16	0.188	3.03	0.197
19:00	3.28	0.175	3.14	0.182
20:00	3.37	0.163	3.23	0.172
21:00	3.46	0.156	3.22	0.162
22:00	3.55	0.146	3.41	0.153
23:00	3.65	0.139	3.51	0.143
00:00	3.75	0.129	3.61	0.135

Table 6.3.2: COP and compressor work from CoolProp and Excel for lettuce cooling throughout a day in April.

6.3.1 Pump work

The simulation of the fluid pump work needed to circulate a water and sodium chloride mixture in the secondary circuit for cooling purposes is performed using Python and the CoolProp library. From Equation 5.7, only the pressure difference, the specific volume, and the mass flow rate must be known. To obtain exact values, the pressure drop must be calculated extensively. It is assumed that there is a pressure drop of 0.25 bar for each of the heat exchangers, resulting in a total pressure drop of 0.5 bar. From CoolProp, the specific heat capacity of the sodium chloride and water mixture is $C_p = 3.41 \frac{kJ}{kg \cdot K}$ and the specific volume is $v = 0.00087 \frac{m^3}{kg}$. Equation 5.8 determines the mass flow rate as $\dot{m} = 0.07 \frac{kg}{s}$, given a total refrigeration load of $\dot{Q}_{tot} = 0.96$ kW and a temperature difference of $\Delta T = 4^\circ C$. Equation 5.7 provides the calculation for pump work, resulting

in $\dot{W}_{pump} = 3.1$ W.

6.4 Load profile

The load profile was created for a cold storage facility consisting of two temperature controlled rooms, with Room 1 kept at 1°C and Room 2 at 10°C. The cold storage facility includes a compressor and two continuously running fans, summarized in Table 6.4.1:

Table 6.4.1: Power consumption of various appliances

Appliances	Consumption (kWh/yr)	No. appliances	Tot. use (min/day)	Avg. consumption (Wh/day)
Cold Storage	1255	1	1440	3440.8
Fan	1752	2	1440	4800
Total:	3007	3	1440	8240.8

The daily load profile, shown in Figure 6.4.1, represents the aggregate load averaged over a single day for the two seasons. It highlights the variation in power demand at different hours of the day. A noticeable increase in load is observed in the early morning (around 6:00 a.m.), which corresponds to the start of intensive compressor operation during the harvesting period. The load gradually decreases in the afternoon and further decreases during the evening and night as the cooling demand decreases.

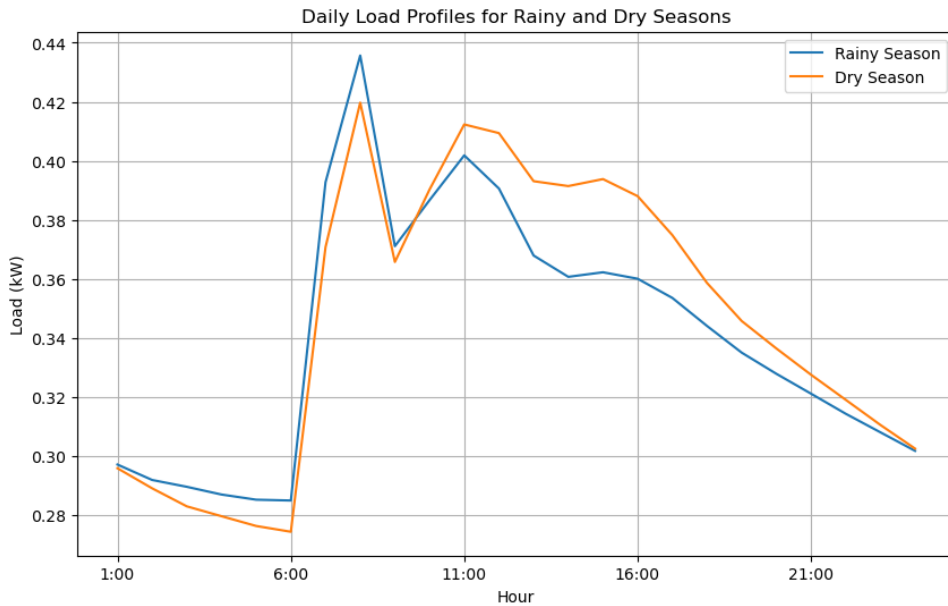


Figure 6.4.1: Daily Seasonal Load Profile of the Cold Storage Facility

The monthly load profile, shown in Figure 6.4.2, indicates the average daily load for each month. The profile differentiates dry season months in yellow and rainy season months in blue. The profile demonstrates relatively consistent power demand throughout the year,

with a slight decrease in the middle of the rainy season. These variations are attributed to seasonal changes in ambient temperatures that affect the cooling requirements of the storage facility. The fan load remains constant, contributing to a stable base load throughout all months.

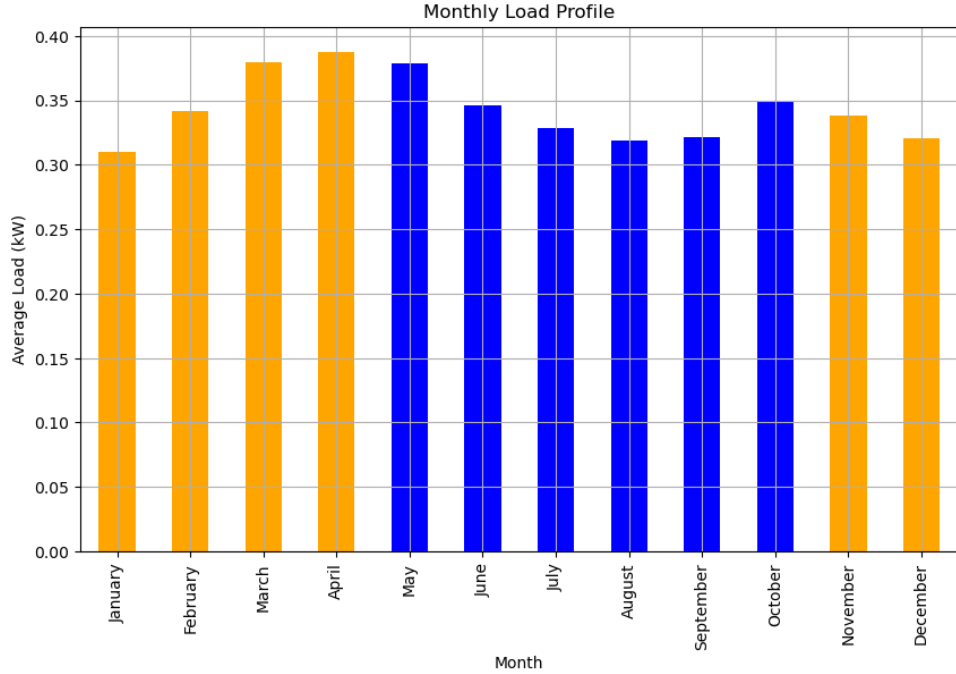


Figure 6.4.2: Daily Load Profile of the Cold Storage Facility

The load duration curve, shown in Figure 6.4.3, provides information on the distribution of power usage over the year. The red line represents the aggregated hourly load sorted in descending order, illustrating the peak and base loads. The peak load is marked by the horizontal orange line at approximately 0.43 kW, and the vertical orange line indicates the number of hours for which the system would need to operate at peak capacity to meet total energy demand. This curve is important in understanding the reliability of the system and evaluating the operating capacity of the cooling system.

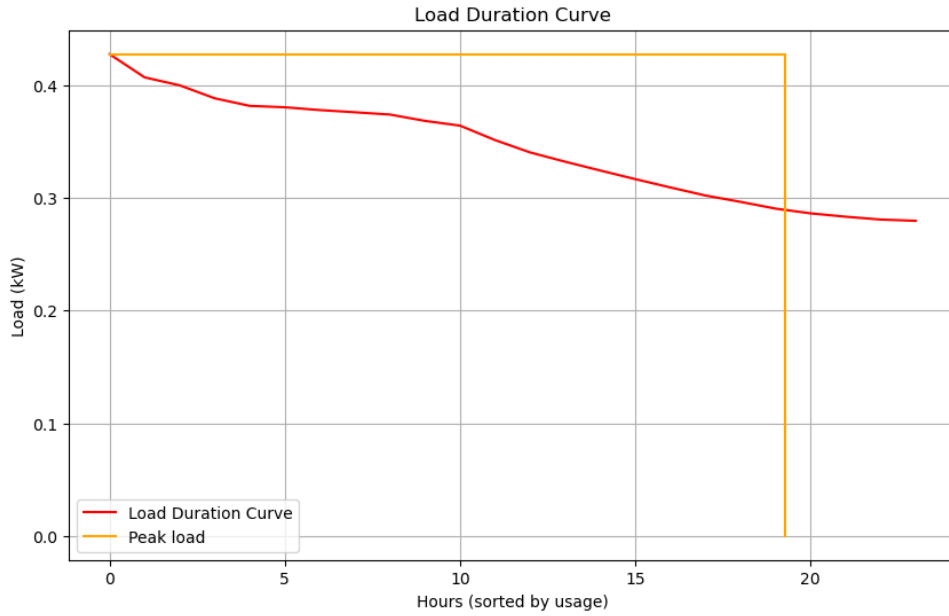


Figure 6.4.3: Daily Load Profile of the Cold Storage Facility

6.5 Microgrid design

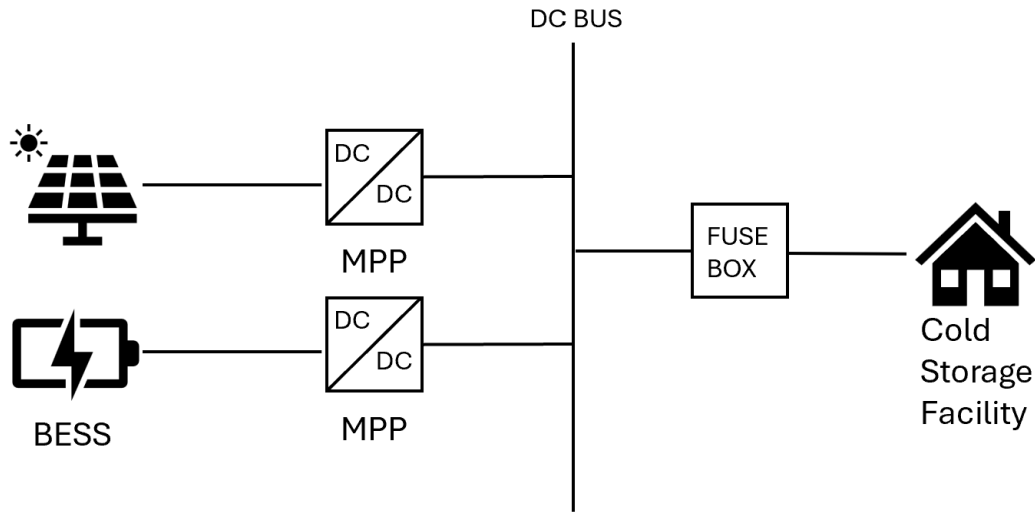


Figure 6.5.1: A simple system topology for the off-grid system after design

Source: All icons are either made by student or taken from Microsoft PowerPoint's icon library

Figure 6.5.1 visualize the topology of the off-grid system for the SPCS facility. An inverter is not required to handle the load, and conversion losses can be neglected as the microgrid is powered by a DC distribution system. The layout includes the PV array mounted above the cold storage facility and the DC components located nearby. The selection of

PV modules and batteries was based on the availability of local suppliers, as indicated in previous invoices, to ensure that all components are accessible and appropriate for the location of the project. A comparative analysis of the available options was conducted.

The following is a summary of the key parameters of the intuitive approach:

- **Daily average load:** 8240.77 Wh/day. The peak load occurred in April, with a value of 488.78 W.
- **Voltage level:** For the DC bus, a nominal voltage of 48 V was selected based on established guidelines. According to Louie (2018b), a 48 V system is recommended when the daily load exceeds 4 kWh, as it minimizes the size of the wire and transmission losses.
- **Battery capacity:** Calculated as 1153.49 Ah, including an end-of-life rating of 80%, a DoD of 20%, and a safety margin of 7.5%.
- **PV system capacity:** Corrected energy production of 3.40 kWp with a tilt angle of 14°.
- **Module area:** The required area of the PV module is 15.48 m², which exceeds the cold storage roof area (9 m²), making additional structural support necessary.

6.5.1 Component selection

The system was designed on the basis of the daily load profile and the peak sun hours during the month with the lowest solar insolation (August). A comparative analysis of PV modules and battery types was performed:

PV Modules:

- *JA Solar JAM72-S30 565W Module:* Cost of 116.55 USD/piece, requiring 6 modules with a maximum of 4 per string.
- *Victron Solar Panel 330W-24V Poly Module:* Cost of 152.21 USD/piece, requiring 11 modules with a maximum of 5 per string.

Decision: The selected PV module, JAM72S30-565 (Appendix C), was chosen for its compatibility, cost-effectiveness, and availability from local suppliers. Although this specific module was not included in the PVsyst database, its technical parameters were manually entered using a similar module by the same manufacturer. The key specifications are summarized in Table 6.5.2. Its high efficiency and optimal performance under local climate conditions made it a suitable choice for this project.

Table 6.5.1: Electrical Parameters at NOCT for JAM72S30-565.

Parameter	Value
Rated Max Power (Pmax)	565 W
Open Circuit Voltage (Voc)	50.28 V
Max Power Voltage (Vmp)	42.42 V
Short Circuit Current (Isc)	14.21 A
Max Power Current (Imp)	13.32 A
Module Efficiency (%)	21.9
NOCT Conditions	Irradiance: 800 W/m ² Ambient Temp: 20°C Wind Speed: 1 m/s

Batteries:

- *BYD LVS 8.0 kWh* Lithium Battery: Cost of 1437.5 USD/piece, with a configuration of 8 batteries in a single string (51.2 V).
- *Victron 12V/220Ah* Gel Deep Cycle Battery: Cost of 572 USD/piece, with a configuration of 6 batteries per string and 4 strings.

Decision: The BYD LVS Lithium batteries were selected due to their higher energy density, longer lifecycle, and lower LCOE compared to Victron Gel batteries.

Table 6.5.2: Electrical Parameters at for BYD LVS 8.0 kWh.

Parameter	Value
Rated Capacity	156 Ah/8 kWh
Nominal Voltage	51.2 V
Max Output Current	130 A
Round Trip Efficiency	≥ 95%

Charge controller:

Since no information on the local availability of charge controllers is successfully retrieved, only recommendations for charge controller specifications are provided:

- Satisfy the voltage, current, and power constraints.
- Include MPPT functionality to extend the lifespan of BESS.
- Ensure that the maximum current does not exceed the BESS rating.

Based on the constraints, the charge controller must satisfy the technical specifications listed in Table 6.5.3:

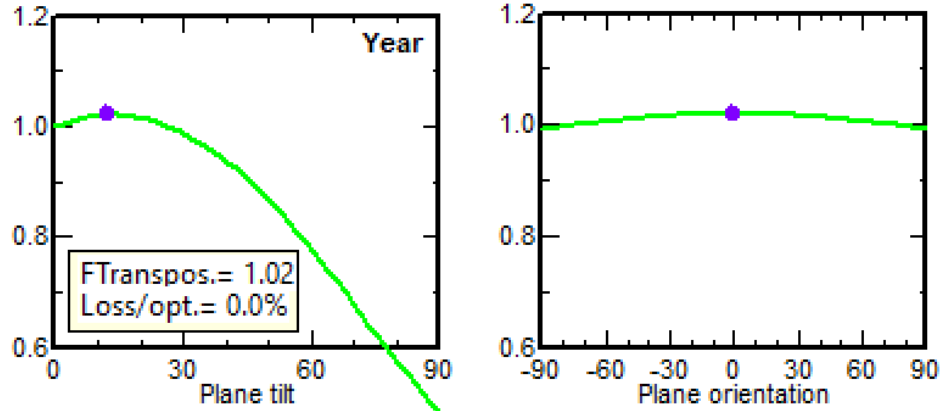
Table 6.5.3: Summary of the specifications of the Charge Controller

Specification	Required
Nom. Controller Power	>3400 W
Short-Circuit Current (I_{sc})	>28.42 A
Maximum Open-Circuit Voltage ($V_{oc, \text{max}}$)	>100.56 V

Optimal orientation

As the cold storage facility is built as an independent building on the site, this allows customization of the module orientation to optimize performance at this location.

According to the sensitivity analysis performed in PVsyst, the ideal plane tilt is between 12° and 14° , with an azimuth of 0° , maximizing the annual yield. This configuration results in an annual incident irradiation of 2086 kWh/m^2 on the collector plane. Designing in relation to annual yield results in a yield loss of -3.4% from April to September (PVsyst definition of Summer) and -4.4% from October to March (Winter) compared to the absolute optimum. The optimization curve is shown in Figure 6.5.2.

**Figure 6.5.2:** Figure of the optimal tilt angle in PVsyst.

Source: “PVsyst | PVsyst 8”, n.d.

6.5.2 Battery design

The DC bus operates at 48 V. The average battery capacity required is calculated based on a daily average load of 8.24 kWh/day. Taking into account an end-of-life rating of 80%, 20% DoD, and a safety margin of 7.5%, the necessary capacity was calculated using Equation 5.39. Finally, the capacity specification as specified in Table 6.5.4 is equal to 1153.49 Ah with a battery bank configuration of 1 series of 8 batteries in parallel, which

corresponds to a 51.2 V battery system operating at 48 V, with an autonomy of 4 days due to the criticality of the load.

Table 6.5.4: Summary of the battery bank configuration

Specification	Value
Number of Series	1
Number of Strings	8
Total Battery Capacity	1153.49 Ah

6.5.3 PV system design

The potential energy production of the PV system is initially calculated as 1.47 kW, using Equation 5.41. Adjusting for a 20% assumed efficiency loss and considering the temperature coefficient of $\alpha_p = -0.35\%/\text{°C}$, it increases to 2.04 kW. Although August is in the rainy season, based on the average from 1991 - 2010, it is not common to have several days with too low insolation. Therefore, a design margin of 0.4 has been chosen due to the criticality of the cold storage facility. With a reliability design margin, the final energy production is approximately 3.40 kWp. For this setup, approximately 6 modules are needed with a maximum of 4 modules per string.

With a PV system design of 2 strings of 3 modules, the total array output is equal to the required 3.40 kW. This results in a short-circuit current of $14.21 \text{ A} \times 2 \text{ strings} = 28.42 \text{ A}$. In addition, the open-circuit voltage, V_{oc} , at the coldest temperature (19°C in January) is 100.56 V.

Table 6.5.5: Summary of the PV system design

Component	Value
Average Insolation (August)	5.04 kWh/m ²
Module W_p	565 W
Corrected Energy Production	3.40 kWp
Modules required	6
Nb. of strings	2 strings
Tilt Angle	14°

PV modules area:

- Area required for one single module (m^2): $2278 \text{ mm} \times 1134 \text{ mm} (\times 30 \text{ mm}) = 2.58 m^2$
- Area required for all modules (m^2): $2.58 \text{ m} \times 6 = 15.48 m^2$
- Cold storage facility area (m^2): $3 \text{ m} \times 3 \text{ m} = 9 m^2$.

6.6 PVsyst simulation

The PVsyst simulation validated the system design and provided detailed information on energy production, system losses, and battery performance. A visualization of the facility is modeled in PVsyst and can be seen in Figure 6.6.1.

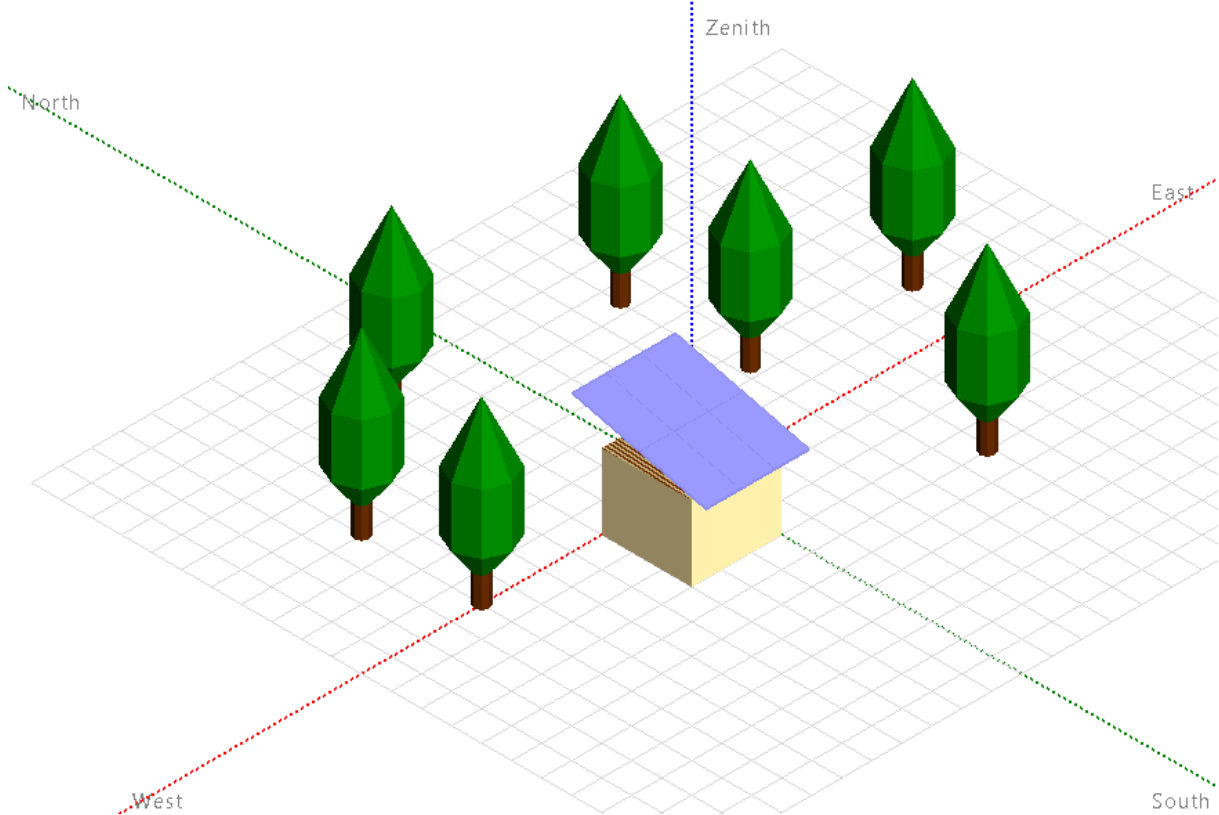


Figure 6.6.1: 3D scene of the cold storage facility with 3 modules on 2 strings . Trees are just for aesthetics.

6.6.1 System overview

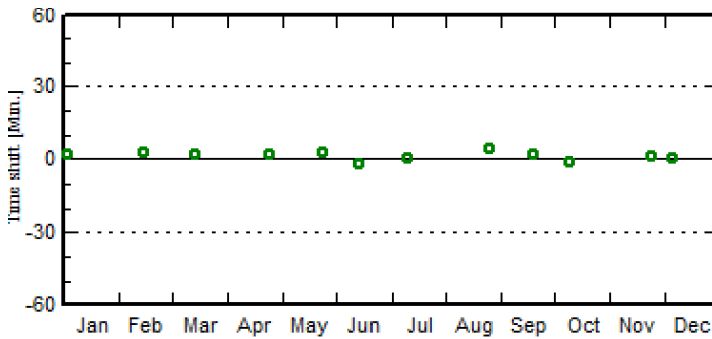
The PV array consists of **4 modules** with a total nominal power of **2260 Wp**. The modules are configured as a single string of 4 modules. The system includes a lithium-ion battery pack (LFP) comprising **5 units**, each with a nominal capacity of **165 Ah at 51 V**. The tilt and azimuth angles of the system were set at 14° and 0° , respectively, to optimize the capture of solar energy.

The PV array was simulated using meteorological data from Bolgatanga, which is the closest weather station to TRAX Ghana, approximately 16 km away. Table 6.6.1 summarizes the geographical details, and Figure 6.6.2 visualizes the data quality check performed in PVsyst, confirming the quality of the data.

Table 6.6.1: Summary of the geographical coordinates.

Input type	Value
Latitude	10.786 °
Longitude	-0.851 °
Altitude	180 m

Figure 6.6.2 illustrates the quality check of Meteonorm data, confirming their suitability for solar simulation.

**Figure 6.6.2:** Data quality check for Meteonorm inputs in PVsyst.

Source: “PVsyst | PVsyst 8”, n.d.

6.6.2 Energy production and demand

The total useful energy provided by the PV system was **3007.4 kWh/year**, matching the annual energy demand of the cold storage facility. This indicates that the system achieved a solar fraction of 100%, which fully met the energy needs. The excess energy, which represents the solar energy that has not been used due to a full battery, amounted to **621.0 kWh/year**. The specific energy production of the PV system was calculated to be **1331 kWh/kWp/year**, with a performance ratio (PR) of **64.16%**. The main results of the simulations are summarized in Table 6.6.2:

Table 6.6.2: Summary of PVsyst simulation results

Parameter	Value
Energy Demand	3007.4 kWh/year
Useful Energy	3007.4 kWh/year
Excess Energy	621.0 kWh/year
Performance Ratio (PR)	64.16%
Specific Production	1331 kWh/kWp/year

Monthly energy distribution

Table 6.6.3 summarizes the monthly distribution of energy supplied to the load, with October showing the highest energy availability, while August and February recorded the lowest output. The system consistently met the load demand throughout all months. Normalized production and loss factors are visualized in Figure 6.6.3.

Table 6.6.3: Monthly energy distribution from PVsyst simulation

Month	Energy available (kWh)	Energy used (kWh)	Excess energy (kWh)
January	318.5	230.7	63.0
February	286.0	229.5	47.5
March	331.9	282.0	37.7
April	326.7	279.0	37.4
May	316.7	281.7	25.0
June	299.3	249.0	39.2
July	308.3	244.3	54.1
August	292.8	237.2	46.9
September	298.2	231.7	60.2
October	338.1	260.2	64.4
November	335.7	243.5	80.9
December	314.9	238.7	64.7

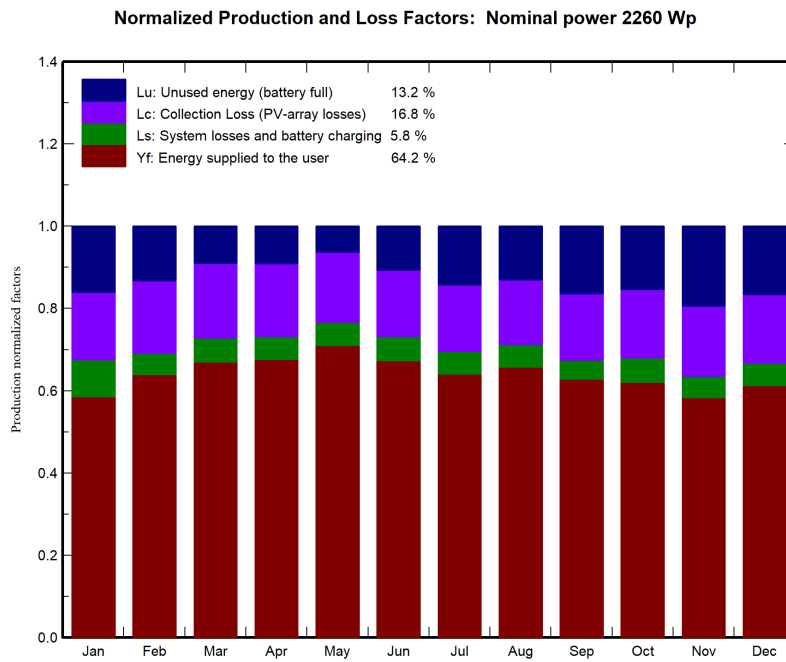


Figure 6.6.3: Normalized production and loss factors from the PVsyst simulations.

Source: “PVsyst | PVsyst 8”, n.d.

6.6.3 Battery performance

The battery system stored 63.9% of the solar energy and supplied 36.1% directly to the load. The State of Wear (SoW) of the battery was calculated at 98.7%, indicating minimal aging during the simulation period.

The battery system was analyzed to ensure continuous power availability during low-sunlight periods. Key results include:

- **Battery Capacity:** A battery capacity of **780 Ah** was recommended, less conservative compared to the intuitive design value of **1153.49 Ah**.
- **Battery Autonomy:** The system provided autonomy for approximately **4 days**, sufficient to maintain operations during cloudy periods.
- **State of Charge (SoC):** The battery maintained a minimum SoC of **20%**, ensuring lifespan.

6.6.4 System efficiency and losses

Below, the parameters that contribute to the annual loss are displayed along with their estimated impact on the system. The loss diagram, shown in Figure 6.6.4, illustrates the PVsyst loss factors and their contributions. The simulation highlighted the following losses in the system:

- Soiling losses: **3.0%**.
- IAM factor: **1.4%**.
- Module mismatch losses: **2.0%**.
- Ohmic wiring losses: **1.5%**.
- Light-induced degradation (LID): **2.0%**.
- PV losses due to temperature: **7.7%**.

The losses amount to approximately 20%, matching the loss factor employed in the intuitive approach. Despite these losses, the system efficiently converted solar energy, resulting in a virtual array energy at the MPP of **3930.1 kWh/year** and a converter output of **3146.2 kWh/year**.

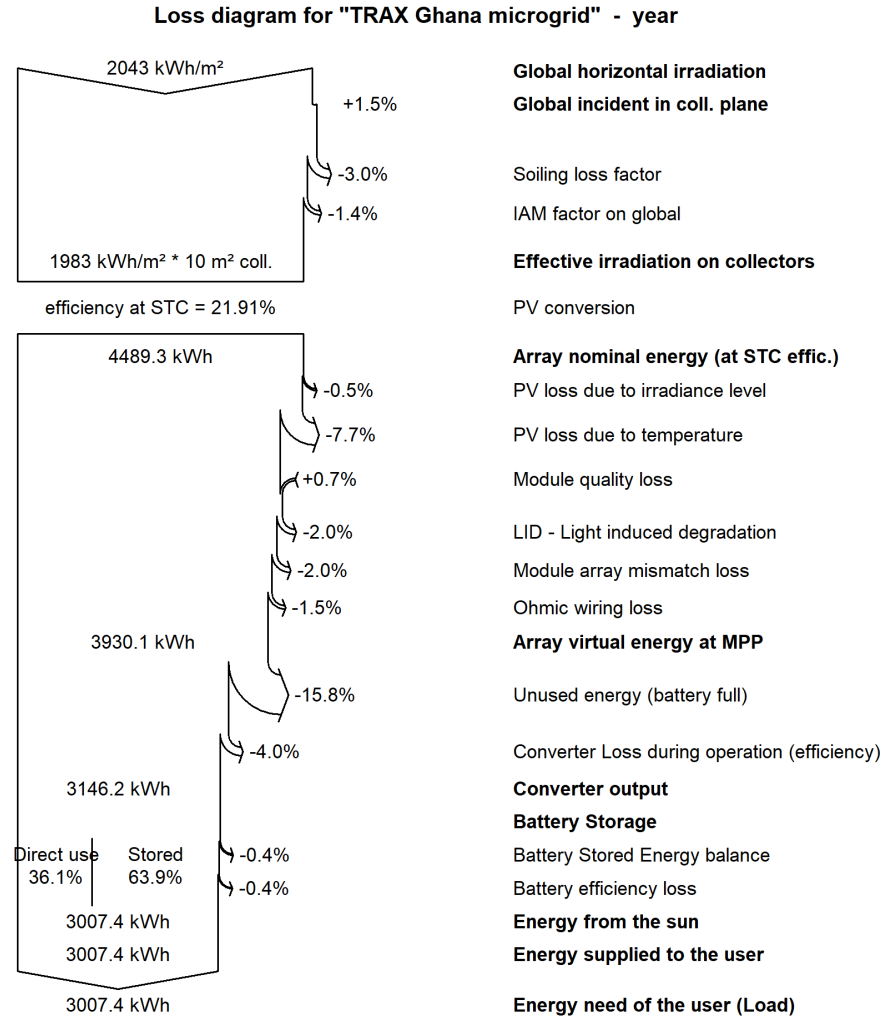


Figure 6.6.4: Loss diagram from PVsyst simulations

6.7 Comparison of design approaches

The intuitive and PVsyst approaches yielded different design configurations as a result of their methodologies and underlying assumptions. Table 6.7.1 summarizes the key design parameters derived from each approach.

Table 6.7.1: Comparison of design parameters between intuitive and PVsyst approaches

Design parameter	Intuitive approach	PVsyst approach
PV Capacity (kWp)	3.40	2.26
Battery Capacity (Ah)	1153.49	780
Energy Demand Met (%)	100	100
Excess Energy (kWh/year)	2528.3 (kWh/year)	621
Performance Ratio (%)	42.77%	64.16

The intuitive approach aimed for simplicity by sizing the PV system and battery according to August, the month with the least solar insolation. Since the load profile corresponds to the peak load of an April day, the results were very conservative. This method led to conservative sizing, favoring reliability with larger battery and PV capacities. However, it lacked detailed loss analysis and did not account for seasonal variations in solar energy availability. When using the results of the intuitive method in PVsyst, the virtual energy generated by the array is 5943.2 kWh and results in a loss of 42. 5% due to unused energy. This confirms that the method is too conservative, leading to a significantly oversized PV array in relation to the load, and thus causing substantial unused energy losses.

The PVsyst approach provided a detailed simulation of energy flows, system losses, and performance metrics over a year. Although it recommended a smaller battery and PV capacity, its results highlighted the potential for unused energy (621 kWh/year), particularly during months of high insolation. This indicates opportunities to optimize system sizing to reduce overproduction.

Optimization of final design

Based on the comparative analysis, the following optimizations are proposed to balance the benefits of both approaches:

PV system optimization

The PV capacity of the intuitive approach (3.40 kWp) was conservatively overestimated compared to the PVsyst result (2.26 kWp). To balance reliability and cost:

- Increase PV capacity to 2.80 kWp, which provides a reliability margin for low-insolation periods while reducing excess energy. Results in a number of five modules on a module area of $13\ m^2$.
- Retain the tilt angle of 14° and azimuth of 0° to maximize the annual energy yield, as indicated by the analysis of the sensitivity of PVsyst.

Battery optimization

The sizing of the battery in the intuitive approach (1153.49 Ah) offers high autonomy but increases the cost and complexity of the system. The PVsyst simulation suggested a smaller battery capacity (780 Ah) with sufficient autonomy. Based on this:

- Increase the number of batteries to 6 in parallel to have a battery capacity of 936 Ah, balancing autonomy (approximately 4 days) and cost efficiency.
- Lithium-ion batteries are selected for their longer life cycles and higher energy density, as recommended by the intuitive approach.

The optimized design combines elements of both approaches to achieve a balanced system configuration. Table 6.7.2 summarizes the final design parameters.

Table 6.7.2: Summary of final optimized design

Design parameter	Optimized value
PV Capacity	2.83 kWp
Battery Capacity	936 Ah
Tilt Angle	14°
Energy Demand Met	100%
Excess Energy	1560 kWh/year
Autonomy	4 days
No. PV modules	5 in series x 1 string
No. Batteries	6 in parallel x 1 series

Chapter 7

Discussion

7.1 Plausibility

Although the initial draft provides a strong starting point, its assumptions must be validated and adjusted to the on-site implementation. The plausibility of the system proposal would be significantly increased by fieldwork and visits. It should also be mentioned that the components and solutions chosen are based on what is known to be available in the area, which helps to increase plausibility. It will be important to consult with local suppliers and experts in order to increase adaption to the real context and situation. However, as key data sources are based on interviews and internal reports, some factors cannot be known until they are realized in the future.

7.2 Climate and weather considerations

The system design took into account local climate and weather on average between 1991 and 2010, with the tilt angle and azimuth optimized for the annual solar yield. However, reliance on Meteonorm data introduces potential inaccuracies in predicting solar energy availability, climate variability, and potential long-term changes in solar insolation. In addition, the potential Meteonorm inaccuracies can affect the predicted required refrigeration capacity. The system's autonomy of approximately four days ensures operational reliability during brief periods of low sunlight, but extended cloudy periods could strain it. The integration of additional renewable energy sources, such as wind, or the exploration of hybrid system configurations should be examined to improve resilience.

7.3 Cold storage

The dimensioning of the cold storage and its capacity is based on information from TRAX Ghana and has not been extensively fact checked. Therefore, the predicted capacity of 1500-2250 kg of produce could be misleading. There are also uncertainties regarding the amount of penetration of the vapor barrier and/or insulation from pipes and electrical wiring. This could be a factor that affects the transmission load through weakened insulation and condensation in the insulation. Relative humidity inside the cold storage could also be affected, which could pose an issue. In addition, the design includes a door between the two cold storage rooms which could pose an issue due to ethylene circulating between the rooms. If one of the rooms stores ethylene-producing vegetables and the other stores ethylene-sensitive vegetables, it could result in faster deterioration of the ethylene-sensitive vegetables.

The relative humidity in the cold storage is assumed to be maintained at approximately 90% to avoid loss of mass in the crops. However, the heat exchangers are not dimensioned in the initial design of the cold storage, so in reality it is uncertain whether relative humidity can be maintained. This could especially be an issue for the room with 10°C, as the refrigerant will be around 0°C, resulting in a large temperature difference that can cause dehumidification. Therefore, it could be necessary to have a humidifier in the room to ensure optimal relative humidity.

7.4 Refrigeration loads

Cooling time:

The simulation of the cooling time assumes a uniform initial temperature distribution in the food, a constant temperature of the surrounding medium, constant thermophysical properties, and a convective heat exchange on the surface. There are situations where some of these assumptions could be wrong. This is especially the case for the initial temperature distribution, e.g. variable time spent in the shade / direct sunlight, resulting in different initial temperatures. Furthermore, there is a generalization of the geometries and sizes of the produce. The bell peppers are calculated as slabs, which is a simplification of the actual geometric shape. Hot peppers and cucumbers are classified as cylinders, but can vary widely in shape and thickness throughout the vegetable. In addition, the thickness of each crop is considered constant, but will vary in reality. The heat transfer coefficient is defined as $25 \frac{W}{m^2 \cdot K}$, which will not be the case for each vegetable as they are cooled in bulk. All of these factors influence the validity of the predicted cooling time. Nonetheless, the results are deemed appropriate for this thesis.

Product load:

The product load does not take into account the cooling of the storage boxes. This decision was made on the basis of equation Equation 5.25, as the mass strongly influences the product load. Since the storage box should contain approximately 20 kg of produce and weigh 1.9 kg itself, the product load of the vegetables would be roughly ten times that of the storage box. Therefore, the additional product load is neglected. However, if the product load is estimated to be too low, the result would be an increase in cooling time, which in most cases would not be critical to the quality of the product. Harvest temperatures can influence the product load, as the actual temperature is rarely the same as the calculated temperature. However, the product load is calculated with values and assumptions that are considered the worst case, resulting in a lower real product load in almost all cases.

Transmission load:

The only variations in transmission load will be fluctuations in ambient temperature and the desired temperature within the storage, as there will be no change in the geometry of the building. There is a case to be made regarding thicker insulation. However, this was decided against because the available storage area would decrease, there is a higher initial cost, and the decrease in transmission load would not be significant enough. In addition, the floor of the cold storage is estimated to be 3°C below the outside temperature, which should be investigated more closely.

Infiltration load:

The infiltration load is based upon several assumptions, namely the number of times the door is opened, the total time spent open, the effectiveness of the doorway protection device, the chosen time interval, and the open-closing time of the door. However, since all of these in reality could vary heavily, the infiltration load is assumed to be a constant load throughout the two hours of harvest, making it an overestimation in practically all cases. The load is quite small compared to the others, so it will not greatly affect the total load if it is over- or underestimated.

Internal load:

The internal load neglects additional heat from fans and the defrosting of the evaporator due to the predicted insignificant load increase. Therefore, the internal load comes from people who occupy the cold storage and is considered a constant load for the duration of harvest. In reality, people will not be occupying the room during the specified harvest time. However, the amount of activity in the cold storage is partially unknown, so a constant load is added as a buffer. The removal of vegetables from the cold storage to sell on the market will also occur in the morning, reducing the overestimation of the internal load.

Total load

An additional increase of 10% is added to the total load to account for unexpected loads or errors in calculations. Each of the loads are calculated for the worst case, resulting in an overestimation for most days. However, some potential loads, such as the cooling of the storage boxes and the defrosting of the evaporator, have been neglected due to their predicted small nature. This will in turn result in a slightly larger refrigeration load, which will make the overestimation smaller. The total load, calculated as 0.96 kW, results in a small compressor. The total load is deemed a credible result due to the small amount of vegetables cooled simultaneously. Furthermore, if the compressor capacity is larger than the estimated refrigeration load, it will result in faster cooling of the vegetables, and vice versa.

7.5 Refrigeration system

The simulation of the refrigeration cycle is conducted with CoolProp, a well established Python-library. The other method to calculate the thermodynamic states and properties is to look at relevant thermodynamic tables, which can easily result in human error. Furthermore, a simple way to improve the compressor COP and ensure that only liquid enters is by integrating a liquid receiver into the primary refrigeration cycle. However, the compressor is relatively small, making the difference in compressor work with and without a liquid receiver minimal. In addition, from the log P-H diagram in Figure 5.2.1, compression is not made too close to the liquid line. Therefore, with small changes in pressure, liquid should not enter the compressor, eliminating the need for a liquid receiver.

Furthermore, since the compressor work was calculated in both subsection 6.2.2 and section 6.3, providing almost identical results, the values are deemed credible. However, both calculations are based on a predicted refrigeration load. If this is not accurately estimated, both values of the compressor work will be incorrect.

R744 was considered a secondary refrigerant using evaporators instead of heat exchangers. However, this option was dismissed because the critical pressure of 73.7 bar (ToolBox, 2018) could create a safety hazard within the cold storage area due to its proximity to people.

7.6 Simulation vs. Calculation

Two different models were created to calculate the compressor work. subsection 6.2.2 used a roughly estimated COP, and section 6.3 used the built-in thermodynamic properties of CoolProp. Although widely similar, there are some variations between the two models,

summarized in Table 7.6.1.

Time	\dot{W}_{comp} [kW]		Deviation [%]
	Excel	Coolprop	
01:00	0,129	0,124	3,9
02:00	0,122	0,119	2,5
03:00	0,118	0,114	3,4
04:00	0,114	0,11	3,5
05:00	0,112	0,109	2,7
06:00	0,111	0,109	1,8
07:00	0,234	0,227	3,0
08:00	0,289	0,278	3,8
09:00	0,22	0,211	4,1
10:00	0,243	0,232	4,5
11:00	0,267	0,254	4,9
12:00	0,266	0,255	4,1
13:00	0,242	0,233	3,7
14:00	0,225	0,215	4,4
15:00	0,228	0,221	3,1
16:00	0,224	0,214	4,5
17:00	0,212	0,205	3,3
18:00	0,197	0,188	4,8
19:00	0,182	0,175	3,8
20:00	0,172	0,163	5,2
21:00	0,166	0,156	3,7
22:00	0,153	0,146	4,6
23:00	0,143	0,139	2,8
00:00	0,135	0,129	4,4

Table 7.6.1: Comparison of estimated compressor work from both Excel and Coolprop.

The largest compressor work in subsection 6.2.2 is chosen as the final design. Although the two models are widely similar, with an average difference of 3.8%, the Excel model predicts slightly higher compressor work, giving an additional margin of error in the calculations. One possible explanation for the deviation between the two models is the slight difference in COP, as the simulated results in python and coolprop are consequently higher. The COP calculated in the excel sheet assumes an efficiency of 0.4, which is most likely the reason behind the deviations. Another factor that could affect compressor work is errors in total refrigeration load. Nevertheless, the size of the compressor would not differ much

for both models, so the final choice is in reality merely a formality.

7.6.1 Pump Work

Although the simulated pump work required for this refrigeration system is small, it could be a feasible result due to the small mass flow rate. To validate the result, the specific heat capacity was cross referenced with ToolBox (2007), which proved a value similar to the simulation in CoolProp. In addition, the mass flow rate for the secondary refrigerant is approximately 20 times larger than that of the primary refrigerant. The sodium chloride and water mixture operates only as a single-phase fluid, which means that the required mass flow rate will be higher than that of refrigerants, such as R290, which operates in multiple phases. However, the pressure differences should be calculated further as the small mass flow rate could lead to a higher pressure drop. If the pressure drop was 1.5 bar instead of 0.5 bar, the corresponding pump work would be 9.2 kW, which is still relatively low.

7.6.2 Defrosting the Evaporator

As the evaporator in the main system operates at temperatures below the freezing point of water, the condensation of air could cause frost on the evaporator. However, for this refrigeration system, a possible design is to place the evaporator inside the external structure along with the primary circuit. In this storage, the temperature is for all intents and purposes equal to the ambient temperate. Therefore, by halting the evaporative cooling, the evaporator could naturally defrost, especially at high ambient temperatures in northern Ghana. There are other methods to defrost the evaporator, such as hot gas defrosting (Pearson, 2008), which should be explored further.

7.7 Uncertainty in microgrid design

7.7.1 Load profiles

Uncertainty and stochasticity in the load profile also arise from variations in harvest schedules, crop removal activities, and cooling requirements driven by external factors such as ambient temperature and crop type. These elements were not explicitly modeled, creating potential inconsistencies between predicted and actual energy demand.

The input parameters for this model were derived from conversations with staff, which may not be fully in line with real-world behavior. Furthermore, the estimation of behavior and harvest cycles is based on assumptions about weekly activities and observed use, which introduces further uncertainty. This inconsistency could lead to an overestimated demand

compared to actual requirements. Given the absence of historical energy consumption data for the facility, future work should focus on collecting and analyzing operational data. Such efforts would enable a more accurate calibration of load models and better alignment of the system with real-world demand dynamics.

7.7.2 System design considerations

The decision to use a DC microgrid configuration was driven by the need to minimize system complexity and energy losses. By eliminating the inverter, the system achieves greater efficiency and lower maintenance requirements, which are critical in rural, off-grid settings. However, the lack of an inverter imposes limitations on future expansions if AC loads are introduced. Careful consideration must be given to the trade-offs between initial cost savings and long-term scalability.

The selected components, including lithium-ion batteries and high-efficiency PV modules, align with the sustainability and scalability objectives. Lithium-ion batteries offer longer lifespans and lower life cycle costs compared to alternatives such as lead-acid batteries. Similarly, the use of high-efficiency PV modules minimizes the physical footprint of the installation. However, the higher upfront costs of these components could pose a financial barrier to maintaining this solution and replication in other rural settings. Future projects must balance these considerations with the declining prices of solar components, which could make such systems more accessible over time.

7.7.3 Additional losses

The intuitive approach does not explicitly consider the impacts of extreme temperatures or wind conditions, potentially leading to an underestimation of energy losses and thus higher losses than anticipated, reducing system efficiency and reliability. However, the approach included conservative calculations, leading to overestimates compared to the PVsyst simulations. Furthermore, the degradation of the BESS under extreme temperature conditions was not addressed, despite its significant implications for both performance and lifecycle costs. High or low temperatures can accelerate battery aging, reduce usable capacity, and decrease overall efficiency. To mitigate these additional losses, PV modules and batteries should be selected according to the adopted temperature tolerance and ventilation strategies.

Another factor affecting production accuracy is shading. Although the current design assumes no shading due to the optimal placement of the storage facility, this assumption may not hold in practice. Unforeseen shading from surrounding vegetation, structures, or seasonal sun angles could reduce overall PV production. This highlights the importance of continuous monitoring and adjustments to account for real-world conditions, ensuring

that production estimates align with actual performance.

Finally, soiling losses introduce uncertainty dependent on the geographic location, complicating precise loss estimation. Creating location-specific monthly soiling intervals could improve estimation precision and aid maintenance strategies, particularly considering Harmattan winds.

7.7.4 PVsyst

Although the conservative nature of the intuitive approach reduces the likelihood of system failure, it can result in inefficiencies, such as excess energy production and under-utilized capacity. This aligns with the objective of the intuitive method of ensuring reliability over optimal cost-efficiency. However, the numerical approach, using PVsyst, offered a more precise analysis by incorporating detailed simulations of weather patterns, system losses and load profiles, and balanced cost-efficiency. However, the numerical approach relies heavily on the quality of the input data and the accuracy of the simulation assumptions.

One significant challenge lies in the assumptions in the weather data. The MET files in PVsyst include hourly weather data such as global horizontal irradiation and temperature, but quality assurance for these datasets can be difficult. Potential errors, such as time shifts caused by discrepancies in summer and winter time adjustments, may introduce inaccuracies into the results. Therefore, post-implementation monitoring and the comparison of actual operational data with simulation output are essential for refining the models and improving their accuracy.

Another area of precision involves the transposition of irradiation data. PVsyst employs the Perez transposition model to calculate incident irradiation in the collector plane based on global horizontal irradiation (“PVsyst | PVsyst 8”, n.d.). Although this model is considered highly sophisticated, the accuracy of its results is highly dependent on the quality of the horizontal data supplied. Including diffuse irradiation data directly in the simulation through the Hay model, also available in PVsyst, further improves the reliability of these calculations, ensuring that the system performance is closely aligned with real-world conditions.

Estimation of thermal and wind loss is also a critical factor in ensuring the accuracy of the simulation results. Measured ambient temperature and wind data play a key role in this context, particularly for systems with modules mounted close to the roof or at a small tilt. Conservative thermal loss constants, such as $U_c = 29 \text{ W/m}^2\text{K}$ and $U_v = 0 \text{ W/m}^2\text{K m/s}$, were applied to account for air circulation around the collectors. For systems installed with greater roof clearance or in areas with high wind velocities, incorporating wind loss factors into the model becomes even more critical. Due to the lack of reliable hourly

wind velocity data in these simulations, adjustments should be investigated as it can significantly impact thermal loss calculations and the accuracy of the results.

7.8 Future work

The current design represents a foundation for the implementation of a reliable and efficient solar-powered cold storage system. However, there are several opportunities to further improve the robustness, scalability, and alignment of the system with real-world demands. Future work should focus on the following areas:

- Design and dimension heat exchangers to identify the necessity of incorporating an external humidity source to ensure optimal storage humidity levels.
- Predict the storage life of the vegetables and investigate the potential effect of ethylene transfer between the two rooms.
- Calculate a more accurate representation of the heat transfer coefficient in the cooling tunnel, thus adjusting the cooling time of the crops and the product load.
- Include the additional product load from cooling of the storage boxes.
- Identify the total pressure drop in the secondary refrigeration system to accurately calculate the mass flow rate and required fluid pump work.
- Defrosting the evaporator: Consider the assumption that the mechanisms for defrosting the evaporator are unnecessary.
- Conduct extensive field research to better predict the infiltration load.
- Create an accurate temperature profile of the heat gain from the ground below the cold storage.
- Assess the possibility and potential benefits of using other natural refrigerants, such as R717, in the primary refrigeration system.
- Conduct comprehensive economic and social impact studies to evaluate the feasibility and benefits of the system in rural communities.
- Integrate advanced dynamic load modeling tools to better capture stochastic variations in energy demand, such as crop harvest and removal patterns. This would improve the accuracy and reliability of system sizing and performance predictions.
- Investigate excess energy applications, such as water pumping, lighting, or powering additional facilities.

- Integrate energy management systems to dynamically adjust loads and further optimize energy utilization. In addition, periodic monitoring of system performance to validate design assumptions and make iterative improvements.
- Focus on collecting and analyzing operational data post-implementation to calibrate the simulated models and align them with real-world performance. A comparison of simulated energy output with actual production and consumption would highlight areas for further refinement.
- Establish maintenance and knowledge-sharing measures to increase the level of competence among consumers.

Chapter 8

Conclusions

In this report, an initial design for a solar-powered cold storage facility is developed to support the operations of the TRAX Ghana Farm and Youth Empowerment Center (YEC). This includes a full design with a corresponding refrigeration system to facilitate optimal storage conditions of relevant crops. The initial design provides a reliable and cost-effective system solution within the TRAX Ghana project-specific boundaries. The boundaries were set to be an off-grid facility supplied by solar energy, where all components should be eco-friendly and available locally. The integration of the SPCS facility will ensure sustainability and adaptability to the rural off-grid environment of northern Ghana.

The report details a refrigeration load profile that illustrates the cold storage energy demand based on product, transmission, infiltration, and internal loads. This reflects the operational cycle influenced by factors such as harvesting cycles, human behavior, storage geometry, insulation, internal conditions, and outside temperature. This is also used in designing the microgrid, ensuring a consistent power supply throughout the year.

The cold storage and refrigeration system

The final design facilitates the different storage requirements of the relevant vegetables, thus mitigating post-harvest losses at the farm. This allows the storage of vegetables during periods of low market prices, which in turn could lead to increased economic independence for farmers at TRAX Ghana.

For the cold storage, the transmission load is mainly determined by the outer geometry, insulation, and outside temperature. The product load is directly related to the type, harvested mass and the cooling time of the product, where the cooling time is influenced by the geometry, diameter, and heat transfer coefficient. In terms of the infiltration load, it is largely determined by the opening time of the doorway and the protection device.

Finally, the internal load is related to the time people spend inside the cold storage. The designed cold storage will have an indirect refrigeration system with a minimum of 0.289 kW compressor and a 3 W fluid pump, using R290 and a mixture of 18.8% sodium chloride and water as primary and secondary refrigerants, respectively. The compressor is dimensioned according to an estimated maximum total refrigeration load of 0.96 kW, where it will cool 40 kg of vegetables at 29.9°C.

The microgrid design

The proposed system topology is a self-sufficient microgrid supplied by PV panels in combination with batteries. All major components, including fans, compressor, and battery, operate on DC power. This eliminates the need for an inverter, reducing both initial costs and energy losses associated with DC-AC conversion. The final design ensures that the solar-powered microgrid meets the energy demands of the cold storage facility while trying to optimize costs and system complexity. Based on the advantages of both intuitive and numerical methods, adjustments were made in sizing the PV system and battery to balance reliability and cost. This contributed in ensuring sustained operation during low-insolation periods and avoiding excessive overproduction. This final result is found by slightly reducing the PV capacity from the conservative estimate of the intuitive method into a more cost-effective solution. The proposed battery capacity provides sufficient autonomy without unnecessary costs and complexity. Through these adjustments, the final initial design ensures reliability and efficiency, meeting 100% of the energy demand while minimizing excess energy. This integrated approach results in a solid foundation for further design.

Future work

Future work on the solar-powered cold storage system aims to improve the robustness, scalability, and real-world alignment of the design. This includes focusing on improving heat exchanger designs, predicting vegetable storage life, optimizing heat transfer in the cooling tunnel, and accurately calculating pressure drops in the refrigeration system. It also involves exploring natural refrigerants, conducting economic and social impact studies, integrating dynamic load modeling and energy management systems, and investigating possible excess energy applications. Additionally, efforts will be directed towards better data collection and analysis post-implementation for model calibration, and establishing maintenance and knowledge-sharing frameworks for user competence.

References

- Abas, N., Nawaz, R., & Khan, N. (2015). Parametric Quantification of Low GWP Refrigerant for Thermosyphon Driven Solar Water Heating System. In *Procedia Computer Science* (pp. 804–811, Vol. 52). Retrieved November 28, 2024, from <https://www.sciencedirect.com/science/article/pii/S1877050915009369>
- Abdelaziz, G., Hichem, H., & Gharbi, R. (2022, January). *Shading effect on the performance of a photovoltaic panel*. <https://doi.org/10.1109/SCC53769.2021.9768356>
- Abdelrazik, M. K., Abdelaziz, S. E., Hassan, M. F., & Hatem, T. M. (2022). Climate action: Prospects of solar energy in Africa. *Energy Reports*, 8, 11363–11377. <https://doi.org/10.1016/j.egyr.2022.08.252>
- Adekanbi, M. L., Alaba, E. S., John, T. J., Tundelao, T. D., & Banji, T. I. (2024). Soiling loss in solar systems: A review of its effect on solar energy efficiency and mitigation techniques. *Cleaner Energy Systems*, 7, 100094. <https://doi.org/10.1016/j.cles.2023.100094>
- Aemu, T. T. (2023). Review on the Role of Improved Storage Technologies in Post-Harvest Loss Reduction of Perishable Crops and Enhancing Food and Nutrition Security. *Journal of Nutrition & Food Sciences*, 13(2). Retrieved December 13, 2024, from <https://www.longdom.org/open-access/review-on-the-role-of-improved-storage-technologies-in-postharvest-loss-reduction-of-perishable-crops-and-enhancing-food-and-nutri-99770.html>
- Africa Energy Outlook 2019. (2019).
- A-GAS. (2018). R600A (ISOBUTANE). *FSW*. Retrieved November 27, 2024, from https://www.fsw.uk.com/wp-content/uploads/2023/12/r600a_sds_0.pdf
- agricultural organization, F. a. (2021). The state of food security and nutrition in the world 2021. *Food and agricultural organization of the United Nations*. Retrieved November 29, 2024, from <https://openknowledge.fao.org/server/api/core/bitstreams/191ee56e-2d4f-46cb-9710-0ca167ca314d/content/cb4474en.html>
- Ahmed, Y. E., Maghami, M. R., Pasupuleti, J., Danook, S. H., & Basim Ismail, F. (2024). Overview of Recent Solar Photovoltaic Cooling System Approach [Number: 9 Pub-

- lisher: Multidisciplinary Digital Publishing Institute]. *Technologies*, 12(9), 171. <https://doi.org/10.3390/technologies12090171>
- Akorede, M. F. (2022, January). 2 - Design and performance analysis of off-grid hybrid renewable energy systems. In M. Lo Faro, O. Barbera, & G. Giacoppo (Eds.), *Hybrid Technologies for Power Generation* (pp. 35–68). Academic Press. <https://doi.org/10.1016/B978-0-12-823793-9.00001-2>
- Alegbeleye, O., Odeyemi, O. A., Strateva, M., & Stratev, D. (2022). Microbial spoilage of vegetables, fruits and cereals. *Applied Food Research*. <https://doi.org/https://doi.org/10.1016/j.afres.2022.100122>
- American society of heating, R. a. A.-C. E. (2010, January). *2010 ASHRAE Handbook: Refrigeration*. American Society of Heating, Refrigerating, Air-Conditioning Engineers, 2010. Retrieved November 22, 2024, from https://books.google.no/books/about/2010_ASHRAE_Handbook.html?id=fWOZMgEACAAJ&redir_esc=y
- Ameur, A., Berrada, A., Loudiyi, K., & Adomatis, R. (2021, January). Chapter 6 - Performance and energetic modeling of hybrid PV systems coupled with battery energy storage. In A. Berrada & R. El Mrabet (Eds.), *Hybrid Energy System Models* (pp. 195–238). Academic Press. <https://doi.org/10.1016/B978-0-12-821403-9.00008-1>
- Amjad, W., Munir, A., Akram, F., Parmar, A., Precoppe, M., Asghar, F., & Mahmood, F. (2023, June). Decentralized solar-powered cooling systems for fresh fruit and vegetables to reduce post-harvest losses in developing regions: A review. In *Clean Energy* (pp. 635–653, Vol. 7). Oxford University Press. Retrieved December 13, 2024, from <https://academic.oup.com/ce/article/7/3/635/7174941>
- Amoah, M. (n.d.). Geographical and Climate Change Implications on Solar Photovoltaic Performance.
- Amoah, M. (2022, November). *Geographical and Climate Change Implications on Solar Photovoltaic Performance* [doctoral]. Buckinghamshire New University (Awarded by Staffordshire University). Retrieved December 14, 2024, from <https://bnu.repository.guildhe.ac.uk/id/eprint/18706/>
- Ampadu, B., Sackey, I., & Cudjoe, E. (2020, March). *Rainfall Distribution in the Upper East Region of Ghana, 1976 -2016*. <https://doi.org/10.13140/RG.2.2.17924.07042>
- Antwi-Agyei, P., Dougill, A. J., & Abaidoo, R. C. (2021). Opportunities and barriers for using climate information for building resilient agricultural systems in Sudan savannah agro-ecological zone of north-eastern Ghana. *Climate Services*, 22, 100226. <https://doi.org/10.1016/j.cliser.2021.100226>
- Apollo.learn. (n.d.). From Hot to Cold: Harnessing Heat Exchanger Temperature Difference. Retrieved December 12, 2024, from <https://learn.apolloheatpumps.com/en/heat-exchanger-temperature-difference/>

- Appleyard, S. (2006). Simple photovoltaic cells for exploring solar energy concepts. *Physics Education*, 41. <https://doi.org/10.1088/0031-9120/41/5/005>
- Arunkumar, T., Raj, K., Kabeel, A.-E., & Lee, S. J. (2021). Effects of solar geometry and operation period on stability of solar desalination systems: A review. *Environmental Science and Pollution Research*, 28(46), 65014–65032. <https://doi.org/10.1007/s11356-021-16566-8>
- Ashetehe, A. A., Gessesse, B. B., & Shewarega, F. (2022). Development of Optimal Tilt Angle Models of a Photovoltaic Module for Maximum Power Production: Ethiopia [eprint: <https://onlinelibrary.wiley.com/doi/pdf/10.1155/2022/8729570>]. *International Journal of Photoenergy*, 2022(1), 8729570. <https://doi.org/10.1155/2022/8729570>
- Asumadu Sarkodie, S., & Owusu, P. A. (2016). A review of Ghana's solar energy potential. *AIMS Energy*, 4, 675–696. <https://doi.org/10.3934/energy.2016.5.675>
- Ayeng'o, S., Schirmer, T., Kairies, K.-P., Axelsen, H., & Sauer, D. U. (2018). Comparison of off-grid power supply systems using lead-acid and lithium-ion batteries. *Solar Energy*, 162, 140–152. <https://doi.org/10.1016/j.solener.2017.12.049>
- Baharudin, N., Tunku Mansur, T. M. N., Hamid, F., Ali, R., & Irwanto, M. (2017). Topologies of DC-DC converter in solar PV applications. *Indonesian Journal of Electrical Engineering and Computer Science*, 8, 368–374. <https://doi.org/10.11591/ijeecs.v8.i2.pp368-374>
- Baladhiya, C., & Doshi, J. (2016, June). Precooling techniques and applications for fruits and vegetables. In *International journal of processing and post harvest technology*. Retrieved November 30, 2024, from <https://www.cabidigitallibrary.org/doi/pdf/10.5555/20163325599>
- Baldwin, E. A. (2003). Coatings and Other Supplemental treatments to Maintain vegetable Quality. *U.S Department of Agriculture*. Retrieved November 3, 2024, from <https://ucanr.edu/datastoreFiles/608-259.pdf>
- Bamakan, S., & Manshadi, S. D. (2021). Blockchain-enabled pharmaceutical cold chain: Applications, key challenges, and future trends. *Journal of cleaner production*. Retrieved November 29, 2024, from <https://www.sciencedirect.com/science/article/pii/S0959652621012403>
- Bell, I. H., Wronski, J., Quoilin, S., & Lemort, V. (2014). Pure and Pseudo-pure Fluid Thermophysical Property Evaluation and the Open-Source Thermophysical Property Library CoolProp. *ACS Publications*, 54(6). Retrieved December 13, 2024, from <https://pubs.acs.org/doi/full/10.1021/ie4033999>
- Bello, A., Usman, A., Alexander, Y., Abdullahi, C., & Gadom, A. (2022). COMPARATIVE STUDY ON EFFECT OF HUMIDITY, WIND AND HARMATTAN DUST ON THE OUTPUT VOLTAGE OF SOLAR PANELS IN THE SAVANNAH AREA. 8, 22–28.

- Ben, L. (n.d.). Utility-scale solar photovoltaic power plants : A project developer's guide. Retrieved November 29, 2024, from <https://documents.worldbank.org/en/publication/documents-reports/documentdetail/690161467992462412/Utility-scale-solar-photovoltaic-power-plants-a-project-developer-s-guide>
- Bernstad, A. K., Canovas, A., & Valle, R. (2016). Consideration of food wastage along the supply chain in lifecycle assessments: A mini-review based on the case of tomatoes. <https://doi.org/10.1177/0734242X16666945>
- Berwal, A. K., Kumar, S., Kumari, N., Kumar, V., & Haleem, A. (2017). Design and analysis of rooftop grid tied 50 kW capacity Solar Photovoltaic (SPV) power plant. *Renewable and Sustainable Energy Reviews*, 77, 1288–1299. <https://doi.org/10.1016/j.rser.2017.03.017>
- Broom, D. (2020, November). This is why food security matters now more than ever. Retrieved December 13, 2024, from <https://www.weforum.org/stories/2020/11/food-security-why-it-matters/>
- Brosnan, T. (2001). Precooling techniques and applications for horticultural products — a review. *International Journal of Refrigeration*, 24(2), 154–170. [https://doi.org/https://doi.org/10.1016/S0140-7007\(00\)00017-7](https://doi.org/https://doi.org/10.1016/S0140-7007(00)00017-7)
- campus, B. (2022). 6.4 Carnot cycles. In *Introduction to Engineering Thermodynamics*. Retrieved December 11, 2024, from <https://pressbooks.bccampus.ca/thermo1/chapter/6-4-carnot-cycles/>
- Castañer, L., Bermejo, S., Markvart, T., & Fragaki, K. (2012, January). Chapter IIA-2 - Energy Production by a PV Array. In A. McEvoy, T. Markvart, & L. Castañer (Eds.), *Practical Handbook of Photovoltaics (Second Edition)* (pp. 645–658). Academic Press. <https://doi.org/10.1016/B978-0-12-385934-1.00018-0>
- Chanchangi, Y. N., Ghosh, A., Sundaram, S., & Mallick, T. K. (2020). Dust and PV Performance in Nigeria: A review. *Renewable and Sustainable Energy Reviews*, 121, 109704. <https://doi.org/10.1016/j.rser.2020.109704>
- Chaurey, A., & Kandpal, T. C. (2010). Assessment and evaluation of PV based decentralized rural electrification: An overview. *Renewable and Sustainable Energy Reviews*, 14(8), 2266–2278. <https://doi.org/10.1016/j.rser.2010.04.005>
- Chege, C., & Carson, M. (2017). Food loss and waste Africa. *Dalberg Intelligence*. Retrieved November 29, 2024, from <https://dalberg.com/wp-content/uploads/2017/06/FOOD-LOSS-QUARTERLY-VOL9.pdf>
- Choudhari, C., & Sapali, S. N. (2018). Testing of Environment Friendly Refrigerant R290 for Water Cooler Application. *International Journal of*. Retrieved November 27, 2024, from https://www.researchgate.net/publication/323812686_Testing_of_Evironment_Friendly_Refrigerant_R290_for_Water_Cooler_Application
- Coalition, C. (2020, November). Taking Cold Chains Off-Grid: How Solar Powered Cold Rooms Could Dramatically Reduce Food Waste in Sub-Saharan Africa. Retrieved

- December 13, 2024, from <https://coolcoalition.org/taking-cold-chains-off-grid-how-solar-powered-cold-rooms-could-dramatically-reduce-food-waste-in-sub-saharan-africa/>
- Constable, G., & Sommerville, B. (2003). *A Century of Innovation: Twenty Engineering Achievements That Transformed Our Lives*. Joseph Henry press. Retrieved November 28, 2024, from https://books.google.no/books?hl=en&lr=&id=IyVFweSZu0cC&oi=fnd&pg=PR6&ots=xvcm5AuGxa&sig=dDNduXXPAvuLzqs6omgK9GAVHredir_esc=y#v=onepage&q&f=false
- Dagnas, S., & Membre, J.-M. (2013, January). Predicting and Preventing Mold Spoilage of Food Products. In *Journal of food protection* (pp. 538–551, Vol. 76). Retrieved November 28, 2024, from <https://www.sciencedirect.com/science/article/pii/S0362028X23054819>
- Danfoss. (2000). Practical Application of Refrigerant R600a isobutane in Domestic Refrigerator Systems. *Danfoss*. Retrieved November 27, 2024, from [https://skoge.folk.ntnu.no/book-cep/diagrams/additional_diagrams/more_on_refrigerants/isobutane\(R600A\)-Danfos.pdf](https://skoge.folk.ntnu.no/book-cep/diagrams/additional_diagrams/more_on_refrigerants/isobutane(R600A)-Danfos.pdf)
- de Souza Silva, J. L., Costa, T. S., de Melo, K. B., Sakô, E. Y., Moreira, H. S., & Villalva, M. G. (2020). A Comparative Performance of PV Power Simulation Software with an Installed PV Plant [ISSN: 2643-2978]. *2020 IEEE International Conference on Industrial Technology (ICIT)*, 531–535. <https://doi.org/10.1109/ICIT45562.2020.9067138>
- Decorexpo. (2024). 10 påviste tykkveggede paprika. Retrieved December 12, 2024, from <https://grow.decorexpo.com/no/samoe-interesnoe/10-proverennyx-sortov-tolstostennogo-perca.html>
- Diarra, D. .-, & Akuffo, F. O. (2002). Solar photovoltaic in Mali: Potential and constraints. *Energy Conversion and Management*, 43(2), 151–163. [https://doi.org/10.1016/S0196-8904\(01\)00019-X](https://doi.org/10.1016/S0196-8904(01)00019-X)
- Dilshad, S., Kalair, A. R., & Khan, N. (2019). Review of carbon dioxide (CO₂) based heating and cooling technologies: Past, present, and future outlook. Retrieved November 28, 2024, from https://onlinelibrary.wiley.com/doi/epdf/10.1002/er.5024?getft_integrator=sciencedirect_contenthosting&src=getftr&utm_source=sciencedirect_contenthosting
- Dirlik, E., Gezegin, C., Ahmad, S., & Dost Mohammadi, S. A. (2024). Comparison of PVsyst, PVSOL and HOMER Simulation Software Results with Real Production Data of Solar Power Plants in Different Provinces of Turkey.
- Donev, J. (2024). Coefficient of performance. Retrieved December 10, 2024, from https://energyeducation.ca/encyclopedia/Coefficient_of_performance

- Dubey, S., Sarvaiya, J. N., & Seshadri, B. (2013). Temperature Dependent Photovoltaic (PV) Efficiency and Its Effect on PV Production in the World – A Review. *Energy Procedia*, 33, 311–321. <https://doi.org/10.1016/j.egypro.2013.05.072>
- Eddie Sembatya, Joel Essien, Julius Magala, Mathilde Brix Pedersen, & Padmasai Lakshmi Bhamidipati. (2022). Uganda Captive Solar PV Market – Insights Report. Retrieved October 31, 2024, from <https://unepccc.org/publications/uganda-captive-solar-pv-market-insights-report/>
- Edeogu, I., Feddes, J., & Leonard, J. (1997, April). Comparison between vertical and horizontal air flow for fruit and vegetable precooling. In *Canadian Agriculture engineering* (pp. 107–112). Retrieved November 30, 2024, from <https://www.scopus.com/record/display.uri?eid=2-s2.0-0031125864&origin=inward&txGid=6ff9f8ca64a6f3aeaea91ec6c2a55440>
- Eltawil, M. A., & Zhao, Z. (2013). MPPT techniques for photovoltaic applications. *Renewable and Sustainable Energy Reviews*, 25, 793–813. <https://doi.org/10.1016/j.rser.2013.05.022>
- Energypedia. (n.d.). Cold Storage of Agricultural Products. Retrieved December 13, 2024, from https://energypedia.info/wiki/Cold_Storage_of_Agricultural_Products
- F. Faubion, D., & A. Kader, A. (1997). Influence of Place packaging or tray packaging on the cooling rate of palletized "Anjou" pears. *HortTechnology*, 7(4), 378–382. <https://doi.org/https://doi.org/10.21273/HORTTECH.7.4.378>
- Fage, J. D., & Maier, D. J. (2024, January). Ghana | History, Flag, Map, Population, Language, Currency, & Facts | Britannica. Retrieved November 19, 2024, from <https://www.britannica.com/place/Ghana>
- Famoso, F., Lanzafame, R., Maenza, S., & Scandura, P. F. (2015). Performance Comparison between Micro-inverter and String-inverter Photovoltaic Systems. *Energy Procedia*, 81, 526–539. <https://doi.org/10.1016/j.egypro.2015.12.126>
- for Community Health, U. C. (n.d.). Ethylene in fruits and vegetables. Retrieved November 22, 2024, from https://ucsdcommunityhealth.org/resources/?fwp_resource_keywords=ethylene
- Fordham, R., & Biggs, A. G. (2008, October). *Principles of Vegetable Crop Production*. Experimental Agriculture. doi:10.1017/S0014479700014289
- Franklin, D. E. (2018). Solar Photovoltaic (PV) System Components.
- Freeman, J., Whitmore, J., Blair, N., & Dobos, A. P. (2014). Validation of multiple tools for flat plate photovoltaic modeling against measured data [ISSN: 0160-8371]. *2014 IEEE 40th Photovoltaic Specialist Conference (PVSC)*, 1932–1937. <https://doi.org/10.1109/PVSC.2014.6925304>
- FrigoSys. (n.d.). Cold Storage Humidity Control. Retrieved December 12, 2024, from <https://www.frigosys.com/cold-storage-humidity-control/>

- Ghana [Page Version ID: 142152180]. (2024, November). Retrieved November 19, 2024, from <https://it.wikipedia.org/w/index.php?title=Ghana&oldid=142152180>
- Gloel, J. (2022). GHANA REFRIGERATION and AIR CONDITIONING (RAC) roadmap. *Environmental Protection Agency*, 64. Retrieved November 27, 2024, from https://www.green-cooling-initiative.org/fileadmin/user_upload/220621_Ghana_Roadmap_med.pdf
- Google Maps. (n.d.). Retrieved December 15, 2024, from https://www.google.com.gh/maps/place/Trax+Ghana+Farm/@10.8570919,-0.7329899,17z/data=!3m1!4b1!4m6!3m5!1s0xe2b25bfb0e248a1:0x5e90fc9899e8b41f!8m2!3d10.8570866!4d-0.730415!16s%2Fg%2F11r3yls880?entry=ttu&g_ep=EgoyMDI0MTIxMS4wIKXMDSoASAFQAw3D%3D
- Goossens, D., & Van Kerschaever, E. (1999). Aeolian dust deposition on photovoltaic solar cells: The effects of wind velocity and airborne dust concentration on cell performance. *Solar Energy*, 66(4), 277–289. [https://doi.org/10.1016/S0038-092X\(99\)00028-6](https://doi.org/10.1016/S0038-092X(99)00028-6)
- Granyd, E., Ekroth, I., & Lundquist, P. (1999). *Refrigerating engineering* (Vol. 590). Royal Institute of Technology, KTH.
- Gürel, A., Ağbulut, Ü., Bakır, H., Ergün, A., & Yıldız, G. (2023). A state of art review on estimation of solar radiation with various models. *Heliyon*, 9, e13167. <https://doi.org/10.1016/j.heliyon.2023.e13167>
- Hannes, E., & Brits, B. (2020, September). Solar: A power(full) alternative for the cold chain. Retrieved December 13, 2024, from <https://coldlinkafrica.co.za/solar-a-powerfull-alternative-for-the-cold-chain/>
- Harmailil, I. O., Sultan, S. M., Tso, C. P., Fudholi, A., Mohammad, M., & Ibrahim, A. (2024). A review on recent photovoltaic module cooling techniques: Types and assessment methods. *Results in Engineering*, 22, 102225. <https://doi.org/10.1016/j.rineng.2024.102225>
- Haukås, H. T. (2016). *CO₂ (R744) som kuldemedium: Kompendium*. Norsk kjøleteknisk forening.
- Hazardous Substance Fact Sheet. (2015, June). Retrieved November 27, 2024, from <https://nj.gov/health/eoh/rtkweb/documents/fs/1594.pdf>
- Hennessy, D. (2009). Crop Yield Skewness and the Normal Distribution. 34. Retrieved November 27, 2024, from https://www.researchgate.net/publication/227345486_Crop_Yield_Skewness_and_the_Normal_Distribution
- Hiroyuki, T., Futoshi, Y., Dauda, B., O, K., Salaudeen, O, E., Hyacinth, & A, H., Manuel. (2021, October). *Solar-powered cold-storages and sustainable food system transformation: Evidence from horticulture markets interventions in northeast Nigeria* [Google-Books-ID: Mt5IEAAAQBAJ]. Intl Food Policy Res Inst.

- Hofstad, K. (2024, June). Solenergi. Retrieved September 16, 2024, from <https://snl.no/solenergi>
- How a PV Module Works. (n.d.). Retrieved September 16, 2024, from <https://www.apricus.com/solar-pv-systems-pv-panels-19.html>
- Ibegbulam, C., Adeyemi, O., & Fogbonjaiye, O. (2023). Adoption of Solar PV in Developing Countries: Challenges and Opportunity. *International Journal of Physical Sciences Research*, 36–57. <https://doi.org/10.37745/10.37745/ijpsr.17/vol7n13657>
- Iderawumi, A. M. (2021). Quality of Fruits and Vegetables during Storage: An Overview. *ResearchGate*. Retrieved November 22, 2024, from https://www.researchgate.net/publication/353445848_Quality_of_Fruits_and_Vegetables_during_Storage_An_Overview
- IEA. (n.d.). Key findings – Africa Energy Outlook 2022 – Analysis. Retrieved December 13, 2024, from <https://www.iea.org/reports/africa-energy-outlook-2022/key-findings>
- Installasjon av solcelleanlegg. (n.d.). Retrieved November 28, 2024, from <https://iug.no/vaart-arbeid/oppdrag/oppdrag-detalj/article/1656871>
- Intro - Meteonorm (de). (n.d.). Retrieved November 21, 2024, from <https://meteonorm.com/en/>
- Jakica, N. (2018). State-of-the-art review of solar design tools and methods for assessing daylighting and solar potential for building-integrated photovoltaics. *Renewable and Sustainable Energy Reviews*, 81, 1296–1328. <https://doi.org/10.1016/j.rser.2017.05.080>
- Jordan, D. C., & Kurtz, S. R. (2013). Photovoltaic Degradation Rates—an Analytical Review. *Progress in Photovoltaics: Research and Applications*, 21(1), 12–29. <https://doi.org/10.1002/pip.1182>
- Just, R. E., & Weninger, Q. (1999, May). ARE CROP YIELDS NORMALLY DISTRIBUTED? In *American Journal of Agricultural Economics* (pp. 257–499, Vol. 81). Retrieved November 27, 2024, from <https://onlinelibrary.wiley.com/doi/epdf/10.2307/1244582>
- Justo, J. J., Mwasilu, F., Lee, J., & Jung, J.-W. (2013). AC-microgrids versus DC-microgrids with distributed energy resources: A review. *Renewable and Sustainable Energy Reviews*, 24, 387–405. <https://doi.org/10.1016/j.rser.2013.03.067>
- Kader, A. A. (1980). Prevention of ripening in fruits by use of controlled atmosphere. In *Food Technology*. Retrieved November 30, 2024, from https://scholar.google.com/scholar_lookup?title=Prevention%20of%20ripening%20in%20fruits%20by%20use%20of%20controlled%20atmosphere&publication_year=1980&author=A.A.%20Kader

- Kalogirou, S. A. (2014). Chapter 9 - Photovoltaic Systems. In S. A. Kalogirou (Ed.), *Solar Energy Engineering (Second Edition)* (Second Edition, pp. 481–540). Academic Press. [https://doi.org/https://doi.org/10.1016/B978-0-12-397270-5.00009-1](https://doi.org/10.1016/B978-0-12-397270-5.00009-1)
- Kimber, A., Mitchell, L., Nogradi, S., & Wenger, H. (2006). The Effect of Soiling on Large Grid-Connected Photovoltaic Systems in California and the Southwest Region of the United States [ISSN: 0160-8371]. *2006 IEEE 4th World Conference on Photovoltaic Energy Conference*, 2, 2391–2395. <https://doi.org/10.1109/WCPEC.2006.279690>
- Kipkoech, R., Takase, M., Ahogle, A. M. A., & Ocholla, G. (2024). Opportunities and challenges in Ghana's renewable energy sector. *Discover Applied Sciences*, 6(10), 530. <https://doi.org/10.1007/s42452-024-06148-x>
- Kumari, S., Bhende, A., Pandit, A., & Rayalu, S. (2023). Efficiency enhancement of photovoltaic panel by heat harvesting techniques. *Energy for Sustainable Development*, 73, 303–314. <https://doi.org/10.1016/j.esd.2023.02.007>
- Lalwani, M., Kothari, D., & Singh, M. (2010). Investigation of Solar Photovoltaic Simulation Softwares. *INTERNATIONAL JOURNAL OF APPLIED ENGINEERING RESEARCH*, 1.
- Lambert, T., Gilman, P., & Lilienthal, P. (2005, December). Micropower System Modeling with Homer. In F. A. Farret & M. G. Simões (Eds.), *Integration of Alternative Sources of Energy* (1st ed., pp. 379–418). Wiley. <https://doi.org/10.1002/0471755621.ch15>
- Lange, B., Priesmann, C., Geiss, M., & Lambrecht, A. (2016). Promoting Food Security and Safety via Cold Chains. *Deutsche Gesellschaft für Internationale Zusammenarbeit (GIZ) GmbH*.
- Liu, Y., Songtao, B., Wei, S., & Li, L. (2024). Estimating the frost damage index in lettuce using UAV-based RGB and multispectral images. *ResearchGate*. <https://doi.org/10.3389/fpls.2023.1242948>
- Liu, Y., Yao, L., Jiang, H., Lu, N., Qin, J., Liu, T., & Zhou, C. (2022). Spatial estimation of the optimum PV tilt angles in China by incorporating ground with satellite data. *Renewable Energy*, 189, 1249–1258. <https://doi.org/10.1016/j.renene.2022.03.072>
- Louie, H. (2018a). Design and Implementation of Off-Grid Systems. In H. Louie (Ed.), *Off-Grid Electrical Systems in Developing Countries* (pp. 387–445). Springer International Publishing. https://doi.org/10.1007/978-3-319-91890-7_12
- Louie, H. (2018b). Off-Grid System Converters and Controllers. In H. Louie (Ed.), *Off-Grid Electrical Systems in Developing Countries* (pp. 261–306). Springer International Publishing. https://doi.org/10.1007/978-3-319-91890-7_9
- Mahmood, R. A., Ali, O. M., & Noor, M. M. (2020). Mechanical Vapour Compression Refrigeration System: Review Part 1: Environment Challenge. *Research Gate*. Retrieved November 28, 2024, from <https://www.ijame-poland.com/Mechanical->

- Vapour-Compression-Refrigeration-System-Review-Part-1-Environment-Challenge, 166819,0,2.html
- Maina, P., & Huan, Z. (2015). A review of carbon dioxide as a refrigerant in refrigeration technology. *South African Journal of Science*. Retrieved November 28, 2024, from https://www.scielo.org.za/scielo.php?pid=S0038-23532015000500007&script=sci_arttext
- Makola, C. S., Le Roux, P. F., & Jordaan, J. A. (2023). Comparative Analysis of Lithium-Ion and Lead-Acid as Electrical Energy Storage Systems in a Grid-Tied Microgrid Application [Number: 5 Publisher: Multidisciplinary Digital Publishing Institute]. *Applied Sciences*, 13(5), 3137. <https://doi.org/10.3390/app13053137>
- Makule, E. E., & Dimoso, N. (2022). Precooling and Cold Storage Methods for Fruits and Vegetables in Sub-Saharan Africa—A Review. *ResearchGate*. <https://doi.org/10.3390/horticulturae8090776>
- Mani, M., & Pillai, R. (2010). Impact of dust on solar photovoltaic (PV) performance: Research status, challenges and recommendations. *Renewable and Sustainable Energy Reviews*, 14(9), 3124–3131. <https://doi.org/10.1016/j.rser.2010.07.065>
- Martinez-Gracia, A., Arauzo, I., & Uche, J. (2019, January). Chapter 5 - Solar energy availability. In F. Calise, M. D. D'Accadia, M. Santarelli, A. Lanzini, & D. Ferrero (Eds.), *Solar Hydrogen Production* (pp. 113–149). Academic Press. <https://doi.org/10.1016/B978-0-12-814853-2.00005-9>
- Mavromatidis, G., Orehounig, K., & Carmeliet, J. (2018). A review of uncertainty characterisation approaches for the optimal design of distributed energy systems. *Renewable and Sustainable Energy Reviews*, 88, 258–277. <https://doi.org/10.1016/j.rser.2018.02.021>
- McDonald, K., & Sun, D.-W. (2000). Vacuum cooling technology for the food processing industry: A review. *FRCFT Group, Department of Agricultural and Food Engineering, University College Dublin*. Retrieved December 1, 2024, from https://belinrae.inrae.fr/doc_num.php?explnum_id=3074
- McLinden, M. O., & Huber, M. L. (2020). (R)Evolution of Refrigerants. *ACS Publications*. <https://doi.org/https://doi.org/10.1021/acs.jced.0c00338>
- Mehdi, M., Ammari, N., Alami Merrouni, A., Benazzouz, A., & Dahmani, M. (2023). Experimental investigation on the effect of wind as a natural cooling agent for photovoltaic power plants in desert locations. *Case Studies in Thermal Engineering*, 47, 103038. <https://doi.org/10.1016/j.csite.2023.103038>
- Meier, D. C. (n.d.). Using XPS to Find Evidence of Ammonia Corrosion of Copper. Retrieved November 29, 2024, from <https://www.mccrone.com/mm/xps-find-ammonia-corrosion-of-copper/>

- Mekhilef, S., Saidur, R., & Kamalisarvestani, M. (2012). Effect of dust, humidity and air velocity on efficiency of photovoltaic cells. *Renewable and Sustainable Energy Reviews*, 16(5), 2920–2925. <https://doi.org/10.1016/j.rser.2012.02.012>
- Melinder, Å. (2015, August). *Handbook on indirect refrigeration and heat pump systems*. Retrieved November 29, 2024, from <https://varmtochkallt.se/wp-content/uploads/Projekt/Effsys2/P02/ke-Melinder-engelsk-handbok.pdf>
- Mishra, S., & Viral, R. K. (2022, January). Chapter 6 - Introduction to hybrid AC/DC microgrids. In J. M. Guerrero & R. Kandari (Eds.), *Microgrids* (pp. 159–189). Academic Press. <https://doi.org/10.1016/B978-0-323-85463-4.00005-8>
- Moran, M. J., Shapiro, H. N., Boettner, D. D., & Bailey, M. B. (2014, May). *The fundamentals of engineering* (8th ed.). Retrieved November 28, 2024, from <https://www.amazon.com/Fundamentals-Engineering-Thermodynamics-Michael-Moran/dp/1118412931>
- National Electrification Scheme. (n.d.). Retrieved November 19, 2024, from <https://www.iea.org/policies/4956-national-electrification-scheme>
- Nations, U. (n.d.). What is renewable energy? [Publisher: United Nations]. Retrieved September 16, 2024, from https://www.un.org/en/climatechange/what-is-renewable-energy?gad_source=1&gclid=Cj0KCQjwrf-3BhDgARIsAEWJ6SzUgAubOesuV5jwMEgSRIJ9MaAlmSEALw_wcB
- Ndiaye, A., Kébé, C., Ndiaye, P., Charki, A., Kobi, A., & Sambou, V. (2013). Impact of dust on the photovoltaic (PV) modules characteristics after an exposition year in Sahelian environment: The case of Senegal. *International journal of physical sciences*, 8.
- of Agriculture, U. S. D. (1961). Cooling apples and pears in storage rooms. *United states department of agriculture*. Retrieved November 30, 2024, from https://books.google.no/books?hl=en&lr=&id=Cso8AAAAYAAJ&oi=fnd&pg=PA2&dq=Sainsbury+GF.+Cooling+apples+and+pears+in+storage+rooms.+US+Dept.+Agri.+Mtkg.+Res.+Rep.,+1961.+p.+474.&ots=E75zsVwqG3&sig=WVNZjAcCgBQnkcG1-ZdwnbsdbVA&redir_esc=y#v=onepage&q&f=false
- Olosunde, W. A., Aremu, A. K., & Onwude, D. I. (2016). Development of a Solar Powered Evaporative Cooling Storage System for Tropical Fruits and Vegetables [_eprint: <https://onlinelibrary.wiley.com/doi/pdf/10.1111/jfpp.12605>]. *Journal of Food Processing and Preservation*, 40(2), 279–290. <https://doi.org/10.1111/jfpp.12605>
- Onar, O. C., & Khaligh, A. (2015, January). Chapter 2 - Energy Sources. In M. H. Rashid (Ed.), *Alternative Energy in Power Electronics* (pp. 81–154). Butterworth-Heinemann. <https://doi.org/10.1016/B978-0-12-416714-8.00002-0>
- Organization, F. a. A. (2011). Global food losses and food waste. *Food and Agriculture Organization of the United Nations*. Retrieved November 29, 2024, from <https://www.fao.org/faostat/en/#/>

- //www.fao.org/fileadmin/templates/wsfs/docs/expert_paper/How_to_Feed_the_World_in_2050.pdf
- Organization, W. H. (2024, July). Hunger numbers stubbornly high for three consecutive years as global crises deepen: UN report. Retrieved December 13, 2024, from <https://www.who.int/news/item/24-07-2024-hunger-numbers-stubbornly-high-for-three-consecutive-years-as-global-crises-deepen--un-report>
- Owusu - Brown, B. (2016). The effect of settling harmattan dust on photovoltaic modules in Walewale, Northern Ghana. Retrieved October 30, 2024, from <https://ir.knust.edu.gh/handle/123456789/9320>
- Paudyal, B. R., & Shakya, S. R. (2016). Dust accumulation effects on efficiency of solar PV modules for off grid purpose: A case study of Kathmandu. *Solar Energy*, 135, 103–110. <https://doi.org/10.1016/j.solener.2016.05.046>
- Pearson, A. (2008). *Ammonia as a refrigerant*. International Institute of Refrigeration.
- Pros & Cons: Solar Microinverter vs Inverter | Blogs | Growatt. (n.d.). Retrieved December 4, 2024, from <https://en.growatt.com/media/news/pros-cons:-solar-microinverter-vs-inverter>
- PVsyst | PVsyst 8. (n.d.). Retrieved November 26, 2024, from <https://www.pvsyst.com/pvsyst-8/>
- Qazi, S. (2017, January). Chapter 2 - Fundamentals of Standalone Photovoltaic Systems. In S. Qazi (Ed.), *Standalone Photovoltaic (PV) Systems for Disaster Relief and Remote Areas* (pp. 31–82). Elsevier. <https://doi.org/10.1016/B978-0-12-803022-6.00002-2>
- Qviller, A. (n.d.). Pumper, shunter og ventiler. Retrieved December 6, 2024, from <https://www.abkqviller.no/bolig/pumper-shunter-og-ventiler/>
- Rajput, S. (2017, April). *SOLAR ENERGY- Fundamentals, Economic and Energy Analysis First Edition: 2017 ISBN: 978-93—81125-23—6*.
- Ramirez, O. A. (2001). ARE CROP YIELDS NORMALLY DISTRIBUTED? *ResearchGate*. Retrieved November 27, 2024, from https://www.researchgate.net/publication/23504554_ARE_CROP_YIELDS_NORMALLY_DISTRIBUTED
- Rana, S., Barholia, A., Lekhi, R., Pippal, R., & Rana, P. (2019). Vegetative growth of cabbage (*Brassica Oleracea* var. *capitata* l.). cv. Pusa drum head in relation to plant spacing, boron and molybdenum. In *Journal of Pharmacognosy and Phytochemistry* (pp. 933–936). Retrieved December 12, 2024, from <https://www.phytojournal.com/archives/2019/vol8issue2S/PartX/SP-8-2-255-611.pdf>
- Relative humidity. (n.d.). Retrieved December 4, 2024, from <https://www.sciencedirect.com/topics/agricultural-and-biological-sciences/relative-humidity>
- Ritchie, H. (2024, June). Solar panel prices have fallen by around 20% every time global capacity doubled. Retrieved September 16, 2024, from <https://ourworldindata.org/solar-panel-prices>

- org/data-insights/solar-panel-prices-have-fallen-by-around-20-every-time-global-capacity-doubled
- Rutta, E. (2022). Understanding barriers impeding the deployment of solar-powered cold storage technologies for post-harvest tomato losses reduction: Insights from small-scale farmers in Tanzania. *Frontiers in Sustainable Food Systems*, 6. <https://doi.org/10.3389/fsufs.2022.990528>
- Safety Data Sheet R290. (2021). *National refrigerations inc.* Retrieved November 27, 2024, from <https://refrigerants.com/wp-content/uploads/2019/12/SDS-R290-Propane.pdf>
- Said, S. A., Hassan, G., Walwil, H. M., & Al-Aqeeli, N. (2018). The effect of environmental factors and dust accumulation on photovoltaic modules and dust-accumulation mitigation strategies. *Renewable and Sustainable Energy Reviews*, 82, 743–760. <https://doi.org/10.1016/j.rser.2017.09.042>
- Schwartz, D., Thompson, A., & Kalring, H.-P. (2014). Guidelines to use tomato in experiments with a controlled environment. 5, 625. <https://doi.org/10.3389/fpls.2014.00625>
- Shuai, Z., Sun, Y., Shen, Z. J., Tian, W., Tu, C., Li, Y., & Yin, X. (2016). Microgrid stability: Classification and a review. *Renewable and Sustainable Energy Reviews*, 58, 167–179. <https://doi.org/10.1016/j.rser.2015.12.201>
- Sicard, A. J., & Baker, R. T. (2020). Fluorocarbon Refrigerants and their Syntheses: Past to Present. *ACS Publications*, 120(17). Retrieved November 28, 2024, from https://pubs.acs.org/doi/10.1021/acs.chemrev.9b00719?src=getftr&utm_source=sciencedirect_contenthosting&getft_integrator=sciencedirect_contenthosting
- Singh, V., & Meher, J. (2014). Postharvest Technology of Fruits and Vegetables: An Overview. Retrieved November 30, 2024, from https://www.researchgate.net/publication/278557269_Postharvest_Technology_of_Fruits_and_Vegetables_An_Overview
- Skouri, S., Ben Haj Ali, A., Bouadila, S., Ben Salah, M., & Ben Nasrallah, S. (2016). Design and construction of sun tracking systems for solar parabolic concentrator displacement. *Renewable and Sustainable Energy Reviews*, 60, 1419–1429. <https://doi.org/10.1016/j.rser.2016.03.006>
- Soni, J., Gupta, V., Joshi, Y., & Singh, S. K. (2023). Investigative comparison of R134a, R290, R600a and R152a refrigerants in conventional vapor compression refrigeration system. Retrieved November 27, 2024, from <https://www.sciencedirect.com/science/article/pii/S2214785323041561>
- Spiers, D. (2012, January). Chapter IIB-2 - Batteries in PV Systems. In A. McEvoy, T. Markvart, & L. Castañer (Eds.), *Practical Handbook of Photovoltaics (Second Edition)* (pp. 721–776). Academic Press. <https://doi.org/10.1016/B978-0-12-385934-1.00022-2>

- Sreejariya, P., Raynaud, T., Dabbadie, L., & Yakupitiyage, A. (2016). Effect of Water Recirculation Duration and Shading on Lettuce (*Lactuca sativa*) Growth and Leaf Nitrate Content in a Commercial Aquaponic System. *Turkish Journal of Fisheries and Aquatic Sciences*. https://doi.org/10.4194/1303-2712-v16_2_11
- Starkeayres. (2020, October). Hot pepper lance. Retrieved December 12, 2024, from <https://www.starkeayres.com/uploads/files/Lance-2020.pdf>
- Stephen A., M., Dutton, G. S., Yu, P., & Ray, E. (2018). An unexpected and persistent increase in global emissions of ozone-depleting CFC-11. *Nature*, 557. Retrieved November 28, 2024, from <https://www.nature.com/articles/s41586-018-0106-2>
- Subedi, S., Kattel, D., & Thokar, N. (2022). A REVIEW ON POST-HARVEST PRE-COOLING METHODS OF FRUITS AND VEGETABLES. *Research Gate*. Retrieved November 30, 2024, from https://www.researchgate.net/publication/364690662_A REVIEW ON POST-HARVEST PRECOOLING METHODS OF FRUITS AND VEGETABLES
- Sun, D.-W., & Wang, L. (2001, June). Rapid cooling of porous and moisture foods by using vacuum cooling technology. In *Trends in Food Science & Technology* (pp. 174–184, Vol. 12). Retrieved December 1, 2024, from <https://www.sciencedirect.com/science/article/pii/S0924224401000772>
- Suwi, O., & Justo, J. J. (2024, January). Chapter Seven - Comprehensive discussions on energy storage devices: Modeling, control, stability analysis with renewable energy resources in microgrid and virtual power plants. In R. C. Bansal, J. J. Justo, & F. A. Mwasilu (Eds.), *Modeling and Control Dynamics in Microgrid Systems with Renewable Energy Resources* (pp. 139–177). Academic Press. <https://doi.org/10.1016/B978-0-323-90989-1.00001-4>
- Takase, M., Aboah, M., & Kipkoech, R. (2022). A review on renewable energy potentials and energy usage statistics in Ghana. *Fuel Communications*, 11, 100065. <https://doi.org/10.1016/j.fueco.2022.100065>
- Tapia-Hernandez, J., & Katouzian, I. (2017). Relative Humidity. *Nanoencapsulation Technologies for the Food and Nutraceutical Industries*. Retrieved November 23, 2024, from <https://www.sciencedirect.com/topics/agricultural-and-biological-sciences/relative-humidity>
- The World Bank Group. (n.d.). Ghana - Climatology. Retrieved October 29, 2024, from <https://climateknowledgeportal.worldbank.org/country/ghana/climate-data-historical>
- Thompson, J. F. (1998). Pre-cooling and storage facilities. *Department of Biological & Agricultural Engineering*. <https://citeseerx.ist.psu.edu/document?repid=rep1&type=pdf&doi=22614073b39b01a03ae62876a935455f368ae9d0>
- ToolBox, T. E. (2007). Sodium Chloride Water Solutions. Retrieved December 13, 2024, from https://www.engineeringtoolbox.com/sodium-chloride-water-d_1187.html

- ToolBox, T. E. (2018). Carbon Dioxide - Thermophysical Properties. Retrieved December 11, 2024, from https://www.engineeringtoolbox.com/CO2-carbon-dioxide-properties-d_2017.html
- Touati, F., Al-Hitmi, M., & Bouchech, H. J. (2013). Study of the Effects of Dust, Relative Humidity, and Temperature on Solar PV Performance in Doha: Comparison Between Monocrystalline and Amorphous PVS. *International Journal of Green Energy*, 10. <https://doi.org/10.1080/15435075.2012.692134>
- Unal, F. (2019). CONDENSATION ANALYSIS OF THE INSULATION OF WALLS ACCORDING TO DIFFERENT LOCATIONS IN MARDIN PROVINCE. *European Journal of Technique*, 9, 253–262. <https://doi.org/10.36222/ejt.648601>
- United Nations. (n.d.). Indicator 12.3.1 | Sustainable developments Goals. Retrieved December 14, 2024, from <https://sdgs.unep.org/indicator1231>
- Upper East Region [Page Version ID: 1256667968]. (2024, November). Retrieved November 19, 2024, from https://en.wikipedia.org/w/index.php?title=Upper_East_Region&oldid=1256667968
- Ustun, T. S., Ozansoy, C., & Zayegh, A. (2011). Recent developments in microgrids and example cases around the world—A review. *Renewable and Sustainable Energy Reviews*, 15(8), 4030–4041. <https://doi.org/10.1016/j.rser.2011.07.033>
- Utz, V. (2011). Modern Energy Services for Modern Agriculture. *GIZ-HERA – Poverty-oriented Basic Energy Services*. Retrieved December 24, 2024, from https://energypedia.info/images/f/fd/Energy_Services_for_Modern_Agriculture.pdf
- Valentin Software. (2020, March). PV*SOL premium | Photovoltaic design and simulation. Retrieved December 5, 2024, from <https://valentin-software.com/en/products/pvsol-premium/>
- Vuppaladadiyam, A. K., Antunes, E., Vuppaladadiyam, S. S., Baig, Z. T., Subiantoro, A., Lei, G., Leu, S.-Y., Sarmah, A. K., & Duan, H. (2022). Progress in the development and use of refrigerants and unintended environmental consequences. *Science of The Total Environment*, 823. <https://doi.org/https://doi.org/10.1016/j.scitotenv.2022.153670>
- Wageningen, U. a. r. (n.d.). Ethylene management in practice. Retrieved November 23, 2024, from <https://www.freshknowledge.eu/en/longreads/ethylene-management.htm>
- Wang, K., Eisele, M., Hwang, Y., & Radermacher, R. (2010, March). Review of secondary loop refrigeration systems. In *International journal of refrigeration* (pp. 212–234). Retrieved December 6, 2024, from <https://www.sciencedirect.com/science/article/pii/S0140700709002291?via%3Dihub>
- Wang, R., Xing, Y., Xuanlin, L., & Guo, X. (2019). Microstructure and quality of cabbage slices (*Brassica oleracea* L. var. *capitata* L.) as affected by cryogenic quick-freezing

- treatment. *International Journal of Food Properties*, 22. <https://doi.org/10.1080/10942912.2019.1681449>
- Wantira, A., Sugiharto, M., & Setiabudi, B. (2023). Utilization Off-Grid Solar Powered Cold Storage for Economy Improvement of Fishermen in Mangur Island. *International Journal of Multicultural and Multireligious Understanding*, 10, 125. <https://doi.org/10.18415/ijmmu.v10i6.4852>
- Weisstein, E. (n.d.). Bessel Function of the First Kind. Retrieved December 15, 2024, from <https://mathworld.wolfram.com/BesselFunctionoftheFirstKind.html>
- Wenzl, H. (2009, January). BATTERIES AND FUEL CELLS | Lifetime. In J. Garche (Ed.), *Encyclopedia of Electrochemical Power Sources* (pp. 552–558). Elsevier. <https://doi.org/10.1016/B978-044452745-5.00048-4>
- Wikipedia. (n.d.). Agurk. Retrieved December 12, 2024, from <https://no.wikipedia.org/wiki/Agurk>
- Xiang, B., & Zhang, X. (2023). Advancements in the development of field precooling of fruits and vegetables with/without phase change materials. *Journal of energy storage*. Retrieved November 30, 2024, from <https://www.sciencedirect.com/science/article/pii/S2352152X23024052#bb0030>
- Yadav, P., Davies, P. J., & Khan, S. (2020). Breaking into the photovoltaic energy transition for rural and remote communities: Challenging the impact of awareness norms and subsidy schemes. *Clean Technologies and Environmental Policy*, 22(4), 817–834. <https://doi.org/10.1007/s10098-020-01823-0>
- Younis, A., & Onsa, M. (2022). A brief summary of cleaning operations and their effect on the photovoltaic performance in Africa and the Middle East. *Energy Reports*, 8, 2334–2347. <https://doi.org/10.1016/j.egyr.2022.01.155>
- Yuan, D., Guan-Bang, W., Verboven, P., Zhang, X.-R., Wu, D., & Nicolai, B. (2020, June). Postharvest precooling of fruit and vegetables: A review. In *Trends in food science and technology*. Retrieved November 30, 2024, from <https://www.sciencedirect.com/science/article/pii/S0924224420304568#bib38>
- Zheng, L., & Sun, D.-W. (2004, December). Vacuum cooling for the food industry—a review of recent research advances. In *Trends in food science & technology*. Retrieved November 30, 2024, from <https://www.sciencedirect.com/science/article/pii/S0924224404002183>
- Zijdemans, D. (2014, January). *Vannbaserte oppvarmings- og kjølesystemer*. VVSkunnskap.no.

Appendix

A Appendix A: Github repository

All code and latex-files used in this document are included in the Github repository linked below. Further explanations are given in the readme-file.

Github repository link

- https://github.com/ninasalvesen/thesis_latex_template

B Appendix B: Code script

B1 - Code script for creating PVsyst load data file

```
1 def pvssyt_load_profile(data, output_file, fan_consumption_kW=0.2):
2     """
3         Generate a PVsyst-compatible CSV file with constant fan consumption
4             added to the data.
5
6     Parameters:
7         data (pd.DataFrame): Hourly load data for each month (columns)
8             and time (rows).
9         output_file (str): Path to the output CSV file.
10        fan_consumption_kW (float): Constant fan consumption in kW
11            (default 0.2 kW).
12
13    """
14
15    # Read the data and set time as the index
16    data.set_index("Time", inplace=True)
17
18    # Add fan consumption to all load values
19    data += fan_consumption_kW
20
21    # Days in each month for a non-leap year
22    days_in_month = [31, 28, 31, 30, 31, 30, 31, 31, 30, 31, 30, 31]
23
24    # Generate hourly data for the entire year, starting at 01:00
25    hourly_data = []
26    for month, days in enumerate(days_in_month):
27        month_profile = data.iloc[:, month].values
28        hourly_data.extend(np.tile(month_profile, days))
29
30    # Create a datetime range starting at 01:00 on January 1st and
31    # ending at 23:00 on December 31st
32    datetime_range = pd.date_range(start="01/01/2023 01:00",
33                                   periods=len(hourly_data), freq="H")
34
35    # Ensure the data length matches
36    if len(hourly_data) != len(datetime_range):
37        raise ValueError("Data length mismatch. Ensure profiles cover
38                         8760 hours.")
39
40    # Create PVsyst-compatible DataFrame
41    pvssyt_data = pd.DataFrame({
42        "Date": datetime_range.strftime("%d/%m/%Y %H:%M"),
43        "P Load": hourly_data
44    })
45
```

```
38 # Add headers and units
39 with open(output_file, "w", encoding="ansi") as file:
40     file.write("# PVsyst Load Data File\n")
41     file.write("# Generated from Monthly Profiles with Fan Load\n")
42     file.write("#\n")
43     file.write("Date,P_Load\n")
44     file.write(",,[kW]\n")
45 pvsyst_data.to_csv(file, index=False, header=False,
        line_terminator="\n")
```

Listing 1: PVsyst Load Profile Generation

C Appendix C: Data sheet

C.1 PV Module Datasheet



Higher output power



Lower LCOE



Less shading and lower resistive loss

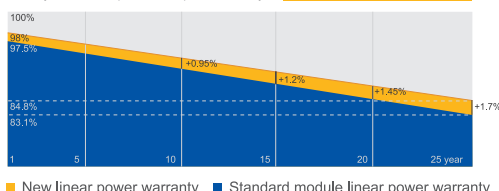


Better mechanical loading tolerance

Superior Warranty

- 12-year product warranty
- 25-year linear power output warranty

0.55% Annual Degradation
Over 25 years



■ New linear power warranty ■ Standard module linear power warranty

Comprehensive Certificates

- IEC 61215, IEC 61730, UL 61215, UL 61730
- ISO 9001: 2015 Quality management systems
- ISO 14001: 2015 Environmental management systems
- ISO 45001: 2018 Occupational health and safety management systems
- IEC 62941: 2019 Terrestrial photovoltaic (PV) modules - Quality system for PV module manufacturing



www.jasolar.com

Specifications subject to technical changes and tests.
JA Solar reserves the right of final interpretation.



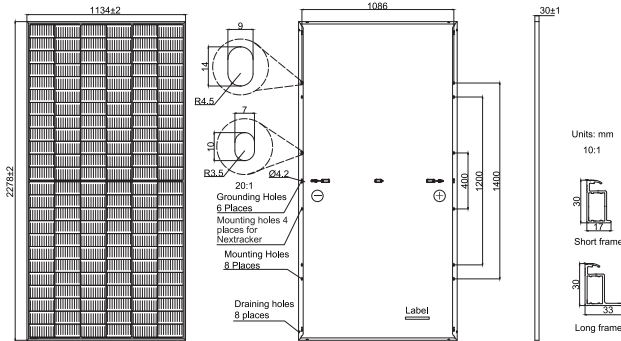
JA SOLAR

C.2 PV Module Datasheet

JA SOLAR

JAM72S30 540-565/GR Series

MECHANICAL DIAGRAMS



Remark: customized frame color and cable length available upon request

SPECIFICATIONS

Cell	Mono
Weight	27.3kg
Dimensions	2278±2mm×1134±2mm×30±1mm
Cable Cross Section Size	4mm ² (IEC), 12 AWG(UL)
No. of cells	144(6×24)
Junction Box	IP68, 3 diodes
Connector	QC 4.10-351 / MC4-EVO2A
Cable Length (Including Connector)	Portrait: 200mm(+)/300mm(-); Landscape: 1300mm(+)/1300mm(-)
Packaging Configuration	36pcs/Pallet 720pcs/40HQ Container

ELECTRICAL PARAMETERS AT STC

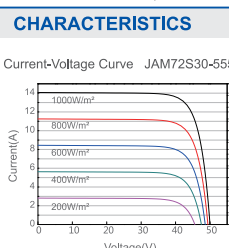
TYPE	JAM72S30 -540/GR	JAM72S30 -545/GR	JAM72S30 -550/GR	JAM72S30 -555/GR	JAM72S30 -560/GR	JAM72S30 -565/GR
Rated Maximum Power(Pmax) [W]	540	545	550	555	560	565
Open Circuit Voltage(Voc) [V]	49.60	49.75	49.90	50.02	50.15	50.28
Maximum Power Voltage(Vmp) [V]	41.64	41.80	41.96	42.11	42.27	42.42
Short Circuit Current(Isc) [A]	13.86	13.93	14.00	14.07	14.14	14.21
Maximum Power Current(Imp) [A]	12.97	13.04	13.11	13.18	13.25	13.32
Module Efficiency [%]	20.9	21.1	21.3	21.5	21.7	21.9
Power Tolerance	0~+5W					
Temperature Coefficient of Isc(α_{Isc})	+0.045%/°C					
Temperature Coefficient of Voc(β_{Voc})	-0.275%/°C					
Temperature Coefficient of Pmax(γ_{Pmp})	-0.350%/°C					
STC	Irradiance 1000W/m ² , cell temperature 25°C, AM1.5G					

Remark: Electrical data in this catalog do not refer to a single module and they are not part of the offer. They only serve for comparison among different module types.

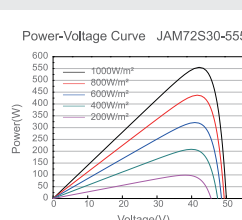
ELECTRICAL PARAMETERS AT NOCT

TYPE	JAM72S30 -540/GR	JAM72S30 -545/GR	JAM72S30 -550/GR	JAM72S30 -555/GR	JAM72S30 -560/GR	JAM72S30 -565/GR	Maximum System Voltage	1000V/1500V DC						
Rated Max Power(Pmax) [W]	408	412	416	420	424	428	Operating Temperature	-40°C ~ +85°C						
Open Circuit Voltage(Voc) [V]	46.43	46.55	46.68	46.85	46.99	47.15	Maximum Series Fuse Rating	25A						
Max Power Voltage(Vmp) [V]	38.99	39.20	39.43	39.66	39.85	40.04	Maximum Static Load Front*	5400Pa(112lb/ft ²)						
Short Circuit Current(Isc) [A]	11.09	11.13	11.17	11.21	11.26	11.31	Maximum Static Load Back*	2400Pa(50lb/ft ²)						
Max Power Current(Imp) [A]	10.47	10.51	10.55	10.59	10.64	10.69	NOCT	45±2°C						
NOCT	Irradiance 800W/m ² , ambient temperature 20°C, wind speed 1m/s, AM1.5G						Safety Class	Class II						
*For Nextracker installations, maximum static load please take compatibility approve letter between JA Solar and Nextracker for reference.														
Fire Performance														

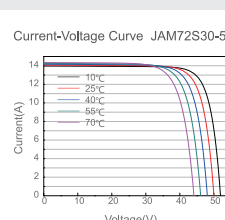
Current-Voltage Curve JAM72S30-555/GR



Power-Voltage Curve JAM72S30-555/GR



Current-Voltage Curve JAM72S30-555/GR



Premium Cells, Premium Modules

Version No. : Global_EN_20220921A

C.3 Battery Datasheet

BATTERY-BOX PREMIUM LVS

- Scalable from 4 kWh to 256 kWh
- Maximum Flexibility for any Application with up to 64 Modules Connected in Parallel
- Compatible with Market Leading 1 and 3 Phase Inverters
- Cobalt Free Lithium Iron Phosphate (LFP) Battery: Maximum Safety, Life Cycle and Power
- Capable of High-Powered Emergency-Backup and Off-Grid Function
- Patented Internal Plug Design Requires No Additional Wiring
- Self-Consumption Optimization for Residential and Commercial Applications



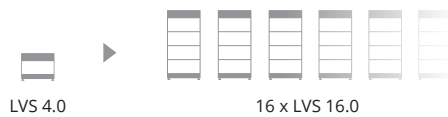
BATTERY-BOX PREMIUM LVS

- 4 kWh Module
- Modular Design Simplifies Transport and Installation

The BYD Battery-Box Premium LVS is a lithium iron phosphate (LFP) battery pack for use with an external inverter. A single Battery-Box Premium LVS contains between 1 to 6 battery modules LVS stacked in parallel and can reach 4 to 24.0 kWh usable capacity in one tower:

- Battery-Box LVS 4.0 (4 kWh)
- Battery-Box LVS 8.0 (8 kWh)
- Battery-Box LVS 12.0 (12 kWh)
- Battery-Box LVS 16.0 (16 kWh)
- Battery-Box LVS 20.0 (20 kWh - single tower only)
- Battery-Box LVS 24.0 (24 kWh - single tower only)

Connect up to 16 Battery-Box LVS 16.0 in parallel for a maximum size of 256 kWh. Ability to scale by adding LVS modules or parallel towers of 1 to 4 modules later.



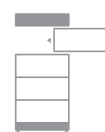
FLEXIBLE, EFFICIENT, SIMPLE



Internal Plug Connection
No Additional Wiring Required



4 - 256 kWh
Tailored Sizing for Each Application



Extend Anytime
Easily Adapts to New Requirements



High Power
Power for Every Application



C.4 Battery Datasheet

TECHNICAL PARAMETERS PREMIUM LVS

	LVS 4.0	LVS 8.0	LVS 12.0	LVS 16.0	LVS 20.0	LVS 24.0
Battery Module	LVS (4 kWh, 51.2 V, 45 kg)					
Number of Modules	1	2	3	4	5	6
Usable Energy [1]	4 kWh	8 kWh	12 kWh	16 kWh	20 kWh	24 kWh
Max Cont. Output Current [2]	65 A	130 A	195 A	250 A	250 A	250 A
Peak Output Current [2]	90 A, 5 s	180 A, 5 s	270 A, 5 s	360 A, 5 s	360 A, 5 s	360 A, 5 s
Dimensions (H/W/D)	528 x 650 x 298 mm	761 x 650 x 298 mm	994 x 650 x 298 mm	1227 x 650 x 298 mm	1460 x 650 x 298 mm	1693 x 650 x 298 mm
Weight	64 kg	109 kg	154 kg	199 kg	244 kg	289 kg
Nominal Voltage	51.2 V					
Operating Voltage	40-57.6 V					
Operating Temperature	-10 °C to +50°C					
Battery Cell Technology	Lithium Iron Phosphate (cobalt-free)					
Communication	CAN / RS485					
Enclosure Protection Rating	IP55					
Round-Trip Efficiency	≥95%					
Scalability [3]	Max. 64 Modules in Parallel (256 kWh)			Single Tower Only		
Certification	VDE2510-50 / IEC62619 / CE / CEC / UN38.3					
Applications	ON Grid / ON Grid + Backup / OFF Grid					
Warranty [4]	10 Years					
Compatible Inverters	Refer to BYD Battery-Box Premium LVS Minimum Configuration List					

[1] DC Usable Energy, Test conditions: 100% DOD, 0.2C charge & discharge at + 25 °C. System Usable Energy may vary with different inverter brands

[2] Charge derating will occur between -10 °C and +5 °C

[3] Parallel tower function only available for 1 to 4 battery modules per tower. LVS 20.0 and LVS 24.0 can only be used as a single tower.

[4] Conditions apply. Refer to BYD Battery-Box Premium Limited Warranty Letter.



BYD Company Limited
www.brydbatterybox.com
Global Sales: batteryboxgrp@byd.com
Global Service: bboxservice@byd.com

Battery-Box EU Service Partner
EFT-Systems GmbH
www.eft-systems.de
info@eft-systems.de

Battery-Box AU Service Partner
Alps Power Pty Ltd
www.alpspower.com.au
service@alpspower.com.au

Battery-Box US Service Partner
EFT-Systems GmbH
www.eft-systems.de/us
USservice@eft-systems.de

v2.1



C.5 Charge Controller Datasheet



SmartSolar Charge Controllers with VE.Can interface
MPPT 250/70 VE.Can up to MPPT 250/100 VE.Can



**SmartSolar Charge Controller
MPPT 250/100-Tr VE.Can
with optional pluggable display**



**SmartSolar Charge Controller
MPPT 250/100-Tr VE.Can
without display**



**Bluetooth sensing:
Smart Battery Sense**



**Bluetooth sensing:
BMV-712 Smart Battery Monitor**



**Bluetooth sensing:
SmartShunt**

Ultra-fast Maximum Power Point Tracking (MPPT)
Especially in case of a clouded sky, when light intensity is changing continuously, an ultra-fast MPPT controller will improve energy harvest by up to 30 % compared to PWM charge controllers and by up to 10 % compared to slower MPPT controllers.

Advanced Maximum Power Point Detection in case of partial shading conditions
If partial shading occurs, two or more maximum power (MPP) points may be present on the power-voltage curve.
Conventional MPPTs tend to lock to a local MPP, which may not be the optimum MPP.
The innovative SmartSolar algorithm will always maximize energy harvest by locking to the optimum MPP.

Outstanding conversion efficiency
No cooling fan. Maximum efficiency exceeds 99 %.

Flexible charge algorithm
Fully programmable charge algorithm, and eight pre-programmed algorithms, selectable with a rotary switch (see manual for details).

Extensive electronic protection
Over-temperature protection and power derating when temperature is high.
PV short circuit and PV reverse polarity protection.
PV reverse current protection.

Bluetooth Smart built-in
The wireless solution to set-up, monitor, update and synchronise SmartSolar Charge Controllers.

Internal temperature sensor and optional external battery voltage, temperature and current sensing via Bluetooth
A Smart Battery Sense, a BMV-712 Smart Battery Monitor or a SmartShunt can be used to communicate battery voltage and temperature (and current, in case of a BMV 712 or a SmartShunt) to one or more SmartSolar Charge Controllers.

VE.Direct or VE.Can
For a wired data connection to a Color Control GX, other GX products, PC or other devices.

Synchronized parallel charging with VE.Can or Bluetooth
Up to 25 units can be synchronized with VE.Can, and up to 10 units with Bluetooth.

Fully discharged battery recovery function
Will initiate charging even if the battery has been discharged to zero volts.
Will reconnect to a fully discharged Li-ion battery with integrated disconnect function.

VE.Can: the multiple controller solution
Up to 25 units can be synchronized with VE.Can.

Remote on-off
To connect for example to a VE.BUS BMS.

Programmable relay
Can be programmed to trip on an alarm, or other events.

Optional: SmartSolar pluggable LCD display
Simply remove the rubber seal that protects the plug on the front of the controller, and plug-in the display.




Victron Energy B.V. | De Paal 35 | 1351 JG Almere | The Netherlands
General phone: +31 (0)36 535 97 00 | E-mail: sales@victronenergy.com
www.victronenergy.com

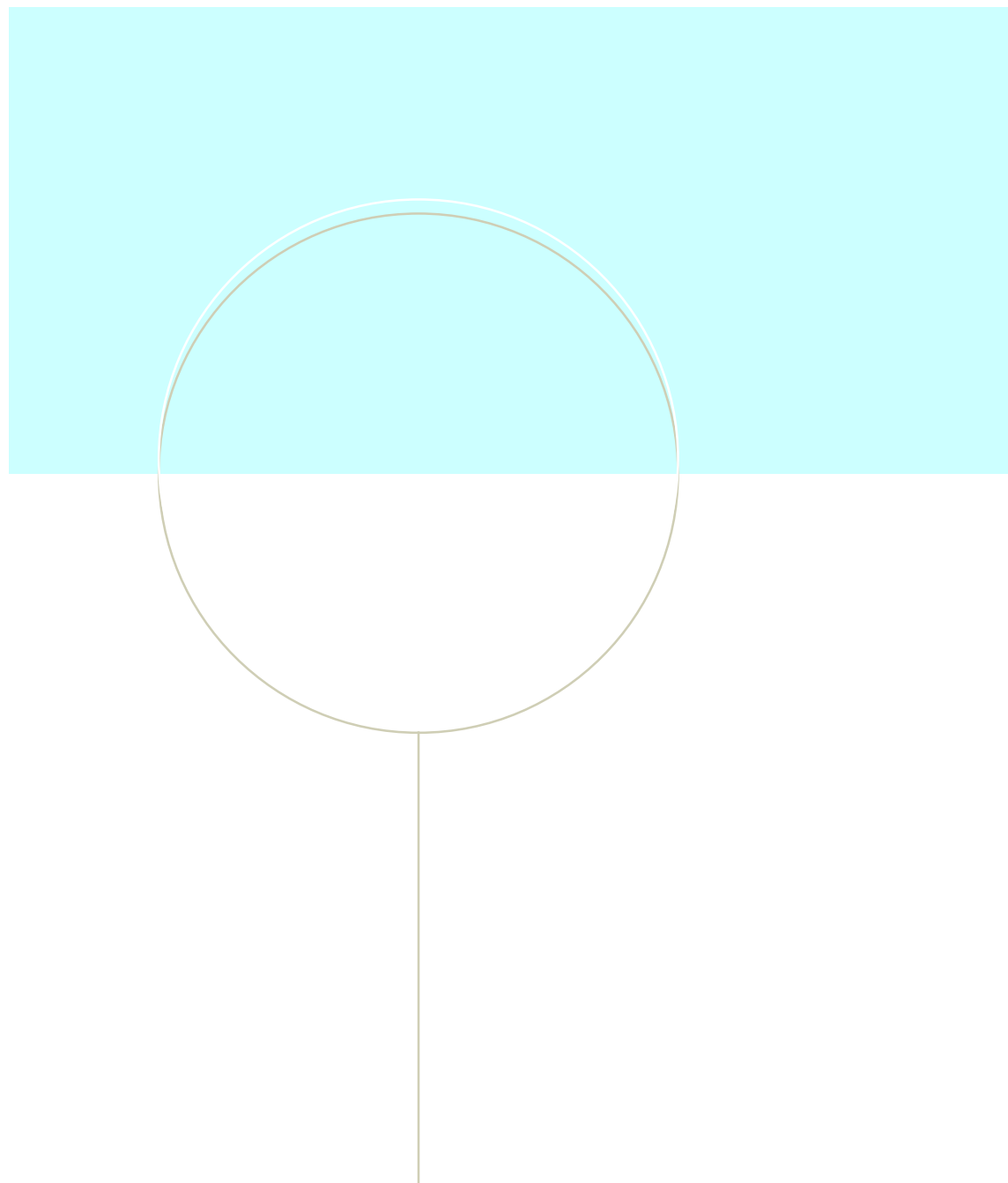


C.6 Charge Controller Datasheet

SmartSolar Charge Controller with VE.Can interface					
	250/70	250/85	250/100		
Battery voltage	12/24/48 V Auto Select (36 V: manual)				
Rated charge current	70 A	85 A	100 A		
Nominal PV power, 12 V 1a,b)	1000 W	1200 W	1450 W		
Nominal PV power, 24 V 1a,b)	2000 W	2400 W	2900 W		
Nominal PV power, 36 V 1a,b)	3000 W	3600 W	4350 W		
Nominal PV power, 48 V 1a,b)	4000 W	4900 W	5800 W		
Max. PV short circuit current 2)	35 A (max 30 A per MC4 conn.)	70 A (max 30 A per MC4 conn.)			
Maximum PV open circuit voltage	250 V absolute maximum coldest conditions 245 V start-up and operating maximum				
Maximum efficiency	99 %				
Self-consumption	Less than 35 mA @ 12 V / 20 mA @ 48 V Default setting: 14,4 / 28,8 / 43,2 / 57,6 V				
Charge voltage 'absorption'	(adjustable with: rotary switch, display, VE.Direct or Bluetooth) Default setting: 13,8 / 27,6 / 41,4 / 55,2 V				
Charge voltage 'float'	(adjustable: rotary switch, display, VE.Direct or Bluetooth)				
Charge voltage 'equalization'	Default setting: 16,2 V / 32,4 V / 48,6 V / 64,8 V (adjustable)				
Charge algorithm	multi-stage adaptive (eight pre-programmed algorithms) or user defined algorithm				
Temperature compensation	-16 mV / -32 mV / -64 mV / °C				
Protection	PV reverse polarity / Output short circuit / Over temperature				
Operating temperature	-30 to +60 °C (full rated output up to 40 °C)				
Humidity	95 %, non-condensing				
Maximum altitude	5000m (full rated output up to 2000m)				
Environmental condition	Indoor, unconditioned				
Pollution degree	PD3				
Data communication	VE.Can, VE.Direct and Bluetooth				
Remote on/off	Yes (2 pole connector)				
Programmable relay	DPST	AC rating: 240 VAC / 4 A DC rating: 4 A up to 35 VDC, 1 A up to 60 VDC			
Parallel operation	Yes, parallel synchronised operation with VE.Can (max. 25 units) or Bluetooth (max. 10 units)				
ENCLOSURE					
Colour	Blue (RAL 5012)				
PV terminals 3)	35 mm ² / AWG2 (Tr models) Two pairs of MC4 connectors (MC4 models)	35 mm ² / AWG2 (Tr models) Three pairs of MC4 connectors (MC4 models)			
Battery terminals	35mm ² / AWG2				
Protection category	IP43 (electronic components), IP22 (connection area)				
Weight	3 kg	4,5 kg			
Dimensions (h x w x d) in mm	Tr models: 185 x 250 x 95 mm MC4 models: 215 x 250 x 95 mm	Tr models: 216 x 295 x 103 MC4 models: 246 x 295 x 103			
STANDARDS					
Safety	EN/IEC 62109-1, UL 1741, CSA C22.2				
1a) If more PV power is connected, the controller will limit input power. 1b) The PV voltage must exceed Vbat + 5 V for the controller to start. Thereafter the minimum PV voltage is Vbat + 1 V. 2) A PV array with a higher short circuit current may damage the controller. 3) MC4 models: several splitter pairs may be needed to parallel the strings of solar panels Maximum current per MC4 connector: 30 A (the MC4 connectors are parallel connected to one MPPT tracker)					



With VE.Can up to 25 Charge Controllers can be daisy-chained and connected to a Color Control GX or other GX device
Each Controller can be monitored individually, for example on a Color Control GX and on the VRM website



NTNU – Trondheim
Norwegian University of
Science and Technology